UCLouvain

epl

École polytechnique de Louvain

Influence of a glow plug on the performances of a methane HCCI engine : a numerical study

Authors: **Nathan Deloge, Pierre Legrand**
Supervisors: **Francesco Contino, Hervé Jeanmart**
Reader: **Matthieu Duponcheel**
Academic year 2020–2021
Master [120] in Mechanical Engineering
Master [120] in Electro-mechanical Engineering

Abstract

In the framework of the ecological transition, a solution proposed to overcome the storage problems linked to the use of renewable energies is the power-to-gas. Homogeneous Charge Compression Ignition (HCCI) engines can be used to reconvert this gas back into electricity. To improve this last step, the present work proposes the installation of a glow plug in an HCCI engine.

The use of a glow plug creates a thermal stratification inside the cylinder which lowers the pressure rise rate. This allows the use of a lower intake temperature and the increase of the engine power density. In this work, numerical simulations are used to simulate HCCI engine combustion based on an experimental bench.

The results of this study show that, in terms of combustion efficiency, similar results are obtained with and without the glow plug but the effect on phasing results in a 5% increase in IMEP. By increasing the load, the rise in IMEP reaches 12% while staying under the ringing limit. The effects of thermal stratification were found to be strongly local, but the glow plug is able to generate an early burn of 1% of the methane, making the total combustion smoother. In terms of emissions, an increase in CO production is observed but remains marginal. Regarding parietal losses, the obtained results do not follow the used correlation. Therefore, it would be preferable to carry out an experimental campaign to confirm the values and the trend obtained with temperature variations.

Acknowledgements

First of all, we would like to thank our supervisors, Pr. Contino and Pr. Jeanmart. Their availability throughout the year combined with their accurate remarks and relevant comments made the completion of this thesis possible. We would like to thank them especially for their reactivity and for having accepted several meetings on a very short notice.

Then we would like to address a special thank to Sara. Her help, her advice and her patience were indispensable. Her daily support gave us back the motivation when we needed it.

In addition, we thank Pr. Duponcheel for accepting the task of reader and member of the jury. We also thank Frank, Julien, Arnaud and Thierry for their availability and valuable advice. Additionally, we are grateful for B. Herman and P. Eliaers advises regarding the safety documents.

Finally, we would like to thank our friends, families and roommates for their patience, support and motivation throughout the writing of this thesis.

Contents

Nomenclature

Abbreviations

AFR	Air-Fuel Ratio
$AHRR$	Apparent Heat Release Rate
$aTDC$	after Top Dead Center
BDC	Bottom Dead Center
$BMEP$	Brake Mean Effective Pressure
$CA10$	Crank angle where 10% of the heat has been released
$CA50$	Crank angle where 50% of the heat has been released
$CA90$	Crank angle where 90% of the heat has been released
CA_{10-90}	Combustion Duration
CAD	Crank Angle Degree
CAS	Compressed Air Storage
CC	Cubic centimeters
$CCGT$	Combined Cycle Gas Turbine
CFD	Computational Fluid Dynamics
CHP	Combined Heat and Power
CHR	Cumulative Heat Release
CI	Compression-Ignition
$COP21$	21^{st} Conference Of the Parties
COV_{IMEP}	Coefficient Of Variation in IMEP
CR	Compression Ratio

DAC	Dynamic Adaptive Chemistry
DOC	Duration Of Combustion
EGR	Exhaust Gas Recirculation
EVO	Exhaust Valve Opening
FAR	Fuel-Air Ratio
FAR_{st}	Stoichiometric Fuel-Air Ratio
$FMEP$	Friction Mean Effective Pressure
$FuelMEP$	Fuel Mean Effective Pressure
GP	Glow Plug
$GPMEP$	Glow Plug Mean Effective Pressure
$HCCI$	Homogeneous Charge Compression Ignition
HRR	Heat Release Rate
ICE	Internal Combustion Engines
$IMEP$	Indicated Mean Effective Pressure
$imep$	Mean Indicated Mean Effective Pressure
$IMEPgross$	Gross Indicated Mean Effective Pressure
$IMEPnet$	Net Indicated Mean Effective Pressure
$IMMC$	Institute of Mechanics, Materials and Civil Engineering
$ISAT$	In Situ Adaptive Tabulation
IVC	Intake Valve Closing
IVO	Intake Valve Opening
LHV	Lower Heating Value
MEP	Mean Effective Pressure
MFC	Mass Flow Controller
$MPRR$	Maximum Pressure Rise Rate
NG	Natural Gas

PDF	Probability Density Function
PM	Particulate Matter
$PMEP$	Pumping Mean Effective Pressure
PRR	Pressure Rise Rate
PS	Pumped Storage
PtG	Power-to-Gas
PtP	Power-to-Power
$QemisMEP$	Heat lost during the combustion Mean Effective Pressure
$QexhMEP$	Heat lost at the exhaust Mean Effective Pressure
$QhrMEP$	Heat released Mean Effective Pressure
$QhtMEP$	Heat lost at the wall Mean Effective Pressure
$QlossMEP$	Heat lost Mean Effective Pressure
RE	Renewable Energy
RI	Ringing Intensity
SI	Spark-Ignition
SOC	Start Of Combustion
SR	Swirl Ratio
$TDAC$	Tabulation of Dynamic Adaptive Chemistry
TDC	Top Dead Center
VCR	Variable Compression Ratio
VVT	Variable Valve Timing
WDI	Water Direct Injection
NO_x	Nitrous Oxides

Greek letters

α	Hohenberg scaling factor [-]
β	Conrod length over crankshaft radius [-]

η_{comb}	Combustion efficiency [-]
η_{ind}	Indicated efficiency [-]
η_{mec}	Mechanical efficiency [-]
η_{th}	Theoretical efficiency [-]
γ	Specific heats ratio [-]
λ	Air-fuel equivalence ratio [-]
ω	Engine speed [rpm]
ϕ	Equivalence ratio [-]
σ_{IMEP}	Standard deviation in Indicated Mean Effective Pressure [-]
τ	Compression ratio [-]
τ_{eff}	Effective compression ratio [-]
θ	Crankshaft angle [CAD]

Symbols

$\bar{v}_p$	Mean piston speed [m/s]
ΔU	Variation of internal energy [J]
A	Surface [m^2]
B	Cylinder bore [m]
c_p	Specific heat at constant pressure [J/mol/K]
c_v	Specific heat at constant volume [J/mol/K]
Co	Courant number [-]
h	Heat transfer coefficient [W/m^2/K]
k	Thermal conductivity [W/m/K]
k_{CH4}	Remaining methane fraction [-]
k_{CO}	CO coefficient [-]
L	Conrod length [m]
M	Molar mass [g/mol]

m_a	Air mass [kg]
m_f	Fuel mass [kg]
n	Number of moles [mol]
p	Pressure [Pa]
P_{GP}	Glow Plug Power [W]
Q	Heat energy [J]
q	Heat flux [W/m^2]
R	Crankshaft radius [m]
R	Ideal gas constant [J/mol/K]
S	Piston stroke [m]
T	Temperature [K]
T_{in}	Intake temperature [K]
T_{wall}	Wall temperature [K]
U	Velocity [m/s]
V	Volume [m^3]
V_d	Displacement volume [m^3]
W	Work [J]

Introduction

Human activities are responsible for the increasing carbon footprint. However, the level of industrialization and energy consumption is not about to decrease. In an attempt to limit the carbon footprint, efforts are made to produce our day-to-day energy with renewable sources. From their very nature, they are intermittent and a capacity of storage is needed to fit the energy production to the consumption. Power-to-gas systems represent a promising technology for renewable energy storage since it allows to store a large amount of energy for a long time. To retrieve this energy stored in the fuel, *Homogeneous Charge Compression Ignition* (HCCI) engines are viable solution for applications under $3MW_{elec}$ [1].

HCCI engines combine the advantages of both Diesel and gasoline engines. Just like the compression ignition engine, the HCCI engine works with a high compression ratio, which leads to a high efficiency. And similarly to a spark ignition engine, the charge is homogeneous which decreases the pollutant emissions. The working principle is based on the auto-ignition : the homogeneous mixture is compressed until self-ignition. However those advantages come with limitations. Since the auto-ignition only relies on chemical kinetics, it is difficult to predict. Moreover the operating range is limited. Also, at low engine load, misfire can happen and at high engine load, the spontaneity of the combustion might damage the engine. This is the reason why HCCI engines are only fueled with lean mixtures [2]. To increase the fueling and thus the power density, thermal stratification can be used [3].

The principle of thermal stratification consists in inducing an in-cylinder gradient of temperature. The mixture would ignite inhomogeneously which will decrease the sudden and violent pressure increase. HCCI engines can therefore run with richer mixture while preventing damage to the engine. The thermal stratification can be achieved with a diesel engine derived glow plug. A glow plug would bring an in-cylinder hot spot and therefore create a temperature gradient. It should also be able to control the start of the combustion. Research on HCCI engines with a glow plug has already been conducted [3], [4]. However, none were found applied to methane and none of them prove the fact that the glow plug can indeed increase the power density.

The thesis is structured as follows. In Chapter 1, HCCI engines are described and their advantages and limitations are reported. Then the principle of thermal stratification will be covered along with a brief overview of its presence in the literature. In Chapter 2, the experimental setup on which this thesis is based will be described as well as the glow plug itself. In Chapter 3, a description of the HCCI simulation model that was used to analyze the glow plug effects is presented. This simulation has then been compared to an experimental case. Finally, in Chapter 4, several analyses on the glow plug were

performed. Among them, studies on its ability to control the combustion, to increase the work produced or to increase the HCCI engine power density.

Chapter 1

Context

1.1 Introduction

1.1.1 Environmental issues

Since the early days of mass industrialization, the effects of pollution and hazardous emissions on climate change and public health have been a growing concern. This resulted in a change of mind among not only the people, but also politicians and industries. As a consequence, more and more concrete actions are being taken to prevent and reduce them. More recently, in the context of the 21^{st} *Conference of the Parties* (COP21), a large number of states agreed on a guideline to follow which is commonly known as the Paris Agreement. This guideline has the ambition to reach carbon neutrality in 2050 or at least a reduction of carbon emissions of 80% depending on the scenario considered [5].

In the path towards zero net carbon emissions, the share of *Renewable Energy* (RE) will grow continuously. Solar panels, wind turbines and other RE sources have been deployed at huge scale around the world for the past years. This trend will most likely continue and the share of renewables in the total energy production is predicted to increase.
Those technologies, while providing solutions to major problems, bring their own set of issues, the main one being their intermittency of energy production. This can be seen more clearly when looking at the most common renewable energy sources, such as wind turbines and photovoltaic panels. Wind turbines depend on the wind, whereas photovoltaic panels depend on the sun to produce their energy. Both sources of energy vary greatly on place, time, season, etc. However, energy consumption is not limited to the time when energy is available. Therefore, to ensure grid stability and avoid blackouts, the need for large-scale and long-term storage will grow continuously in the next years.

1.1.2 Energy Storage

There are many ways for storing energy, from the smallest capacity to the largest one and from seconds to months of storage time. In Figure 1.1 an overview is given of several

commonly known energy storage methods together with an indication of how long and how much they can store.

- For the short term storage, the most common in our daily lives are batteries. Even if there is a lot of research on this topic at the moment to improve them, e.g. in the automotive sector, they are not yet suitable for a long-term storage.
- At the seasonal level, the storage by *Compressed Air Storage* (CAS) and by *Pumping Storage* (PS) are suitable. However, the implementation of those two storage methods requires large spaces. CAS takes place in caves and PS requires large height differences. In Belgium, the hydro potential is very limited, therefore those technologies will not be able to cope for the whole storage capacity needed.
- A final technology worth talking about is the *Power-to-Gas* (PtG) storage. This technology offers long-term storage and, due to its high energy density, higher storage capacities than any of the technologies mentioned above. The gas in question can be either hydrogen or another fuel obtained with the further transformation of hydrogen into methane or ammonia.

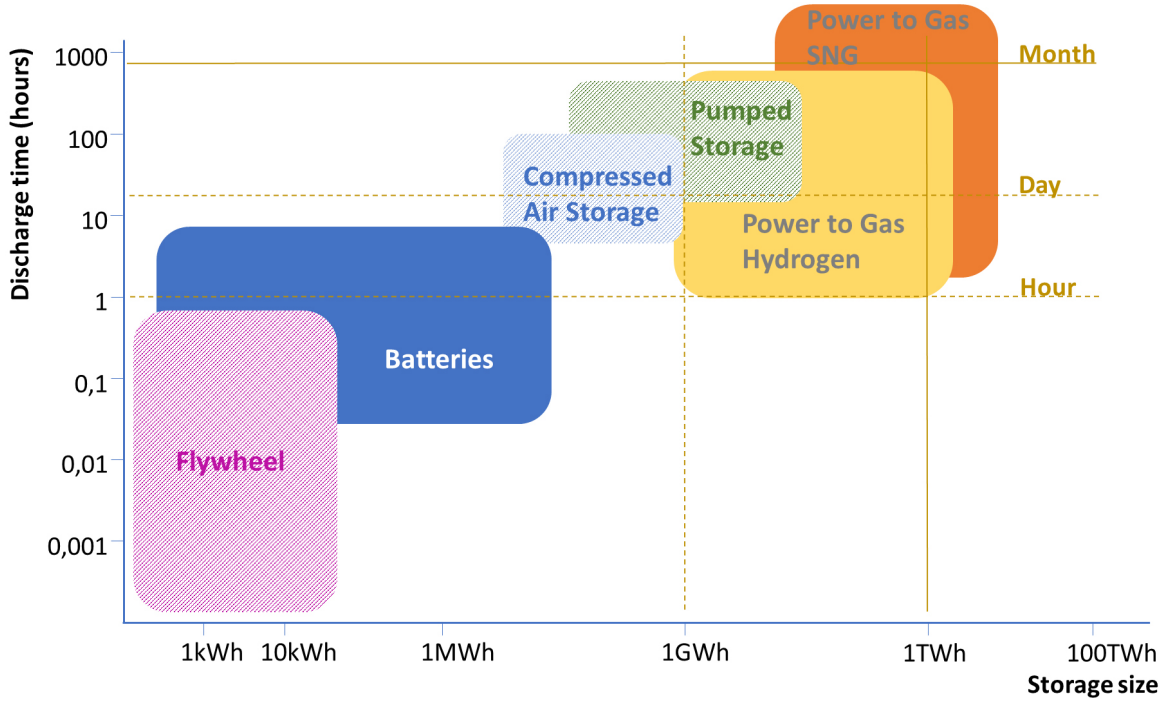

Figure 1.1: *Storage size versus discharge time for common storage technologies. The characteristics vary greatly among them [6].*

The conversion process is the following : During peak production times, when the demand is lower than the production, the excess electricity is used to create hydrogen by hydrolysis. The hydrogen can be used as is or can be transformed into methane or ammonia. The decision to carry out an additional step in the conversion process to obtain methane comes from its perfect compatibility with the existing *Natural Gas* (NG) network. Moreover, the hydrogen in the network is regulated and cannot exceed a certain concentration.
After being stored for varying periods of time, the gas is converted back into electricity.

The full cycle is called *Power-to-Power* (PtP). For small-scale applications, like decentralized cogeneration units, this transformation is generally done thanks to *Internal Combustion Engines* (ICE) [1], fuel cells or *Combined Cycles Gas Turbines* (CCGT).

The main drawback of the PtP is the low overall efficiency due to the losses in each conversion process. The losses for the whole PtP cycle includes the ones depicted in Figure 1.2 and must also take into account the efficiency of the technologies used to recover the energy. For typical ICE, the efficiency ranges from 30% to 50%. When used in a *Combined Heat and Power* unit (CHP), the efficiency can rise up to 95% [7].

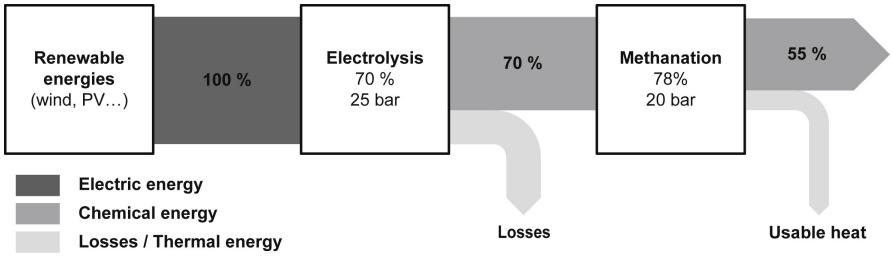

Figure 1.2: *Losses of the different steps of the conversion. Only 55 % of the power is retrieved in the end. [8]*

This thesis will focus on the last part of the PtP cycle and more precisely on the conversion of gas back into electricity using an ICE. The HCCI engine was selected for its many qualities discussed in the following sections.

1.2 HCCI engines

1.2.1 Fundamentals

The description of the engine, its comparison with its gasoline and diesel equivalents and the basic theory on efficiencies and pollutants were partly inspired by the previous theses of Hosselet and Van de Putte. [9], Collette and Gatin. [10] and Pochet [1].

The HCCI engine is an internal combustion engine which relies both on the working mechanism of the *Spark-Ignition* (SI) engine, also called the gasoline engine, and the *Compression-Ignition* (CI) engine, also called the Diesel engine.

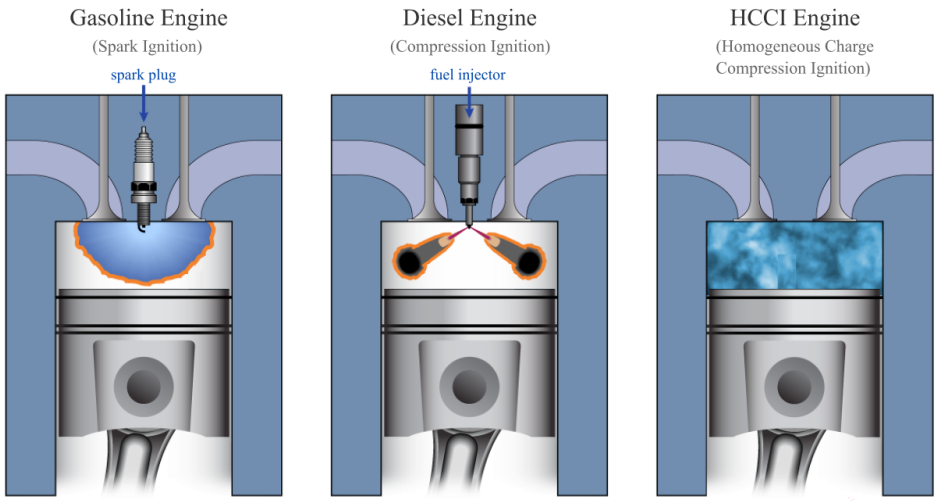

Figure 1.3: *The SI, CI and HCCI engines present different combustion principles. Adapted from [11].*

The basic gasoline engine (SI) (Figure 1.3 left) mixes fuel and air to get a homogeneous in-cylinder mixture. This blend is compressed by the piston and then the combustion occurs thanks to a spark plug that is being lit at the desired timing. The combustion propagates via a flame front starting from the spark. The power delivered depends on the quantity of mixture put inside the cylinder.
For the Diesel engine (CI) (Figure 1.3 middle), the intake mixture consists solely of air. It is compressed by the piston until it exceeds a certain thermodynamic state of pressure and temperature. The combustion occurs thanks to the injection of the fuel which meets a suitable environment for auto-ignition. The combustion propagates from droplets to droplets in the cloud of fuel. The power delivered depends on the quantity of fuel injected each cycle.
The HCCI engine (Figure 1.3 right) relies on a mix of both principles. The intake mixture consists of a homogeneous blend of air and fuel as in a SI engine. The ignition occurs due to the thermodynamic state reached by compression which has to be high enough to start the auto-ignition process as in a CI engine. There are many parameters to adjust the combustion : the compression ratio, the wall temperature, the equivalence ratio, etc. (Figure 1.4).

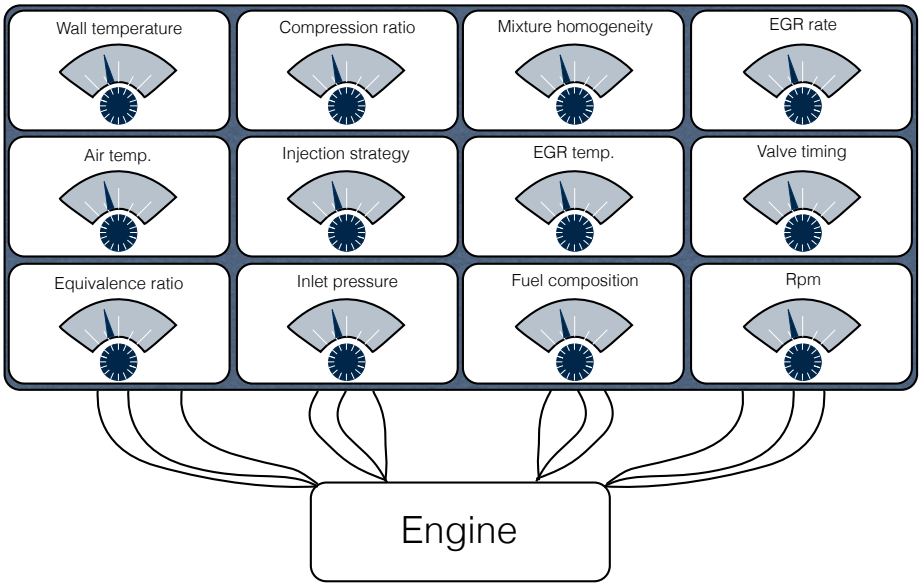

Figure 1.4: *Parameters influencing the combustion in an HCCI engine. There are many of them [2].*

The combustion conditions are therefore very different from one engine to another.

First of all, concerning the compression ratio. On the one hand, for the gasoline engine, the fuel inside the cylinder undergoes the full compression. In order to avoid disastrous consequences, the fuel must not explode before the spark plug starts the combustion. This is why the SI engine works with a relatively low compression ratio, usually around 10:1. The Diesel engine, on the other hand, must reach high compression ratio to ensure auto-ignition to happen. The CI engines will usually have a compression ratio between 12:1 and 23:1. Since the HCCI has the same working principle of compression-ignition, it also uses high compression ratio, around 20:1 and sometimes above.

Secondly, regarding the combustion itself, the HCCI engine has a particularly short *Duration of Combustion* (DOC) compared to the other ICE. For the SI engine, it takes a certain time for the flame to propagate and for the CI a certain time for the fuel droplets to evaporate. The charge homogeneity in the HCCI makes its combustion very short. Because of that, the *Start of Combustion* (SOC) is usually placed quite late compared to the other ICE in order for the combustion to occur around *Top Dead Center* (TDC).

Thirdly, HCCI engines work with very lean mixtures. The almost instantaneous release of heat in the engine causes the pressure to rise sharply. This can cause ringing and destroy the engine by applying too much stress on it. In order to prevent this, the charge has a great excess of air which makes the mixture very lean. In addition, putting too much fuel inside the cylinder could lead to uncontrolled auto-ignition that could also rapidly destroy the engine. For comparison, the SI engine operates close to stoichiometric condition. For the CI engine, since the fuel is injected in the piston right before TDC, it creates very rich regions where the fuel is in excess. In order to prevent a too large amount of unburned hydrocarbons there must be a great excess of oxygen which makes

the global mixture poor.

The lean or rich conditions of a mixture are defined via the equivalence ratio. It represents the ratio between the quantity of fuel and air actually present in the cylinder and the stoichiometric quantity. It is defined as follows :

$$\phi = \frac{FAR}{FAR_{st}} = \frac{m_f/m_a}{(m_f/m_a)_{st}} \tag{1.1}$$

Where FAR is the *Fuel-Air Ratio*, m_f the fuel mass, m_a the air mass and the subscript "st" stands for stoichiometric. The conditions are called lean when there is an excess of air so when ϕ is smaller than one and rich when there is an excess of fuel so when ϕ is larger than one. The air-fuel equivalence ratio, λ, can also be defined as the inverse of ϕ.

1.2.2 Upsides

The choice to operate on an HCCI engine is based on all the advantages this technology can offer compared to other ICE. Despite the greater difficulty to control the combustion timing and the limitations on the HCCI operating range, the efficiency characteristics and the low pollutant emissions make it a worthy and promising engine for the future.

Efficiency

In HCCI engines, the DOC is much shorter compared to conventional SI or CI ones [12]. The fact of having a shorter combustion, ideally taking place when the piston is at the top of its stroke, makes the cycle closer to the theoretical model of the Beau de Rochas cycle, also called Otto cycle (Figure 1.5). The Otto cycle is an idealized thermodynamic cycle which has the best theoretical efficiency for a given compression ratio. In this model, the heat addition phase happens at constant volume.
The cycle occurs as follows : it begins with a heat addition at constant volume and continues with an isentropic expansion. To achieve such a heat addition in an ICE, the heat should be added instantaneously. During both isentropic processes, there are no losses and there is no heat released outside the cylinder. The net mechanical work is the sum of the work added to the system for the compression phase and the heat released by the combustion minus the heat released at the exhaust.

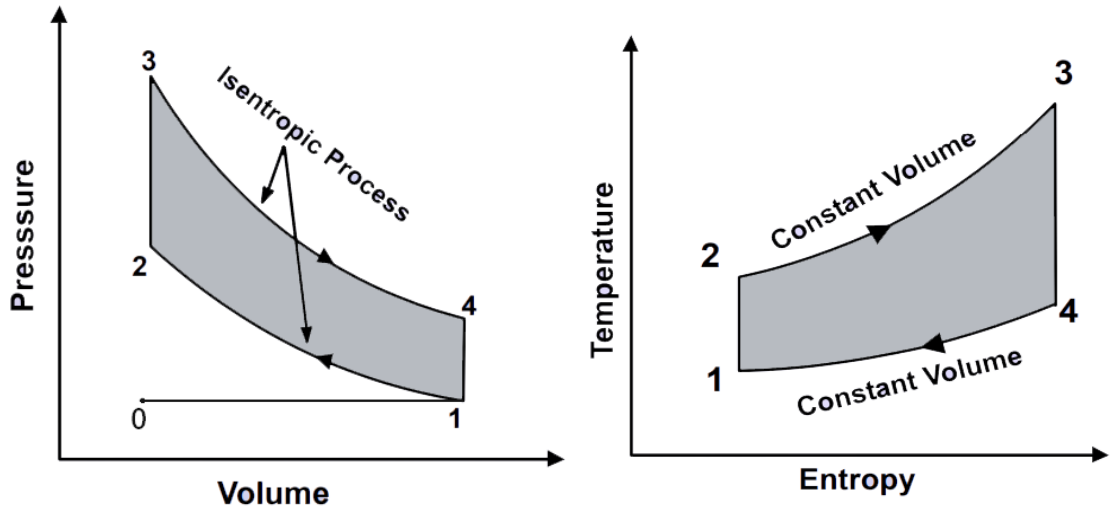

Figure 1.5: *P-V and T-S diagrams of the Beau de Rochas cycle. The heat addition happens at constant volume and the compression and the expansion are isentropic. [13]*

The theoretical efficiency of this cycle can be easily linked to the compression ratio of an engine. It is defined as the ratio of the work applied on a piston over the heat released by the combustion (Equation (1.2)).

$$\eta_{th} = 1 - \frac{1}{\tau^{1-\gamma}} \tag{1.2}$$

Where $\gamma = \frac{c_p}{c_v}$ is the ratio of specific heats. Even if they are temperature dependent and different for each species, a common value used to approximate γ is 1.3 [2]. τ is the *Compression Ratio* (CR) and is defined by the ratio of the in-cylinder volume at *Bottom Dead Center* (BDC) over the one at TDC.
The efficiency is therefore inversely proportional to the compression ratio. As said earlier, the SI engine operates with lower compression ratios than HCCI and CI engines, which is the reason for their lower efficiency. The high efficiency of the HCCI engine is therefore mainly due to its high compression ratio and short combustion.

Then in order to compare two different engines, it is necessary to define a new quantity. Indeed, considering the diversity of existing engines, from a lawnmower to a boat engine, the sizes and powers vary considerably. To cope for this, the work produced is normalized by the displacement volume. This ratio is called *Mean Effective Pressure* (MEP) since its units are the ones of a pressure. Moreover, during the conversion of the fuel chemical energy into mechanical energy at the crankshaft, losses are encountered. It is thus necessary to define an MEP at each step of the conversion (Figure 1.6).

The diagram starts with the $FuelMEP$ (Equation (1.3)) which is the total energy contained in the fuel.

$$FuelMEP = \frac{m_f LHV}{V_d} \tag{1.3}$$

Where LHV is the *Lower Heating Value* (LHV) and V_d the displacement of the engine. The fuel chemical energy is transformed into thermal energy through the combustion,

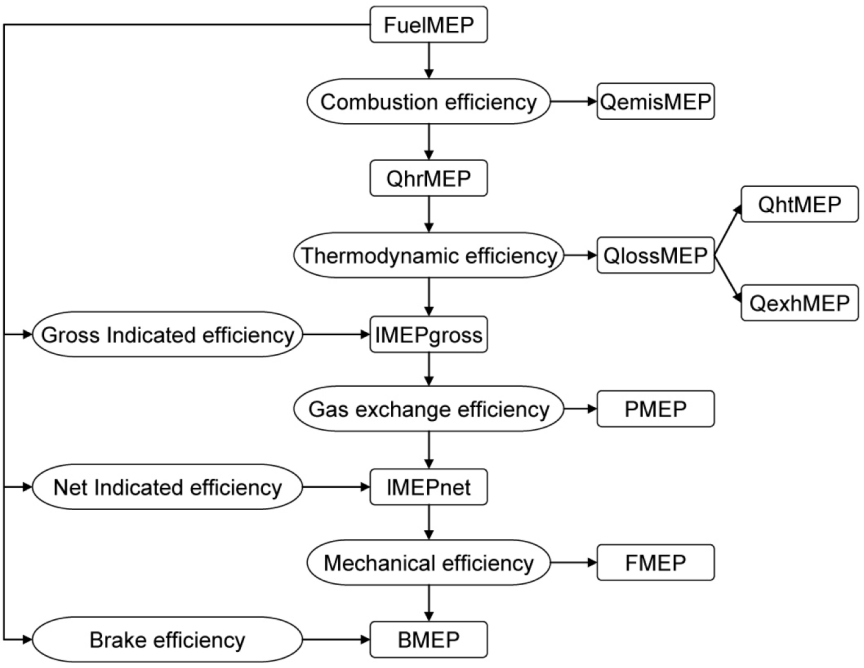

Figure 1.6: *Decomposition of the initial fuel chemical energy into losses and mechanical work. The diagram defines the efficiencies at each step of the fuel conversion. [2]*

which delivers the $QhrMEP$. Their ratio is defined as the combustion efficiency η_{comb} (Equation (1.4)). The losses are taken into account with the $QemisMEP$.

$$\eta_{comb} = \frac{QhrMEP}{FuelMEP} \tag{1.4}$$

The combustion efficiency can also be computed from the energy contained in the remaining exhaust species concentration over the initial energy of the methane at the intake.

$$\eta_{comb} = 1 - \frac{m_i LHV_i}{m_{CH4,init} LHV_{CH4,init}} \tag{1.5}$$

Where m_i and LHV_i are respectively the mass and the LHV of each species present in the exhaust.

The heat is then converted into mechanical work. There are two categories of losses in this process. The first one is the $QhtMEP$ which is the heat lost though the wall and the second one is the $QexhMEP$ which is the heat lost to the exhaust. The thermodynamic efficiency is the ratio between the heat released by the combustion and the energy that is effectively converted into mechanical energy, called the *gross Indicated Mean effective Pressure* (IMEPgross).
However, this energy is not the one transmitted to the crankshaft because of the pumping losses (PMEP). They come from the head losses during the intake and the exhaust stroke. Their work can be expressed as :

$$W_p = (p_{out} - p_{in})V_d = PMEP\, V_d \tag{1.6}$$

Where p_{out} and p_{in} are respectively the exhaust and intake pressure. With those removed, one can get the *net Indicated Mean Effective Pressure* (IMEPnet) (Equation (1.7)).

$$IMEP_{net} = IMEP_{gross} - PMEP = \frac{\oint p \mathrm{d}V}{V_d} \tag{1.7}$$

For the sake of simplicity, when not specified, the IMEP refers to the IMEPgross.

Finally, the final losses before obtaining the useful work are the friction losses (FMEP). The *Brake Mean Effective Pressure* (BMEP) can be defined with the mechanical efficiency (η_{mec}) (Equation (1.8)).

$$\eta_{mec} = \frac{BMEP}{IMEP_{net}} = 1 - \frac{FMEP}{IMEP_{net}} \tag{1.8}$$

For the sake of simplicity, other efficiencies including several steps of the energy conversion process are defined. For instance, the gross indicated efficiency η_{ind} takes into account the losses related to the combustion and the thermodynamic efficiency. The net indicated efficiency takes pumping losses into account (Equation (1.9)) and finally the brake efficiency corresponds to the ratio between the energy contained in the fuel and the energy transmitted to the crankshaft.

$$\eta_{ind} = \frac{IMEP}{FuelMEP} \tag{1.9}$$

Pollutants

The HCCI engine is renowned for its low *Nitrous Oxides* (NO_x) and soot emissions. However, its combustion results in a large amount of unburned hydrocarbon and carbon monoxides emissions [3]. First, the main pollutants will be presented and then their production in the HCCI engine will be analyzed.

- First, the soot, also called the *Particulate Matter* (PM) is a very fine compound. Fine enough to remain in suspension in the air and therefore be inhaled. They can reach the lungs as well as the cardiovascular system and cause illness. Because those particles are carcinogenic, they can lead to numerous human diseases such as cardiovascular disorders, heart attack or respiratory failure [14].

- Then the NO_x are dangerous for both human health and the environment. Exposure has shown to lead to asthma condition. These oxides also cause heart attacks and other deadly hazards. In the environment, they form ground-level ozone layers that contribute to global warming. They can react with other compounds to form nitric acid and cause acid rains.

- Finally, another gas that can be found in the exhaust is the carbon monoxide (CO). It is a product of an incomplete combustion. It is toxic for the human body and can lead to intoxication and often even death.

Note that carbon dioxide (CO_2) is not considered as a pollutant since it is an expected product of the combustion, just like water. Therefore, its emissions are by definition impossible to avoid. However, its polluting effect on the atmosphere and the greenhouse effect it produces should not be overlooked. It is interesting to note that if the fuel comes from renewable energies, there are no net CO_2 emissions.

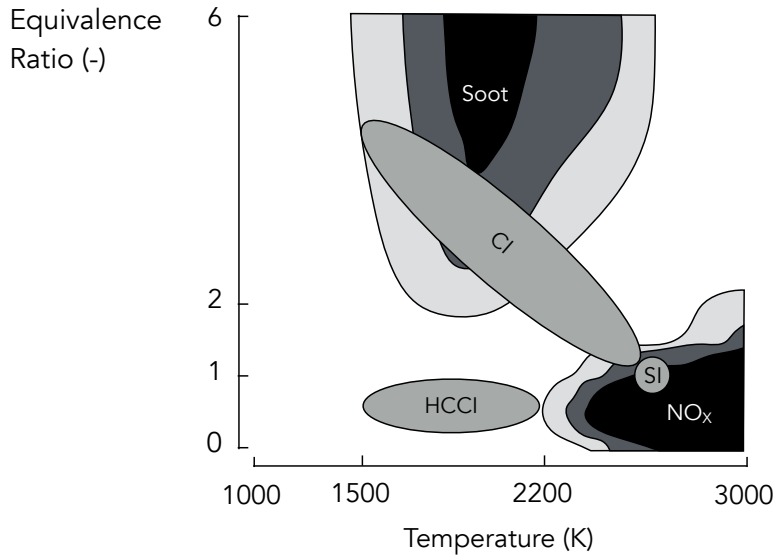

Figure 1.7: *Conditions for soot and NOx production. Both are strongly dependent on the temperature and the equivalence ratio. The different types of engines produce more or less of those pollutant by their very nature. [1]*

The production of pollutants is heavily dependant of the temperature and equivalence ratio conditions.

The soot appears when the equivalence ratio is high (Figure 1.7). Those levels of equivalence ratio can be locally reached due to inhomogeneities in the mixture. The fact that there is no soot production at high temperature is due to their immediate oxidation. The SI engine, with its homogeneous blend has a really low soot production. The CI engine conversely, due to the injection of droplets, presents lots of locally rich zones. Because of the highly diluted charge and the homogeneity in the mixture, the HCCI engine avoids mostly the production of soot.

The NO_x production is favored at high temperatures, when there is enough oxygen to bond with the nitrogen and when the combustion is slow (Figure 1.7). In the SI engine, the temperatures reached are very high and the combustion occurs at stoichiometric conditions, which implicates a high NO_x production. However, since the use of a three-way catalyst is possible, the remaining amount of NO_x emitted is negligible. It is different for the CI engine. Indeed, the temperatures reached inside the cylinder are high enough to produce NO_x and the combustion is slow. The lean conditions make the use of the three-way catalyst ineffective. Some technologies are currently under development and deployed such as AdBlue to lower the emissions, but the levels remain significants.

In the case of an HCCI engine, due to the high dilution of the charge needed to avoid uncontrolled ignition and ringing, local high temperature peaks are avoided and the temperatures remain below the NO_x production zone [2].

The CO production is mainly driven by the equivalence ratio. When the mixture is rich, there is not enough oxygen atoms to bound with the carbon atoms. Thus, instead of CO_2, CO is produced. The emissions of CO are also temperature dependent, as it can be seen in Figure 1.8. For low temperatures, the fuel is not well oxidized. This incomplete combustion leads to a high CO production [15]. Since HCCI are low temperature combustion engines, they present high CO emissions. A very high temperature leads to a dissociation phenomena of the CO_2 which, in turn, increases the carbon monoxide production [16].

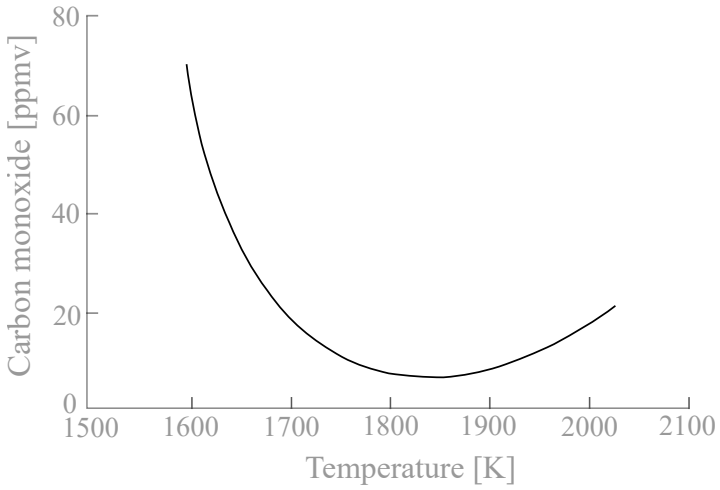

Figure 1.8: *Temperature dependency of the CO production. There is an optimal temperature operating range to limit CO emissions. Adapted from [16].*

In this thesis, the choice has been made to run the HCCI engine with methane as a fuel because of its many advantages. Indeed, its combustion is cleaner with respect to carbon related substances emissions. It is also the only common fuel to have a relatively pure, single-stage combustion. Moreover, the molecules of methane are able to resist decomposition by free radicals during the compression stroke [17].

1.2.3 Limitations

The advantages of the HCCI engine justify the interest that research has in it today. However, in order to take full advantage of it, there are some limitations that need to be taken into account. At the moment, these are the ones that limit its widespread use.

- The first limitation concerns the difficulty to control the combustion. The timing of the combustion depends on many parameters and a small variation of one of them can result in a great loss in efficiency and performances.
- The second major limitation is the limited operating range. The working area is bounded by the risk of misfire on one side and the risk of ringing on the other. The

latter prevents using high fueling rates and thus reaching high power densities.

This shows that the HCCI engine is not meant for automotive applications in view of the constantly changing conditions. Furthermore, as the parameters have to be accurately tuned, the cold start represents an additional difficulty in using this technology. The HCCI engine corresponds much better to stationary conditions with no or small and slow variations of the load. When the engine runs for energetic applications such as electricity production, it is connected to a generator and is set to have a constant rotational speed.

Combustion timing control

On one hand, in conventional engines, combustion can be controlled very precisely : in the SI engine, the spark plug decides the SOC and in the CI engine it is the fuel injection. On the other hand, in the HCCI engine, the SOC depends on the self-ignition of the mixture and is therefore solely dependent on chemical kinetics. This makes the control of the combustion start very difficult because it depends on many parameters as shown in Figure 1.4 [18].
However, not all parameters have the same influence on the SOC. *Amneus et al.* [19] studied the influence of the inlet temperature T_{in} and pressure p_{in} and of the *Air-Fuel Ratio* (AFR). They found that to vary the SOC by one *Crank Angle Degree* (CAD), T_{in} must be varied by 0.6%, p_{in} by 11% and the AFR by 10%, while keeping all the other parameters constant. This study shows that the SOC depends mainly on T_{in}. This is explained by the fact that a higher T_{in} accelerates the oxidation reaction and leads to an earlier SOC [20]. Figure 1.9 shows the phasing variation for a temperature sweep.

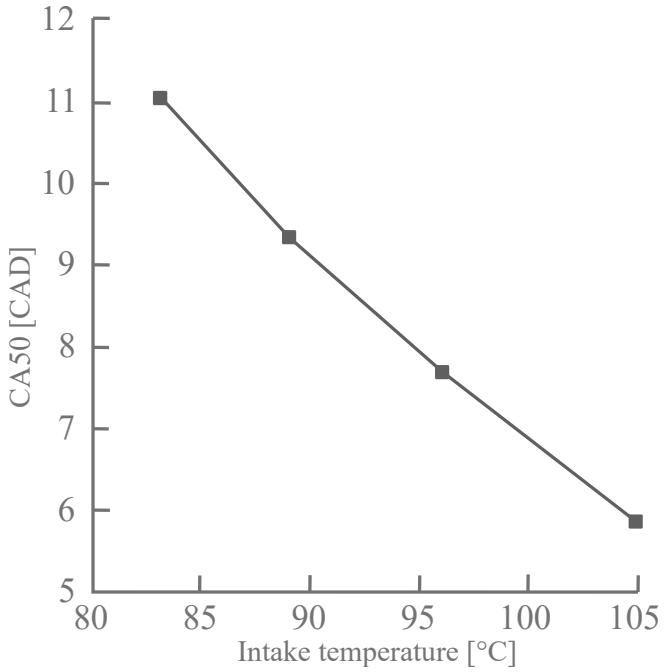

Figure 1.9: *Combustion phasing for an intake temperature sweep. As T_{in} increases the combustion occurs significantly earlier (87 octane gasoline, 550 cc). Adapted from [21]*

To a lesser extent, combustion phasing is also pressure dependent. Increasing the inlet

pressure will lead to higher temperatures and has the same consequences as explained before.
Increasing the compression ratio is another way to influence the pressure in order to get a higher temperature during the cycle.
In addition, increasing the equivalence ratio will make the mixture more reactive and thus lead to an earlier SOC. Finally, the speed of the engine influences the phasing. Since chemical reactions take a certain amount of time, increasing the engine speed will delay the end of the reaction to a later CAD.

In order to control the timing of the combustion in variable conditions, several control mechanisms such as *Variable Valve Timing* (VVT), *Variable Compression Ratio* (VCR) and *Exhaust Gas Recirculation* (EGR) exist today[12], [22]. The VVT and the VCR are particularly interesting due to their fast-time response.

Operating range

The HCCI operating range is bounded by the risk of misfire at low load and the risk of knock at high load. For stationary engines working at constant speed, the load is set by the equivalence ratio and the intake temperature.

At low load, the SOC is too late to sustain the combustion which leads to a misfire. One indicator of misfire in ICE is the Coefficient of Variation in IMEP (COV_{imep}). It represents the variability of the IMEP from one cycle to the other. It is defined as follows:

$$COV_{IMEP} = \frac{\sigma_{IMEP}}{imep} * 100 \qquad [\%] \tag{1.10}$$

Where σ_{IMEP} is the standard deviation in IMEP. The *imep* is the mean IMEP over several engine cycles [23].
In automotive applications the COV_{IMEP} should be limited to 10 % to ensure drivability. For stationary applications, higher values are allowed [24], [25].

At high loads, in SI engines, knock happens when the unburned or end-gases auto-ignite before the flame front reaches the cylinder wall [26]. It is occurring due to high compression ratio or too much spark advance and results usually in engine damage. In CI engines, the "diesel knock" is not detrimental for the engine, but for the comfort, since it creates an unpleasant noise for the driving experience. In an HCCI engine ringing appears at high loads. This phenomenon is characterized by pressure oscillations that increase the engine noise and might damage the engine [27]. The indicator used to characterize ringing is called the *Ringing Intensity* (RI) and is defined in Equation (1.11).

$$RI = \frac{1}{2\gamma} \frac{(\beta \frac{dP}{dt}_{max})^2}{P_{max}} \sqrt{\gamma R T_{max}} \qquad \left[\frac{MW}{m^2}\right] \tag{1.11}$$

Where,

- γ is the ratio of specific heats,
- β is a correction factor for the *Maximum Pressure Rise Rate* (MPRR),

- R is the ideal gas constant,
- $\left(\frac{dP}{dt}\right)_{max}$ is the MPRR in $\left[\frac{k\,Pa}{ms}\right]$,
- P_{max} is the maximum mean in-cylinder pressure,
- T_{max} is the maximum mean in-cylinder temperature.

The coefficient β relates the amplitude of the pressure pulsation to the MPRR. Typically the amplitude of the pressure pulsation represents 5 % of the $MPRR$, thus β is set to 0.05 [27]. The maximal allowable value of the RI depends on the engine itself, its stiffness, speed and peak pressure [28]. According to *Eng et al.* [27] the upper ringing intensity limit varies from 2 $[MW/m^2]$ for an automotive size engine to 6 $[MW/m^2]$ for a larger diesel-based engine. It is reasonable for our small engine to consider an upper limit of 5 $[MW/m^2]$. Those values correspond roughly to a MPRR of 10 - 15 [bar/CAD].

In Figure 1.10, the in-cylinder pressure is represented for several ϕ while keeping a constant phasing. It can be seen that as the load increases, the pressure increases as well. For an equivalence ratio over 0.22, a higher frequency pressure wave starts to appear [28]. Note in Figure 1.10 that 0 CAD is equivalent to the intake TDC and thus 360 CAD is the compression TDC.

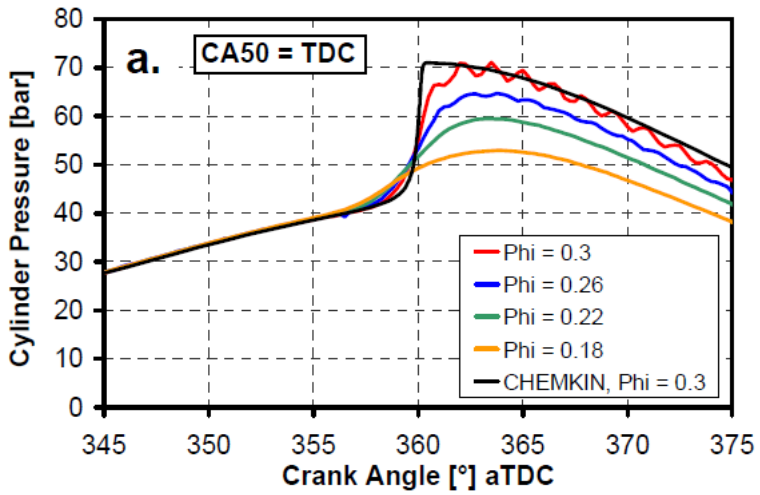

Figure 1.10: *In-cylinder pressure evolution. When the load is too high, ringing characterized by pressure oscillations starts to appear. (iso-octane, 980 cc)[28]*

Figure 1.11 summarizes the operating range of an HCCI engine. If T_{in} is high and λ is low, the mixture is very rich and very reactive, it will lead to ringing. If T_{in} is small and λ is high, the mixture is lean and not very reactive, this would lead to a misfire. Between those extremums there are intermediate cases. If T_{in} is high and λ is high, the IMEP will be small due to a small intake gas density. Finally, if T_{in} is low and λ is low, the mixture will be rich and dense at *Intake Valve Closing* (IVC) which will lead to an optimal operating condition. The optimal operating area is small, thus a slight change

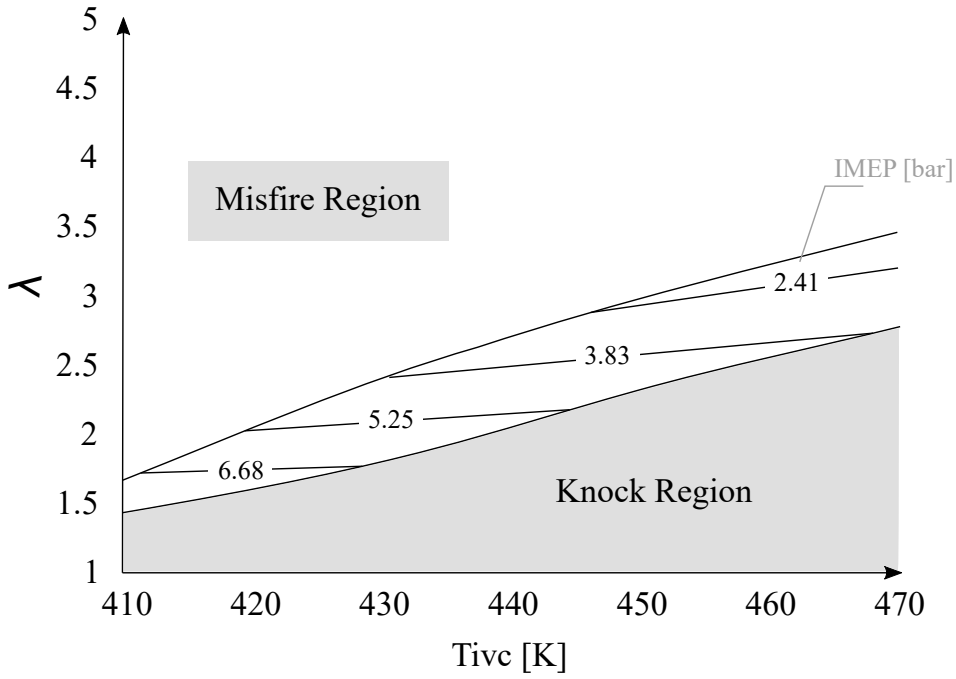

Figure 1.11: *Operating regions and IMEP in function of the load. The working region is small and has a high sensitivity on the load. (Natural gas, 507 cc) Adapted from [23]*

in T_{in} or charge composition will lead to ringing or misfire. The results for a low or high T_{in} and λ are gathered in Table 1.1.

		T_{in}	
		Low	High
λ	Low	High IMEP	Ringing
	High	Misfire	Low IMEP

Table 1.1: *Summary of the HCCI operating conditions.*

Decreasing the fueling rate to reduce the MPRR is not a valuable option. Although it will avoid ringing, it will also lead to a decrease in power density. In order to increase the power density while avoiding ringing, there are solutions in the literature. For example, a blend of fuel with different auto-ignition temperatures allows to extend the DOC and thus have a lower MPRR [1].

Another solution is to add EGR. Because it is adding gases with higher specific heats, the rate of temperature increase during the compression stroke is smaller which results in a lower MPRR. Finally, a lower MPRR can be achieved by charge or thermal stratification. Charge stratification consists in having a broad distribution of ϕ inside the cylinder. The ignition will thus happen sequentially.

1.3 Thermal stratification

The chemistry kinetics is strongly temperature dependent. As the temperature increases, the fuel will be faster oxidized, the intermediate species will be obtained faster as well as the final products. In order to increase the power density, and thus increase the fueling rate while staying under the ringing limit thermal stratification can be used.

1.3.1 Natural stratification

The underlying principle of thermal stratification is to create temperature inhomogeneities inside the cylinder. In this way, there will be hotter and colder mixture areas. The hotter areas will be prone to ignite earlier than the colder areas. The combustion will thus happen sequentially. This leads to a broader *Heat Release Rate* (HRR) and thus a lower MPRR which in the end reduces the ringing intensity.

Figure 1.12 shows an analysis of the *Pressure Rise Rate* (PRR) evolution according to an equivalence ratio sweep for a standard HCCI engine and a numerical simulation. In order to counteract the effects of combustion phasing when ϕ increases, the T_{in} has been decreased such that the phasing (CA50) takes place constantly at TDC. It can be seen that for the same load, the experimental PRR is always lower than the simulated one. *Dec et al.* [28] state that it is not possible to reach perfect homogeneity conditions inside the cylinder, both in terms of mixture and temperature. The difference between the two curves is therefore caused by the natural in-cylinder stratification. Their conclusion is that the thermal stratification reduces the PRR by broadening the HRR [22].

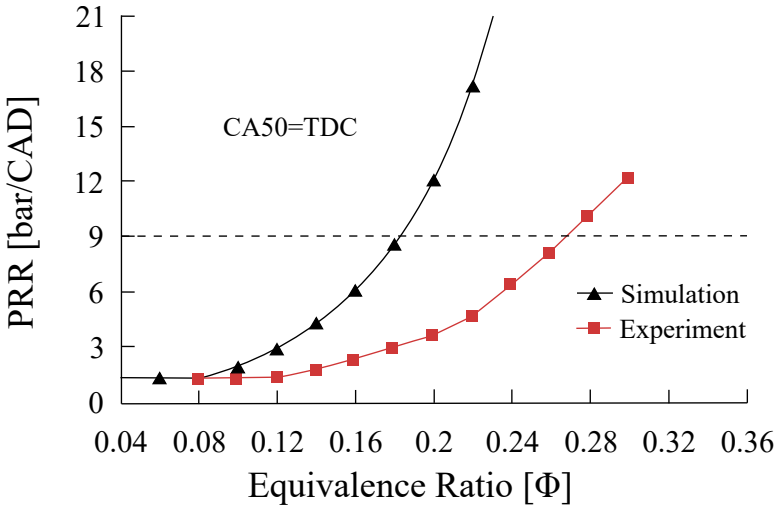

Figure 1.12: *PRR evolution as the load increases for an experimental and a simulation case. The temperature distribution is homogeneous in the simulation case and has a higher PRR. (iso-octane, 980 cc) Adapted from [28]*

With tools such as chemiluminescence imaging or single-line *Planar Laser-Induced Fluorescence* (PLIF) imaging (such as Figure 1.13), it is possible to observe thermal stratification with an optically accessible engine. Figure 1.13 shows the change of temperature relative to the mean temperature of each image (ΔT). The images are taken at the combustion chamber mid plane. Note that for Figure 1.13, 1.14 and 1.16

the 0 [CAD] is taken at the intake TDC, thus the compression TDC is occurring at 360 [CAD].

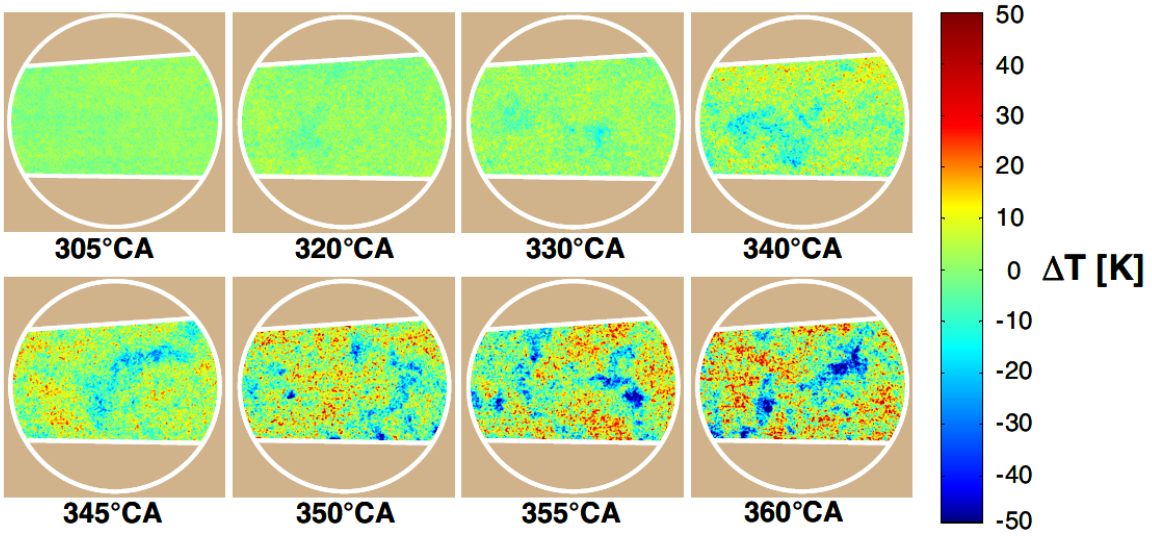

Figure 1.13: *Thermal stratification seen with PLIF imaging. (iso-octane, 980 cc)[29].*

During the earliest part of the compression stroke, the mixture temperature seems homogeneous. *Dec et al* [29]. justify this by stating that the mean gases temperature is not so high at that point and that it takes time for the cold near-wall gases to convect to the cylinder center. It is only in the late phase of the compression, the last 10 CAD, that a significant stratification is visible.

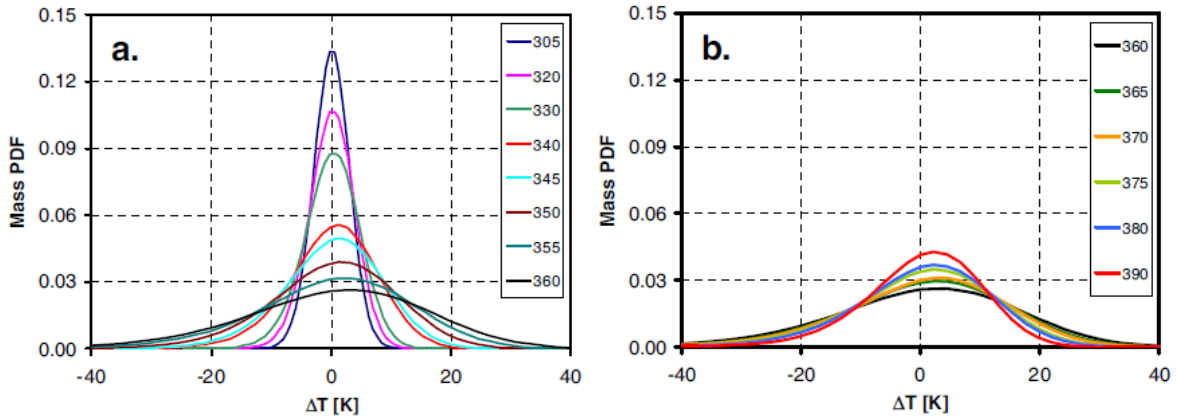

Figure 1.14: *Temperature distribution in mass PDF. As the cycle advances, the mixture temperature is less and less homogeneous (iso-octane, 980 cc)[29]*

The thermal stratification seen in Figure 1.13 can also be represented as ensemble-averaged, mass weighted over several cycles (40 cycles in this case). This representation, as in Figure 1.14, allows to have a clear vizualisation of the deviation of the temperature from the mean temperature in the cylinder. At 305 [CAD], the temperature distribution is very narrow, which means that the temperature is nearly homogeneous in the cylinder. As the piston is going up, the temperature *Probability Density Function* (PDF) gets

wider. At 305 [CAD] the temperature standard deviation is equal to 3.3 [K] and at 360 [CAD], it reaches a value up to 15.9[K]. Note that as the compression phase progresses, the maximal point of the curve is moving to the right. It can be said that it is becoming slightly skewed. At 305 [CAD], the skewing should be large, because the bulk hot gases core has not yet been affected by the near-wall cold gases. It is not seen in Figure 1.14 due to measurement noise induced by the PLIF imaging. At 360 [CAD], the skewing is more visible, this is due to two effects on the skewness. First, the measurement noise is still present but less noticeable due to the broader distribution. Secondly, the cold near-wall gases had time to penetrate into the adiabatic core.

1.3.2 Induced thermal stratification

In the literature, there are several ways to control the in-cylinder thermal stratification. Four of them will be presented here : *Water Direct Injection* (WDI), wall temperature control, hot EGR and actively controlled *Glow Plug* (GP). For all those technologies, the goal is always the same : extend the operating range in order to increase the power density. To do so, a thermal stratification is induced to decrease the RI and allows higher loads.

The principle of WDI is to directly inject water inside the cylinder. The latent heat of vaporization of the water spray cloud will affect the in-cylinder temperature. With this technique, *Collette and Gatin* [10] achieved a 215% increase of IMEP. They also noticed that as the amount of fuel increases, the amount of water injected has to increase drastically in order to reach an acceptable ringing intensity.

The effect of controlling the wall temperature to achieve stratification was studied by *Lawler et al.* [21]. Since the wall temperature is dependent of the coolant temperature, they decided to control it. The first conclusion that they reached is that changing only the wall temperature would lead to a combustion phasing due to heat transfer losses at the intake stroke. Thus, in order to compare the different cases they had to change the intake temperature to always keep the same CA50. In Figure 1.15, the first thing that can be noticed is the change in T_{int} for the sweep in coolant temperature. Then *Lawler et al.* [21] concluded that the thermal stratification is surprisingly negligible. The differences for the different cases are supposedly due to charge variations. Controlling the coolant temperature might not be an effective solution to achieve thermal stratification.

Adding hot EGR induces both thermal and charge stratification. First because there is still oxygen in the residual gases, the local equivalence ratio will be affected. Then because of its high temperature it will act on the mixture temperature.

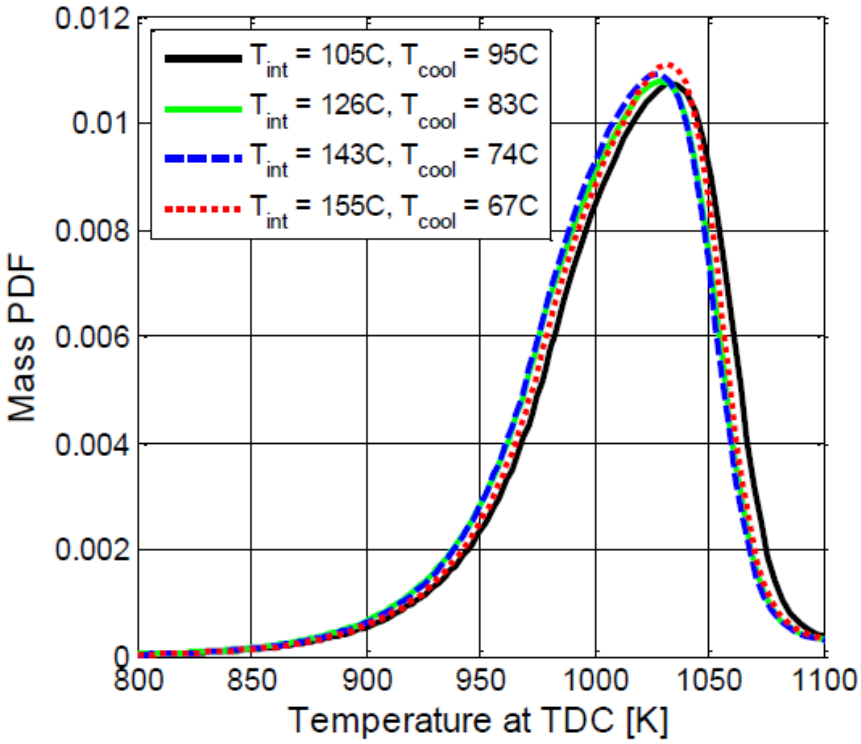

Figure 1.15: *Temperature distribution in PDF. The wall temperature affects greatly the intake temperature to keep the same phasing but not the temperature distribution (87 octane gasoline, 550 cc) [21].*

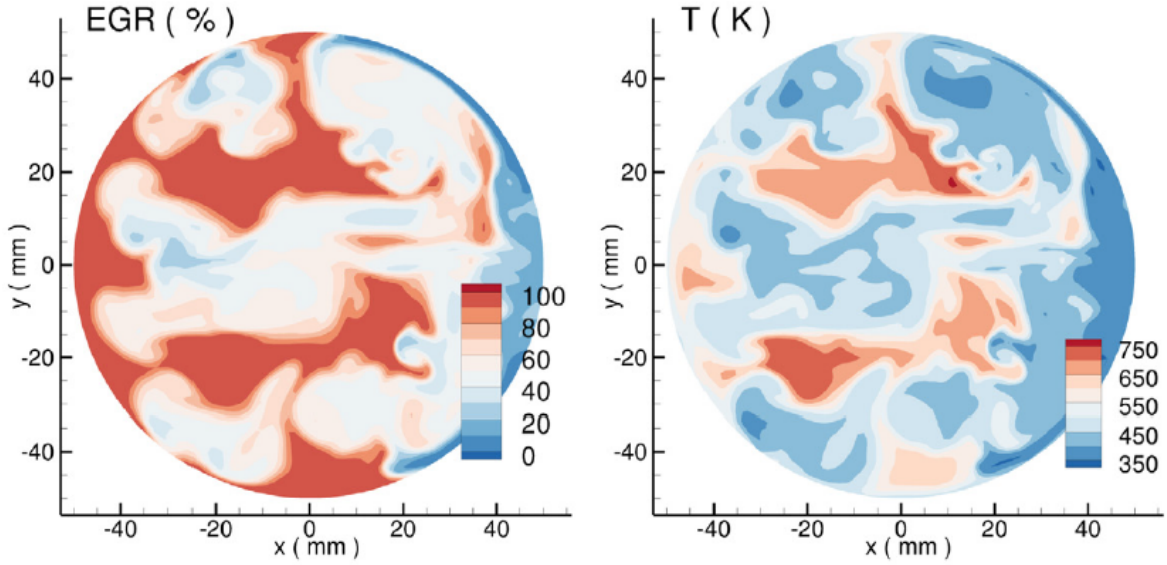

Figure 1.16: *In-cylinder EGR and temperature distribution. At -208 CAD, the EGR and temperature distribution are correlated. (EuroSuper 95, 650 cc) [30].*

The implementation of a GP and its effect on thermal stratification has been studied by *Lawler et al.* [4] and *Pourfallah et al.* [3]. The GP is a resistive element whose original purpose is to preheat the air during cold starts in diesel engines. In this case,

the GP is used as a continuous local heat source. The level of thermal stratification depends on the amount of power transmitted to the GP and therefore on its supply voltage.

Figure 1.17 represents the evolution of the net fuel conversion efficiency (η_{ind}) as a function of the combustion phasing following a temperature sweep or a GP voltage sweep depending on the case.

First, a T_{in} sweep is conducted on the case without GP, represented by the blue line. At late phasing, the low temperature leads to a poor fuel oxidation hence the low net conversion efficiency. As the temperature increases, the combustion efficiency increases and so does the net indicated efficiency. At one point, still increasing the temperature is detrimental for the efficiency since the combustion has reached an optimum but the heat transfer losses and the blow-by losses keep increasing. The resulting efficiency is therefore decreasing for early phasing.

Then, a GP voltage sweep is conducted on the case with GP, represented by the red dotted line. Since the GP brings heat in the cylinder, it is necessary to take a common reference point in order to compare data. By taking two cases with the same phasing, the only effects perceived are due to the addition of the GP. It can be seen that going from low GP voltage to higher ones, the fuel oxidation increases and thus the overall efficiency. This increase is explained by the fact that the GP induces a longer combustion that decreases the reached temperatures and pressures and thus decreases the heat transfer losses to the walls.

Finally, the solid red line is the efficiency when the electrical energy consumption of GP is taken into account, it can be seen that it is not negligible.

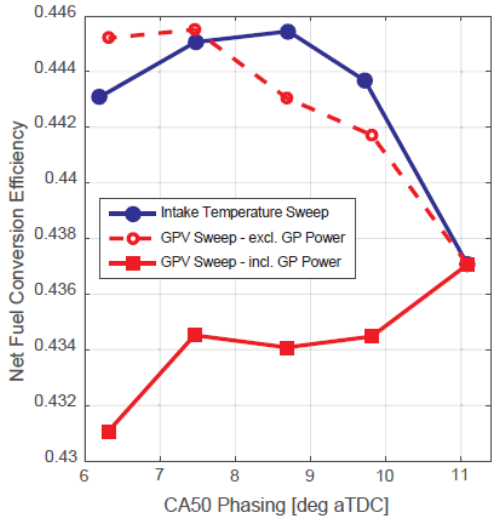

Figure 1.17: *Conversion efficiency for a T_{in} and a GP voltage sweep. As CA50 advances and η_{comb} increases, η_{ind} increases [4].*

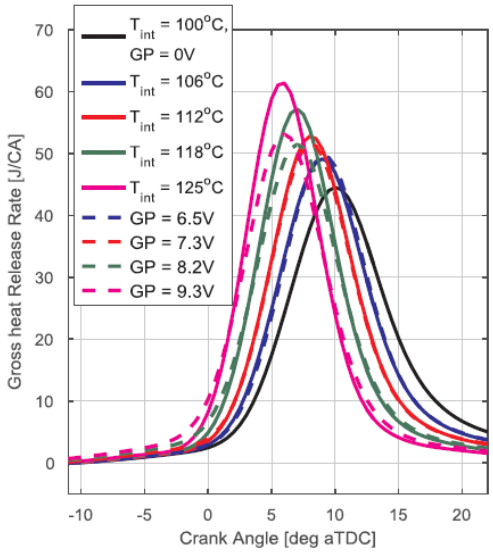

Figure 1.18: *T_{in} and GP voltage sweep. The GP broadens the HHR distribution. [4]*

In Figure 1.18, the solid lines correspond to a T_{in} sweep and the dashed lines to a GP voltage sweep. For low T_{in} and low GP voltage, the curves are very similar. As T_{in} and the GP voltage increase, the difference between the HRRs becomes more and more noticeable. At high GP voltage there is definitely a difference between bringing heat in the cylinder by increasing T_{in} and by using the GP. The combustion duration is longer for the GP case. *Lawler et al.* [4] states the hypothesis that the GP is inducing thermal stratification because the two methods achieve the same phasing but obtain different results.

Finally those results emphasize that a GP can control the phasing of a combustion in order to extend the engine's operating range and that it might induce thermal stratification.

1.4 Data post-process

In order to perform relevant analyses of the engine operation, data are collected via different sensors on the experimental bench. One of them gives the evolution of the pressure and, with the evolution of the volume, allows to calculate the quantity of heat released thanks to the HRR. This quantity is useful to determine the phasing of the combustion via the SOC and DOC. It is also useful to analyze the losses to determine the efficiency of the engine.

1.4.1 Cylinder volume

The volume in our post-processing routine is derived from the theoretical piston position (Figure 1.19). Using simple trigonometric relations, the equation (1.12) determines the piston height as a function of the crankshaft angle.

$$z(\theta) = R\left(1 - \cos(\theta) + \beta - \sqrt{\beta^2 - \sin(\theta)^2}\right) \tag{1.12}$$

Where $\beta = \frac{L}{R}$ is the conrod length over the crankshaft radius. In order to take dead volume of the cylinder into account, the compression ratio and the displacement are used to calculate the volume and its derivative in equations (1.13) and (1.14). τ is the compression ratio and V_d is the displacement.

$$V(\theta) = \frac{V_d}{\tau - 1} + \frac{V_d}{2}\left(\beta + 1 - \cos(\theta) - \sqrt{\beta^2 - \sin(\theta)^2}\right) \tag{1.13}$$

$$\frac{dV}{d\theta} = \frac{V_d \sin(\theta)}{2}\left(1 + \frac{\cos(\theta)}{\sqrt{\beta^2 - \sin(\theta)^2}}\right) \tag{1.14}$$

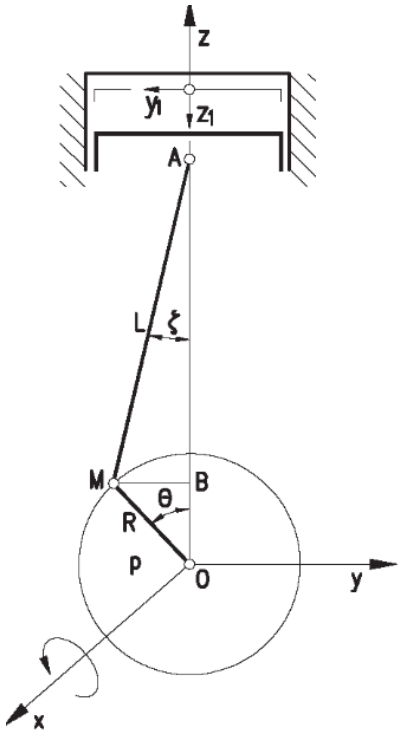

Figure 1.19: *Piston, connecting rod and crankshaft assembly [2].*

1.4.2 Heat release rate

The HRR can be computed from the mean in-cylinder pressure evolution. The first assumption that has to be made is to consider the cylinder as a closed system from IVC to *Exhaust Valve Opening* (EVO). The blow-by losses are neglected. Then the first law of thermodynamics for a closed system can be written as :

$$\Delta U = Q + W. \tag{1.15}$$

Where ΔU is the variation of internal energy, Q the heat energy and W the work received by the mixture. The first law can be differentiated with respect to the crank angle θ to obtain :

$$nc_v \frac{dT}{d\theta} = \frac{dQ}{d\theta} - p\frac{dV}{d\theta}. \tag{1.16}$$

Where c_v is the constant volume heat capacity. Then by assuming that the mixture follows the perfect gas relation and thus that $pV = nRT$ where R is the universal gas constant (R=8.314 J/K/Mol) and n is the number of moles which changes due to the combustion :

$$p\frac{dV}{d\theta} + V\frac{dp}{d\theta} = nR\frac{dT}{d\theta}. \tag{1.17}$$

Then with Equations 1.16 and 1.17, the *Apparent Heat Release Rate* (AHRR) or $\frac{dQ}{d\theta}$ can be obtained.

$$\frac{dQ}{d\theta} = p\frac{dV}{d\theta} + \frac{c_v}{R}\left(p\frac{dV}{d\theta} + V\frac{dp}{d\theta}\right) \tag{1.18}$$

And then :

$$\frac{dQ}{d\theta} = \left(1 + \frac{c_v}{R}\right)p\frac{dV}{d\theta} + \frac{c_v}{R}V\frac{dp}{d\theta} \tag{1.19}$$

With the ratio of specific heat $\gamma = \frac{c_p}{c_v}$ and Mayer's relation $R = c_p - c_v$:

$$\frac{dQ}{d\theta} = \frac{\gamma}{\gamma - 1} p \frac{dV}{d\theta} + \frac{1}{\gamma - 1} V \frac{dp}{d\theta}. \tag{1.20}$$

Q is the total heat exchange between the charge and its environment, it is referred as Q_{net}. It is composed of the heat released during the combustion (Q_{gross}) and the wall heat losses (Q_{loss}).

$$Q_{net} = Q_{gross} - Q_{loss} \tag{1.21}$$

Finally, the HRR, also called RoHR, can be obtained from the AHRR.

$$\frac{dQ_{gross}}{d\theta} = \frac{\gamma}{\gamma - 1} p \frac{dV}{d\theta} + \frac{1}{\gamma - 1} V \frac{dp}{d\theta} + \frac{dQ_{loss}}{d\theta} \tag{1.22}$$

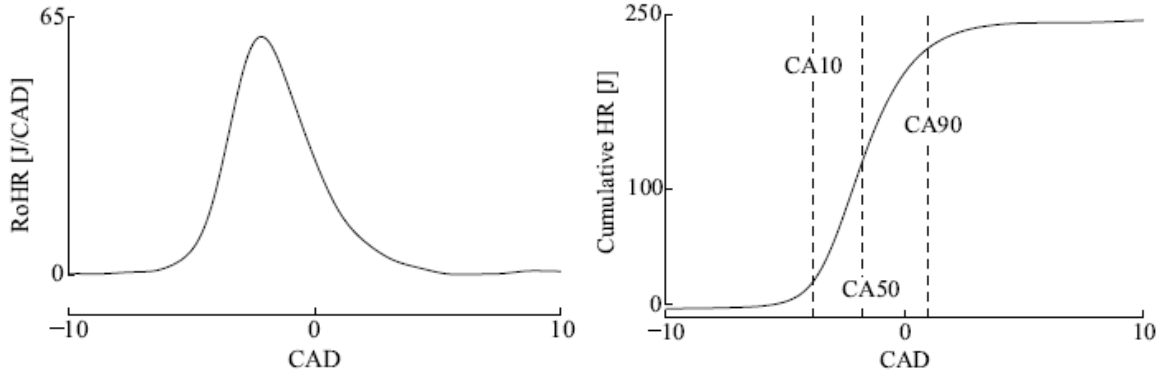

(a) *Heat release rate* ***(b)*** *Cumulative heat release*

Figure 1.20: *A typical HRR and its cumulative. From the cumulative, indicators such as CA10, CA50, CA90 and DOC are defined. [31]*

In Figure 1.20a, a typical representation of the HRR is shown. The HRR is the amount of instantaneous heat released by the combustion reactions. In the Figure 1.20b, the *Cumulative Heat Release* (CHR) is presented. This curve gives a clear view of the heat released at a certain CAD with respect to the total heat that will be released. The parameters CA10, CA50 and CA90 correspond to the crank angles where respectively 10%, 50% and 90% of the fuel has been burnt. The value of CA50 is also a representation of the combustion phasing. The combustion duration CA_{10-90} or DOC is the difference between CA10 which is considered the SOC and CA90 which is considered the end of the combustion.

1.4.3 Losses

As mentioned in the previous subsection, the term Q_{loss} represents the amount of wall heat losses. This term is significant and measuring it experimentally is not an option since mounting a heat flux sensor would require a lot of maintenance and fine-tuning [31].
The choice has been made to model the losses term with Newton's convective law

$$\frac{dQ_{loss}}{dt} = hA(T - T_{wall}) \qquad [W]. \tag{1.23}$$

Where,

- A is the total mixture-wall contact surface [m^2],
- h is the convection coefficient [W/m^2/K],
- T is the mean bulk gas temperature [K],
- T_{wall} is the wall temperature [K].

This choice is motivated by the fact that in HCCI engines, the forced convection from the bulk gases to the combustion chamber walls is the dominant mechanism of heat transfer [32]. This equation can be rewritten as the Equation (1.24) to be expressed in terms of CAD variation.

$$\frac{dQ_{loss}}{d\theta} = hA(T - T_{wall})\frac{1}{\omega} \qquad \left[\frac{J}{CAD}\right] \tag{1.24}$$

Where ω is the engine rotating speed [rpm].
The correlations for the instantaneous heat transfer coefficient ($h(\theta)$) that are the most used are the ones from *Woshni* [33], *Annand* [34] and *Hohenberg* [35]. They were initially designed for CI or SI engine. *Soyhan et al* [32] showed that the Hohenberg correlation might be the most suited for HCCI engines and the easiest to use. The Hohenberg correlation is given in the Equation 1.25.

$$h_{Hohenberg} = \alpha_{scaling} V^{-0.06} p^{0.8} T^{-0.4} (\bar{v}_p + C_1)^{0.8} \qquad \left[\frac{W}{m^2 K}\right] \tag{1.25}$$

Where,

- V is the cylinder volume [m^3],
- p the mean pressure [bar],
- T the mean gas temperature [K]
- $\bar{v}_p$ the mean piston speed [m/s],
- $\alpha_{scaling}$ and C_1 are constants.

Hohenberg determined the coefficient C_1 to be equal to 1.4. The $\alpha_{scaling}$ coefficient depends on the combustion chamber shape, the intake swirl and thus the engine itself. For his study, *Hohenberg* determined $\alpha_{scaling}$ to be equal to 130 [35]. *Bhaduri* used the original Hohenberg scaling factor for the UCLouvain HCCI engine.
Since the scaling factor depends on the operating conditions is usually determined from the Q_{net} trace.

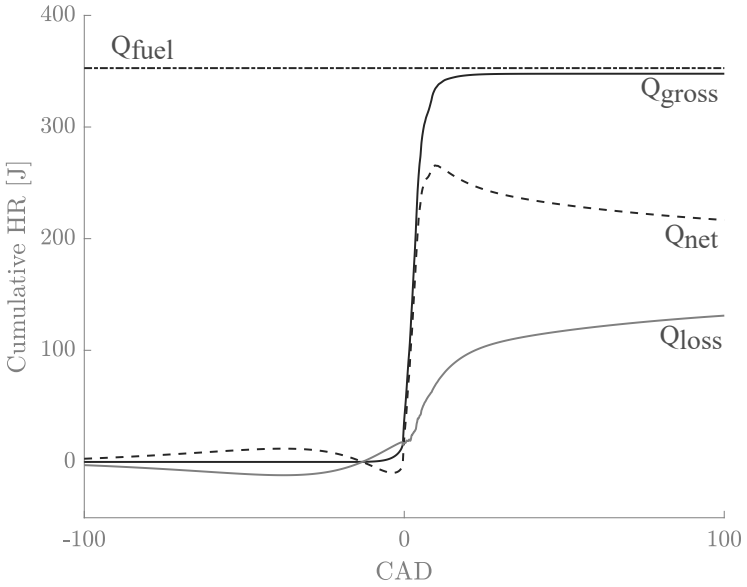

Figure 1.21: *Cumulative heat release with its different contributions. From the initial energy contained in the fuel (Q_{fuel}) only a part is released (Q_{gross}). Then some of this energy is lost through the walls (Q_{loss}). The remaining energy is called Q_{net}. Obtained from our simulation model.*

Figure 1.21 shows the contribution of the terms in Equation (1.21). The Q_{gross} term only takes the heat released during the combustion into account. Since the combustion ends around 0 CAD in Figure 1.20a, it is expected that its value remains constant until the end of the cycle. The Q_{net}, on the other hand, takes the losses into account and is the value computed from the pressure. The Q_{loss} term should thus be adequately tuned through the $\alpha_{scaling}$ factor in order to observe the flatness of Q_{gross} before and after the combustion. The figure also shows the fuel energy contained in a cycle (Q_{fuel}).

Chapter 2

Experimental setup

2.1 Test bench specifications

The test bench was designed in order to perform tests on the combustion in HCCI engines. The bench was used by *Bhaduri* [31] for his research with syngas. Then *Pochet* [1] studied the effects of electrofuels blends with it. It is also worth mentioning that WDI was performed by *Collette and Gatin* [10] and that the possibility of oxy-fuel combustion was introduced by *Hosselet and Van de Putte* [9].
The bench itself is located in the *LEFT* laboratory at the UCLouvain (see Figure 2.1).

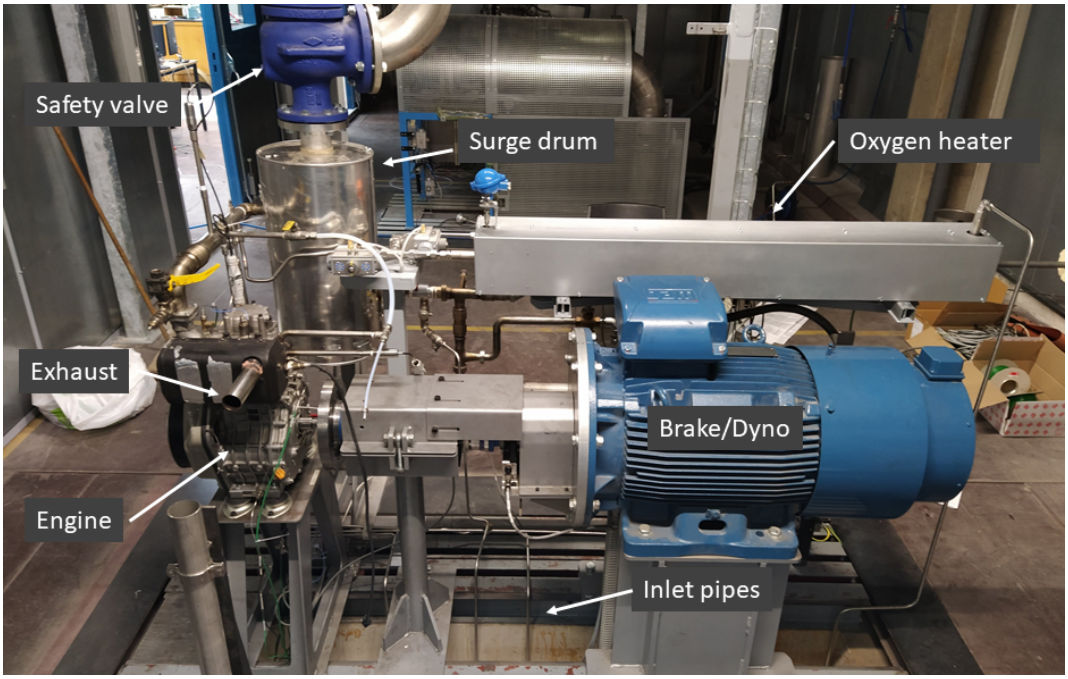

Figure 2.1: *UCLouvain HCCI experimental bench. Note that the installation is not yet finished [9]*

2.1.1 Test bench components

The experimental bench can be divided in four parts : the intake, the exhaust, the engine itself and the brake/dyno. A scheme of the bench setup is shown in Figure 2.2 and its P&ID is available in Appendix A.1. The test bench components are presented successively :

- The fresh gases coming from the gas bottles passes through the *Mass Flow Controllers* (MFC) located in the basement.
- The gases pass through a 2 kW electric heater before flowing into a surge drum that will make the mix fully homogeneous. This description is simplified, for instance there is a bypass to mix the fuel and the oxidizer after the surge drum in order to obtain an inhomogeneous mixture for studies on that particular subject.
- The mixture pressure and temperature is checked with sensors.
- The exhaust will be collected thanks to a flexible hose under the engine. The exhaust gases from the three benches in the casemate will be sent in an unique pipe to the outside.
- Finally, the engine is coupled with a 55kW three-phase induction motor (WEG W22 IE2). As soon as the engine starts, the motor turns into generator mode and induces a braking torque to the engine. A frequency inverter (Mitsubishi FR-1741-55k) controls the electric motor/generator by controlling its rotational speed and delivering the generated power to the grid. The choice has been previously made to set a speed of 1500 [rpm].

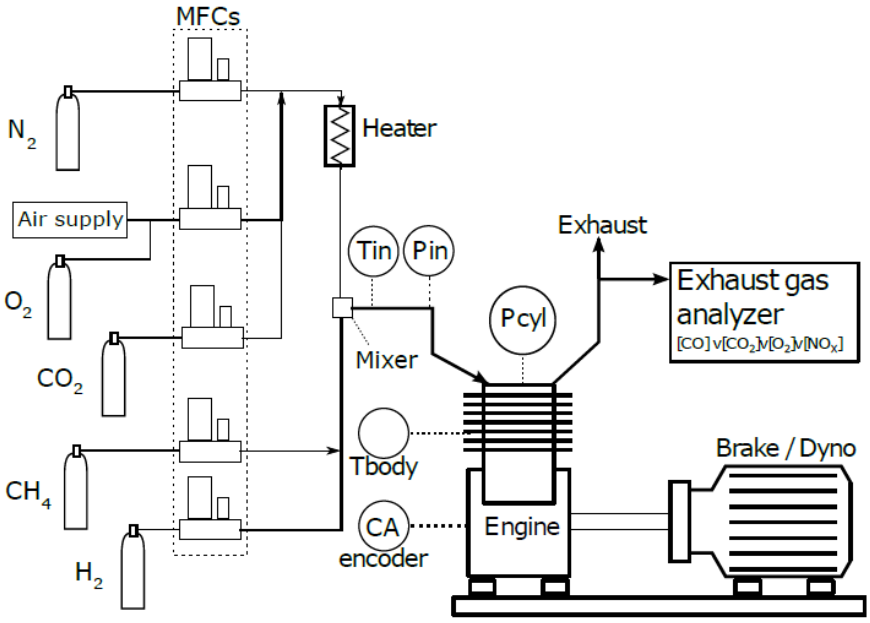

Figure 2.2: *Schematic representation of the UCLouvain HCCI test bench*

In 2019, the IMMC laboratory has built a "casemate", which is a protective room that isolates three benches including the HCCI from the rest of the laboratory hall. The goal

of this ventilated casemate is to protect the users of the laboratory from toxic gases, noise pollution, the risk of mechanical parts breakage and explosions.

2.1.2 Engine specifications

The engine is a modified Yanmar L100V (Figure 2.3). This one was originally an industrial 4-stroke diesel engine. It was selected because it is a mono-cylinder air-cooled engine, which makes it simpler to modify. Also being an industrial engine it has a more rigid construction, which is ideal for high compression applications. The piston head shape was changed from a deep bowl to a low turbulence shallow bowl shape. Then *Pochet* [1], modified it to reach a geometric CR of 23:1. This CR is the maximal attainable with this engine since the piston head is now flat and the minimal clearance to allow valve lift (3.2 [mm]) is now almost reached. For our experiments, since methane needs a high CR, it will not be changed on the engine.
The engine specifications are available in Table 2.1.

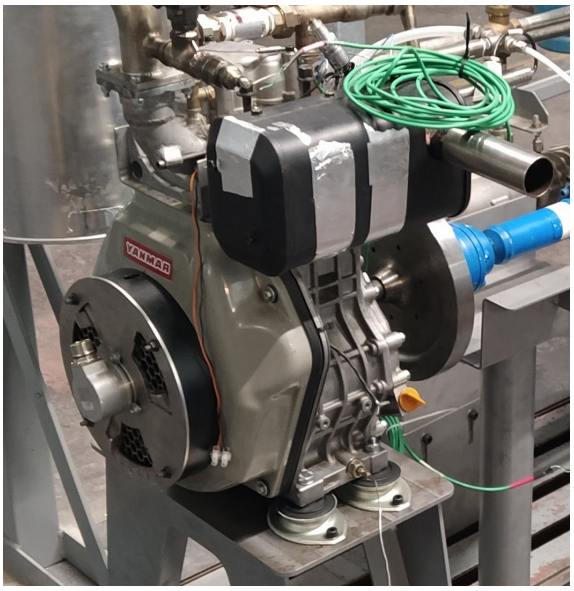

Figure 2.3: *Modified Yanmar L100V*

Table 2.1: *UCLouvain HCCI research engine specifications*

Engine type	Air-cooled 4 stroke Mono-cylinder	
Geometric compression ratio (τ)	23.0 : 1	
Effective compression ratio (τ_{eff})	21.65 : 1	
Displacement volume (V_d)	436	[cm^3]
Clearance	3.5	[mm]
Cylinder bore (B)	86	[mm]
Piston stroke (S)	75	[mm]
Crank radius (R)	37.5	[mm]
Connecting rod length (L)	120.5	[mm]
Intake valve closure (IVC)	-127	[CAD]
Exhaust valve opening (EVO)	127	[CAD]
Rotation speed (ω)	1500	[rpm]

2.2 Glow plug

A glow plug is a heating element used to preheat the air for cold start in diesel engine. For our study it will be used as a hot spot in the cylinder to achieve thermal stratification. In order to see the time needed to warm up the glow plug and the range of temperature attainable, experiments were conducted on a GP.

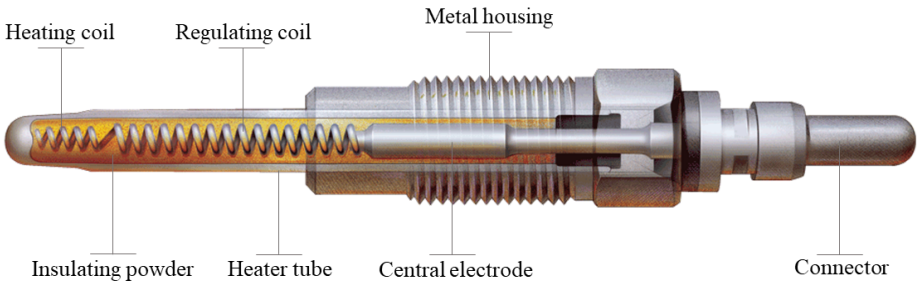

Figure 2.4: *Glow plug see through view [36]*

In the Figure 2.4, the anatomy of a sheathed GP can be seen. First there is the metal housing which is used to hold the GP in the cylinder head. Then there is the heater tube which is the part in contact with the in-cylinder gases. It is usually made of Inconel 310/310S stainless steel for its high resistance to oxidation at very high temperatures (1300 [°C]).
Inside the heater tube there is a powder and two coils connected to each other. The heating coil is usually made of Kanthal D which is an iron-chrome-aluminum alloy, known for its high resistivity and good oxidation resistance. This is the coil that would create the largest amount of heat. The regulating coil is usually made of Vacon CF8. This alloy is used for its specific properties : as the temperature increases its resistance increases sharply. Its purpose is to protect the GP from overheating. The Kanthal resistance does not change significantly while the Vacon resistance will increase linearly with the temperature [37]. Then a powder of magnesium oxide is used as an electrical insulator and for its resistance to high temperatures.
To supply the GP, a voltage needs to be applied between the metal housing and the connector.

2.2.1 Characterization

The experimental setup is presented in Figure 2.5. To characterize it, a 12 V variable DC voltage source was used to supply the GP. A thermocouple was then placed on the tip of the GP.

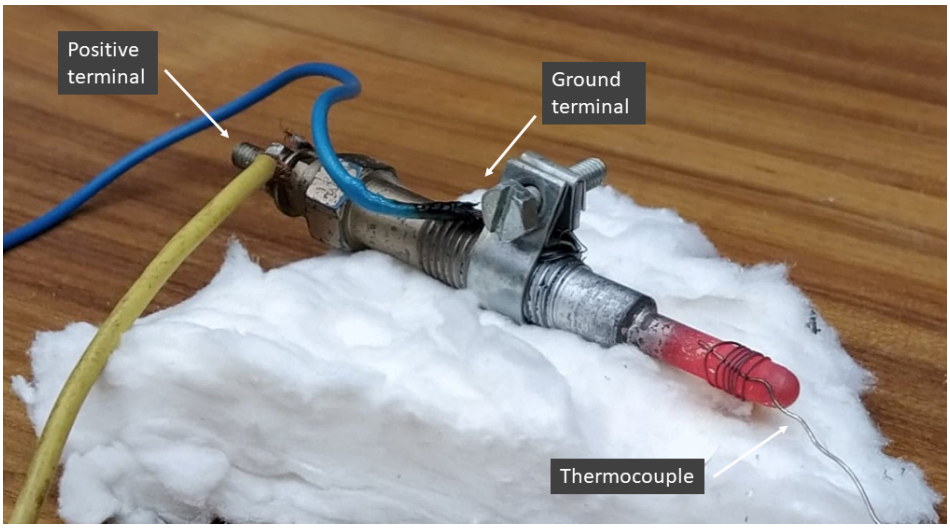

Figure 2.5: *Experimental setup of the GP characterization*

Voltage, current and temperature relations

In order to determine the temperature reached by the GP during its operation, the relationships between current, voltage and temperature must be known.

When the voltage increases, the current passing through the GP also increases. The evolution, visible in figure 2.6, is the characteristic of a non-ohmic element. Thanks to the Joule effect, the current in the heating coil will generate an increase in temperature which is dependant of its resistance. The relationship between the temperature and the resistance of the GP is described in Equation (2.1).

$$R_{wire} = R_0(1 + \alpha(T - T_0)) \tag{2.1}$$

Where,

- $R_0 = 0.6$ [Ω] is the resistance at room temperature,
- T_0 is the room temperature,
- T is the GP temperature,
- α is the temperature coefficient.

According to *Abate* [38] and *Endiz et al.* [37] the GP resistance is directly proportional to the temperature. This effect is confirmed by the data obtained during the characterization shown in Figure 2.7. It represents the GP resistance as a function of its temperature. From this relation it is straightforward to predict the GP temperature in the engine only by measuring its resistance.

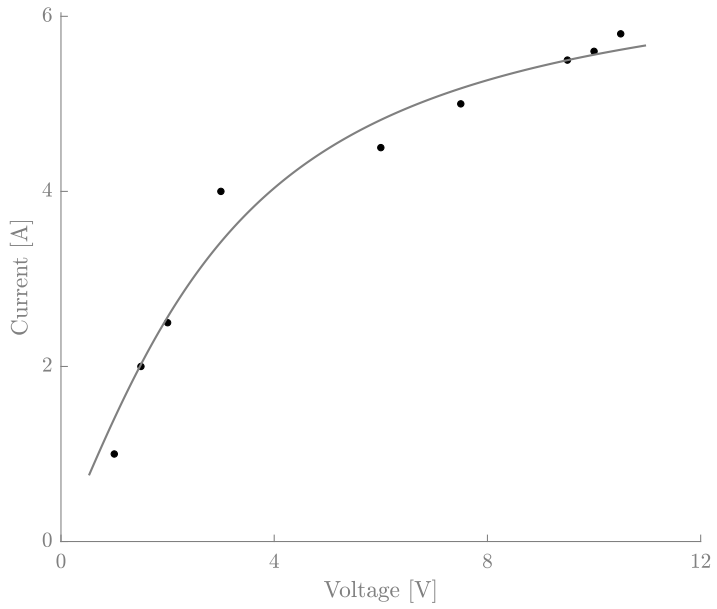

Figure 2.6: *Voltage-Current curve of the GP. This trace is characteristic of non-ohmic elements.*

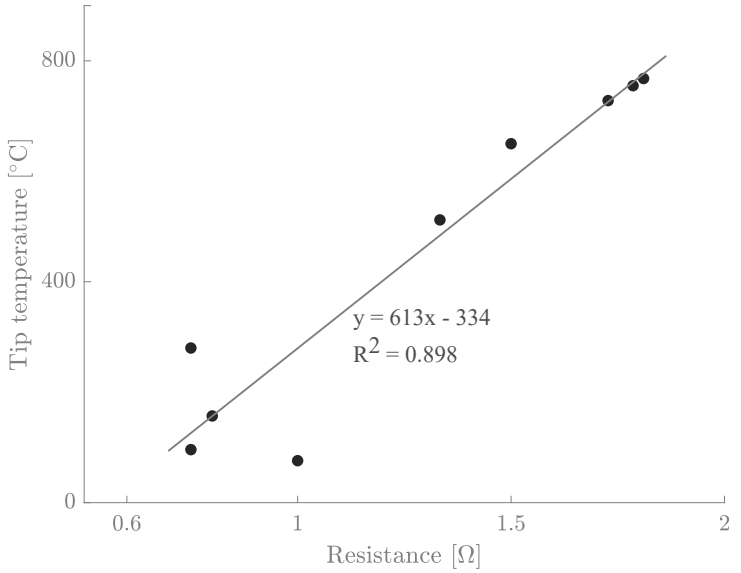

Figure 2.7: *GP resistance in function of its tip temperature. The relation between temperature and resistance is linear. As the temperature increases the GP resistance increases as well.*

As previously mentioned, the GP temperature increases with the GP voltage. However, the temperature is not a good indicator of the power flowing through the GP. The GP temperature depends a lot on its environment. For the characterization experiments the GP was surrounded by air, at room temperature with a low amount of wind. In the engine, the GP will face high temperatures with turbulences and a myriad of gases. Furthermore the environment will continuously change during the engine strokes.

From the Figure 2.6, the maximal power can be computed, it is equal to 60.9 [W]. This power can be normalized by the engine size and be expressed in MEP. A new quantity can be defined: the *Glow Plug Mean Effective Pressure* (GPMEP) (Equation 2.2). The *Glow Plug Power* (P_{GP}) consumption represents around 3 % of the engine power.

$$GPMEP = \frac{120 P_{GP}}{\omega V_d} = 0.112[bar] \tag{2.2}$$

In order to analyze the thermal distribution along the GP, a thermographic camera was used. It is important to mention that the goal was not to obtain absolute values but a representation of the thermal distribution. In Figure 2.8, it can be observed that the heat is dissipated along the whole length of the GP tip. However, from this image it is difficult to predict the amount of heat that will be dissipated in the cylinder head.

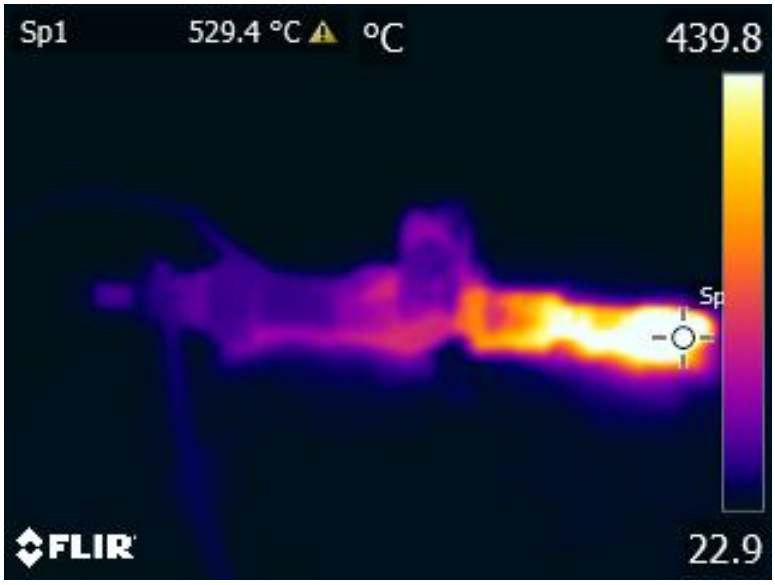

Figure 2.8: *Thermal image of a GP*

Transient analysis

Since the GP has a significant heat capacitance, it can be seen in Figure 2.9 that it takes around 10 seconds for a 50°C temperature increase. Since the GP is an old model, those results are not surprising. Also because the voltage source power was limited, the highest temperature reached is not as high as the one expected once inside the cylinder. In a typical diesel engine, the GP reaches very high temperatures (around 1000 °C) for only a few seconds. The goal of this experiment was to prove that a lower temperature can be obtained for a longer period of time without damaging the GP. In Figure 2.10, it can be seen that even for the latest GP model, a certain time is needed to reach its working temperature. Turning on the GP only for a part of a stroke is excluded. If the engine is running at 1500 [rpm], a full cycle takes 0.08 seconds and the GP would not even have the time to turn on. This is the reason why in our study the GP will be powered continuously. It can be expected that a continuous GP operation will reduce the GP lifetime.

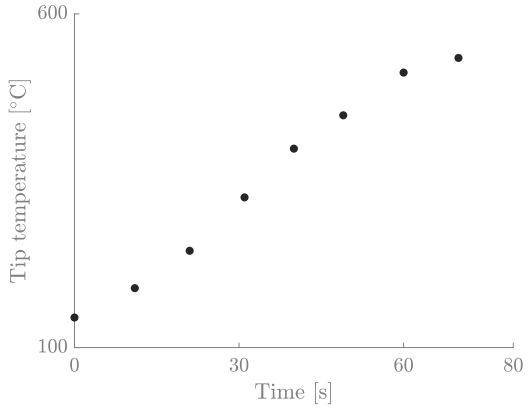

Figure 2.9: *GP tip temperature evolution over time. The time response of the GP is slow compared to an engine cycle.*

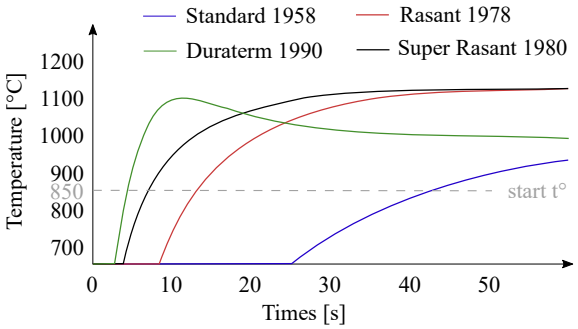

Figure 2.10: *GP temperature over time for several GP models. Adapted from [39]*

2.2.2 Mounting on the engine

The engine was originally a diesel engine. The injector was removed to install a spark plug and then a water injector to perform *Collette and Gatin* [10] experiments. The threaded hole in which they were could be used to fit an adapter that will hold the GP.

Regarding the penetration of the GP in the cylinder, there are different options.

- The first one, allowing the most heat transfer, is to make the GP go deep into the cylinder. Given the low clearance of 3.5 [mm] at the TDC, it will be necessary to modify the piston head. Since the engine is required for other experiments, the piston head will not be modified.
- The second option is to make the GP shorter than the clearance but create a cavity in the cylinder head to increase the exposed surface as in Figure 2.11. This is the choice made by *Lawler et al.* [4] and seems to be the best trade-off between the deepness and the heat transferred.
- The last and simplest option is to flush mount the GP such that the tip does not protrude beyond the clearance. However, the amount of heat transmitted is severely limited since only the very far tip of the GP is exposed.

It is also important to mention the effect of the swirl on the GP. If it is set in the middle of the cylinder, its effect will be less than if it is placed off-center. Indeed, the gas velocities increase along with the distance from the center which will increase the convection effect.

2.3 Safety aspects

Since the installation of the casemate the HCCI bench was dismantled. Due to some modifications on the design to allow oxy-fuel combustion, a new safety validation had to be made. Three documents were necessary to allow the bench to be operational.
First the DRPE (*Document Relatif à la Protection contre les Explosions*, in English :

Figure 2.11: *Possible configuration of the GP mounting in the cylinder head.*

document concerning the protection against explosions), then a risk analysis and finally the "canevas de sécurisation" (caneva of securisation in English).
If the risk analysis reveals that some aspect of the bench is dangerous, measures have to be taken in order to prevent incidents.

2.3.1 Safety documents

The purpose of the DRPE is to point out every possible source of gas leakage and ignition to prevent them. Risky zones are defined and in those zones only ATEX certified equipment can be used. Three zones were detected : the gas bottles heads, the NG arrival and the outlet of the safety valve pipe (see Appendix A.2). Then a study on the casemate ventilation was made. One of the goals of the ventilation is to prevent the creation of an explosive atmosphere in the case of a leakage. To assess that ventilation is sufficient, the fuel dilution was calculated based on the fuel and air mass flows if a line happens to break entirely. With those data the minimal ventilation air flow was computed.

2.3.2 Safety precautions

For some experiments the wall temperature has to be a parameter on the HCCI bench. For water-cooled engines, changing the coolant temperature is sufficient to tune the wall temperature. For air-cooled engines such as the Yanmar L100V, a system that restricted the airflow around the engine was mounted as it can be seen in Figure 2.12. In the past, during the warming up of the engine this flap was closed, then when it reached the right wall temperature it had to be manually opened. Since the variation of the wall temperature is a slow process, the flap had to be moved several times before reaching the desired wall temperature in steady state.
Now the casemate prevents having an easy access to the engine for safety reasons. It is thus inconceivable to get in and out of the casemate every time this flap has to be moved. This is the reason why an automated intake flap was needed.

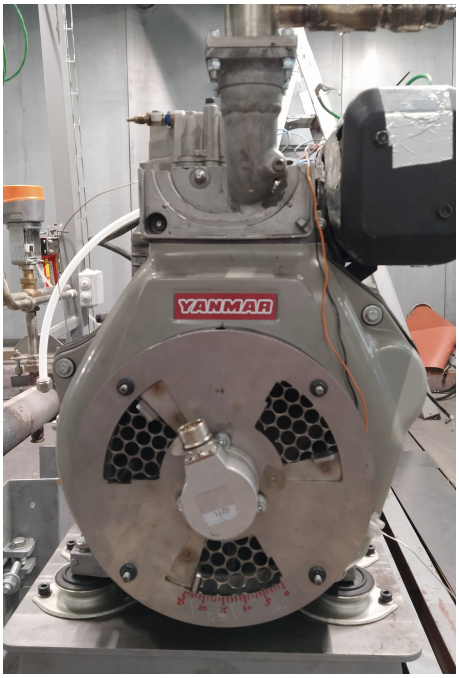

Figure 2.12: *Cooling intake mechanism*

The best solution found for this problem is to use an electrical linear actuator (Figure 2.13). Indeed, this one offers an ease of control because it can be controlled via an analog signal of 0-10V and an ease of assembly because it requires only few adaptations compared to what already exists.

The specifications of this actuator are gathered in Table 2.2.

Table 2.2: *Actuator required specifications*

Travel distance	85 [mm]
Tensile/Compressive force	25-30 [N]
Supply voltage	24 [V]
Command voltage	0-10 [V]

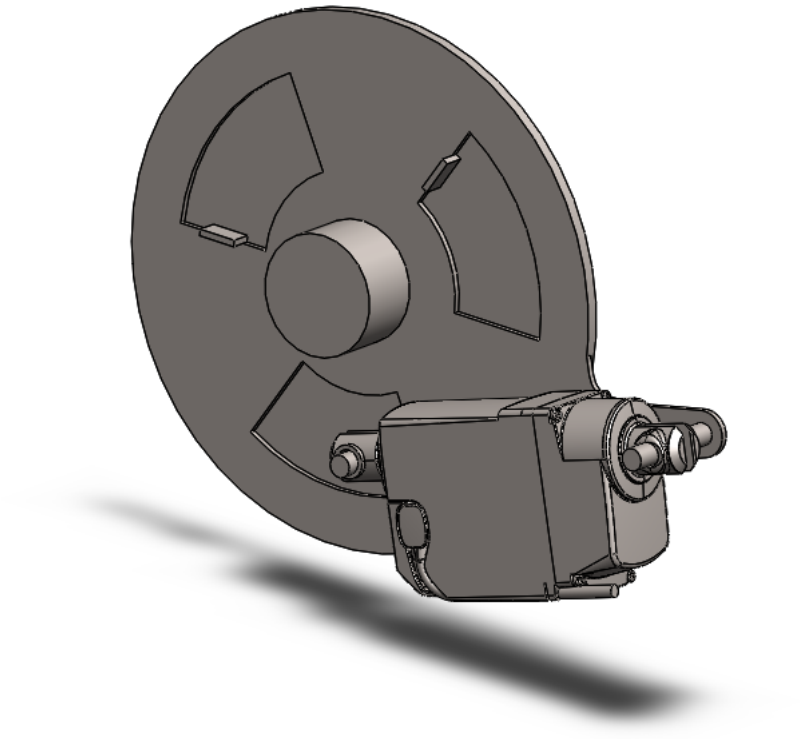

Figure 2.13: *Solution proposal for the cooling intake flap automation. The actuator model comes from [40].*

Chapter 3

Simulation

The final goal of this thesis is to show that a GP would increase the power density of an HCCI engine. Since mounting a GP would affect several parameters on the combustion, performing a simulation beforehand was necessary. Indeed the intake temperature and the equivalence ratio have to be adjusted because the GP will bring heat and change the mixture reactivity. The amount of energy brought by the GP has to be defined. Furthermore since the UCLouvain HCCI engine is not optically accessible, a simulation would allow to have a clear and visual representation of the in-cylinder thermal stratification. Finally, the HCCI model would allow to predict the amount of pollutant emissions in the exhaust.
First, the simulation setup is presented. Secondly, this simulation will be compared with an experimental study to validate the order of magnitude of the results. Finally, the numerical results will be presented.

3.1 Setup

3.1.1 OpenFOAM generalities

OpenFOAM

The simulation tool used for our HCCI combustion simulation is OpenFOAM (Open-source Field Operation And Manipulation). It is an open-source *Computational Fluid Dynamics* (CFD) numerical simulation software. The versions used are OpenFOAM-7 and OpenFOAM-dev. It is a C++ object-oriented library. It is able to solve complex problems such as complex fluid flows involving chemical reactions, heat transfer, solid mechanics, electromagnetics, etc. [41].
OpenFOAM comes with a myriad of tutorials that allow the user to familiarize with the solvers, the pre- and post-processing utilities. The first model of the UCLouvain HCCI engine was developed by *Hosselet and Van de Putte* [9] based on the *freePiston* tutorial. Our model is based on the one they used for oxy-combustion.

OpenFOAM structure

The structure of OpenFOAM is composed of the solving processes and of the pre- and post-processing environments. First the pre-processing allows for instance to set initial

fields. The post-processing environment allows for example to use the *ParaView* tool. It allows to visually analyze the simulation results and retrieve various data.

The structure of an OpenFOAM case is composed of three directories : *system*, *constant* and *time directories*.

First the *system* directory contains all the settings associated with the solution procedure. It is composed of three sub files.

- *controlDict* sets the start and ending time of the simulation. It also defines the solver, time precision, the time step, etc. This file allows as well to call post-processing functions that allow to compute data from the fields that were computed during the simulation. For instance *Qdot* and *dpdt* compute respectively the heat release rate and the pressure derivative.
- *fvSchemes* contains the numerical schemes. For instance derivatives in the equations that are solved during the simulation.
- *fvSolutions* contains the equation solvers and their tolerances.

There are also other files such as *topoSet*, *createPatch* and *extrudeMesh* containing parameters to modify the mesh, create faces, etc. For instance, the *blockMeshDict* defines the main nodes of the geometry.

The *constant* directory contains the description of the mesh in the *polyMesh* sub-directory which is generated by the *blockMesh* utility. This directory contains also physical and chemical properties of the fluids such as their turbulence properties or their chemical reaction. For the specific case of engine simulation, this folder contains the *engineGeometry* file. It specifies the conrod length, the stroke, the engine speed, etc. Then a motion solver determines the motion of the piston based on those parameters. It can also be used to define swirl in the cylinder with the *engineSwirl* utility.

Finally, the other directories are *time directories*. Before launching the simulation, the *case* should contain at least the initial time directory. In this file, the initial and boundary conditions are defined for every field. The fields defined for our specific case are the pressure p [Pa], the temperature T [K], the flow speed U [m/s]. There are also the fields required by the turbulent solver : the turbulent kinetic energy κ $[m^2/s^2]$, the dissipation rate ϵ $[m^2/s^3]$, the thermal diffusivity α_t [kg/m/s] and the turbulent viscosity ν_t $[m^2/\text{s}]$. There is a field for each species concentration and a file *Ydefault* used for unspecified species. During the simulation, files are created every time step. For the particular case of engine simulation, the *time directories* are expressed in CAD.

3.1.2 Case setup

Axi-symmetric geometry

The simulation covers the compression and expansion phase of the engine cycle. As the piston is going up, the mesh is moving and the aspect ratio of the cells is continuously changing. To save computational time, the mesh is axisymmetric. *OpenFOAM* allows that kind of simulation by defining a *wedge* boundary condition. The mesh is one cell thick and one face maps to the opposite face of the same cell. This *wedge* geometry, that

will be called a "slice" to avoid any confusion with the name of the faces, can be seen in Figure 3.1. The slice faces are called patches which is a general name for boundaries. There are several types of patches for axisymmetric meshes such as *wedges*, *wall* and *empty*.
First, the *Front* and the *Back* are called wedges. Then the *CylinderHead*, the *Piston* and the *Liner* are walls. Finally, the *Axis* is of an empty patch type since it is a one dimension patch. The slice is a 2 degree portion of the entire cylinder.

The mesh used in this axisymmetric simulation is presented in Figure 3.2. A mesh with 50 cells between the axis and the liner and with 20 cells between the piston and the cylinder head has been chosen. It is a good trade-off between accuracy and computational time.
The aspect ratio of a mesh can be defined as the ratio of the longest length of the cell over the shortest one. It is used to quantify the quality of the mesh. If the cell has ideal proportion, the aspect ratio would be equal to one. At BDC the cells in the mesh presented in Figure 3.2 present an aspect ratio of 3. And at TDC the aspect ratio is equal to 7.5. This is a good trade-off since satisfying results can then be obtained without a remesh.

The solver used for this engine simulation is called *engineFoam*. It is a transient solver for compressible, turbulent engine flows with a spray particle cloud [41].

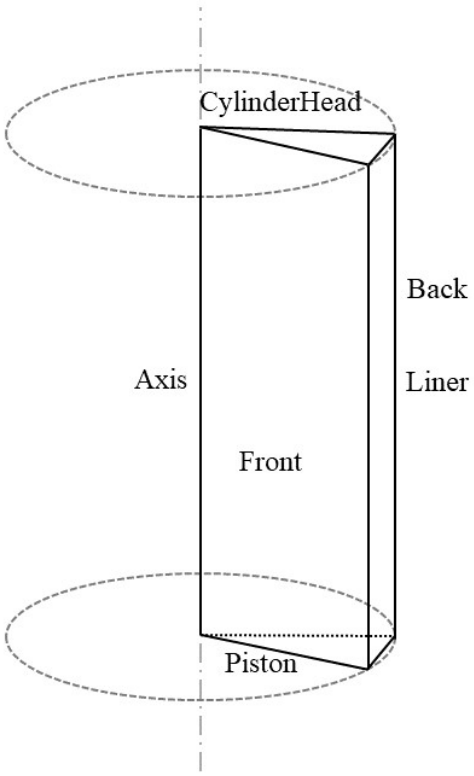

Figure 3.1: *Axisymmetric geometry. Only a slice of the cylinder is modeled to save computational time.*

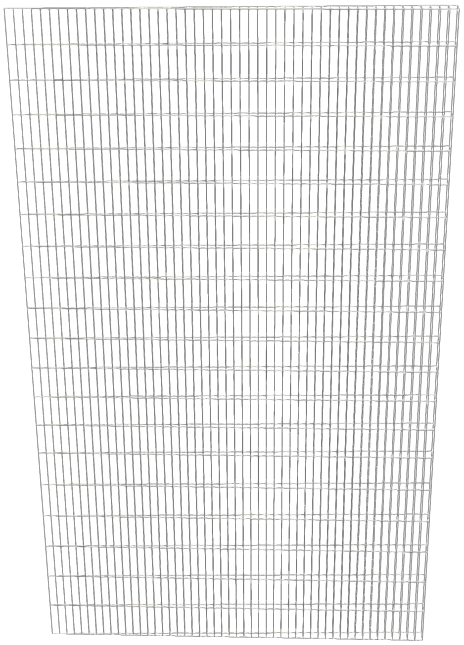

Figure 3.2: *Mesh used for the axisymmetric simulation.The aspect ratio is equal to 3.*

Computational time optimization

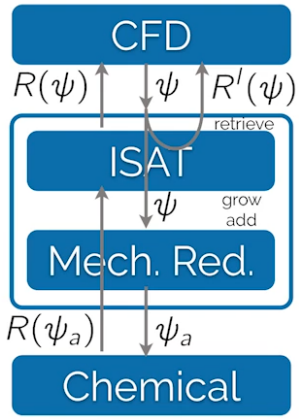

Figure 3.3: *TDAC structure. [42]*

For the purpose of reducing the computational time, *Hosselet and Van de Putte* implemented a *Tabulation of Dynamic Adaptive Chemistry* (TDAC) in the simulation [9]. As it can be seen in Figure 3.3, during the simulation, the CFD which takes care of the thermodynamic aspect, exchanges data with the chemistry which is very computational consuming. The idea behind TDAC is to optimize the chemical computation requirement. In other words, to use the chemistry solver the less possible. Actually, TDAC is the combination of two methods. First, the *In Situ Adaptative Tabulation* (ISAT), is used to retrieve previously computed results. Then the Dynamic Adaptive Chemistry (DAC) is used to remove from the chemistry computation the unused species. With those methods it possible to use as little as possible the chemical computation and thus reduce the computational time.

It is possible to decrease furthermore the computational time by changing the time step from fixed to variable. The variable time step is limited by the maximum *Courant number* (Co number). The Courant number is determined for every cell by Equation 3.1 and is usually set around 0.2.

$$Co = \frac{\delta t|U|}{\delta x} \tag{3.1}$$

Where,

- δt is the time step,
- δx is the cell size in the velocity direction,
- |U| is the magnitude of the velocity through that cell.

A maximal Courant number corresponds to the largest flow velocity through the smallest cell of the mesh. In a variable time step mode, the δt is chosen according to the maximal Co number.

Qdot

OpenFoam comes with a series of useful tools called function objects, those helps extracting data easily from the simulation. A function object of interest is the *Qdot*. It computes the heat release rate for each species, in each cell at each time step. Its computation is given in Equation (3.2).

$$Qdot[cell_i, t_2, Y_j] = Qdot[cell_i, t_1, Y_j] - h[Y_j] * RR[cell_i, Y_j] \tag{3.2}$$

In Equation (3.2),

- Y_j is the concentration of the species j ,
- $cell_i$ is the cell number i,

- $h[Y_i]$ is the enthalpy of formation of the species j in $\left[\frac{J}{kg}\right]$,
- $RR[cell_i, Y_j]$ is the Reaction Rate (RR) of the species j in the cell i in $\left[\frac{kg}{m^3 s}\right]$.

This gives a value of *Qdot* in J/m^3/s.
In order to have the HRR for the whole cylinder, it is necessary to integrate this value over the whole volume of the wedge and then multiply it by 180 to obtain the HRR of the cylinder in [J/s]. In ICE simulations, it is common to express these values as a function of the crankshaft angle, so it is necessary to make a conversion between the time rate and the CAD rate.

Boundaries and initial conditions

The initial temperature will change in function of the simulation purpose. For air-methane combustion, it varies from 460[K] to 500[K] to observe normal combustion.
Then the equivalence ratio is set by specifying initial species mass percentage. To find the mass percentage from the equivalence ratio, first the stoichiometric fuel-air ratio has to be determined from the basic complete and stoichiometric reaction (Equation (3.3)).

$$CH_4 + 2\left(O_2 + \frac{0.79}{0.21}N_2\right) \longrightarrow CO_2 + 2H_2O + 2\frac{0.79}{0.21}N_2 \tag{3.3}$$

Then the FAR_{st} is defined as the Equation (3.4).

$$FAR_{st} = \frac{M_C + 4M_H}{2(2M_O + 2\frac{0.79}{0.21}M_N)} \tag{3.4}$$

Where M_X is the molar mass of the species X. Then the actual fuel-air ratio can be determined with the equation 3.5.

$$FAR = \phi FAR_{st} \tag{3.5}$$

Finally, the mass fractions can be found with the Equations (3.6).

$$\%_{CH_4} = \frac{1}{1 + \frac{1}{FAR}} \qquad \%_{O_2} = 0.21\frac{1}{1 + FAR} \qquad \%_{N_2} = 0.79\frac{1}{1 + FAR} \tag{3.6}$$

The intake pressure, the wall temperature and the swirl ratio were determined by *Hosselet and Van de Putte* [9]. A quick summary will be presented here.

- The pressure boundary conditions are Von Neumann zero gradient conditions set on each wall. Those conditions imply to set the value of the derivative at the boundaries. The UCLouvain HCCI engine is naturally aspirated, thus an intake pressure around 1 bar is expected. *Hosselet and Van de Putte* [9] determined it to be equal to 1.025 bars at IVC.
- The wall temperature is set as a Dirichlet condition. After measurement on the experimental bench, the *cylinderHead* and *Liner* temperatures were set to 380[K] [9]. While the liner and cylinder head are cooled by forced convection, the piston is mainly cooled by oil. The piston head temperature was set to 430[K] [9].

- The eventual presence of swirl has to be modeled in the simulation. The Yanmar L100V is a CI direct-injection with a flat cylinder head and in-piston bowl. It is of common practice that the intake ports are designed to induce in-cylinder air motion. In CI engine, it is used to optimize the air intake and the fuel motion during the injection. In the case of an HCCI engine, since the mixture is homogeneous this swirl will have a great impact on the wall losses and the thermal stratification. It is thus important to implement swirl in our model.

engineSwirl in an OpenFOAM pre-processing utility that is used to set an initial swirl motion. It requires three parameters : the engine speed, the swirl ratio and the swirl profile.
According to *Ferguson* [26] : "The swirl ratio is defined as the ratio of the solid body perpendicular rotational speed of the intake flow ω_s to the engine speed $2\pi N$". Its expression in given in equation 3.7. *Hosselet and Van de Putte* [9] determined it from experimental results and settled for a value of 2.1.

$$SR = \frac{\omega_s}{2\pi N} \tag{3.7}$$

The swirl motion is not constant in the azimuthal direction, the wall affects the gas motion. The swirl profile can be modeled by a Bessel function [43]. It contains a parameter α that will affect the azimuthal velocity. *Hosselet and Van de Putte* [9] used a value of 3.11. The Figure 3.4 shows that the mixture velocity is lower near the axis and the liner. The simulation wall losses are convection based. They depend mainly from the swirl and the wall temperature.

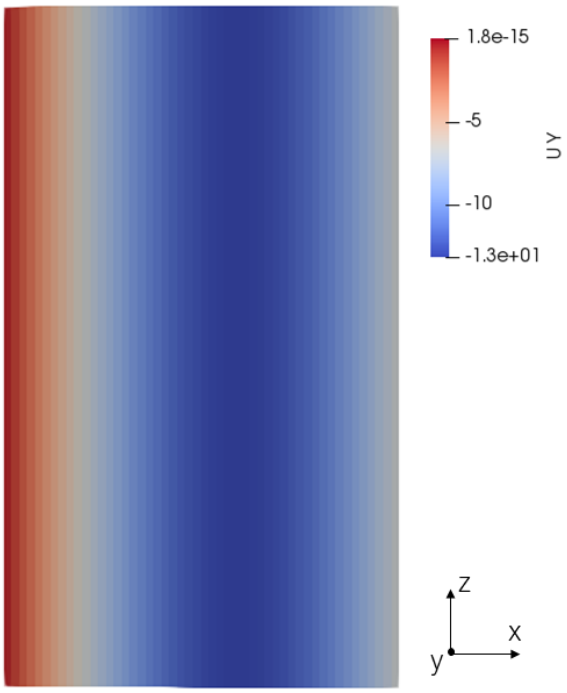

Figure 3.4: *Velocity field in the Y direction at -146 CAD. It corresponds to a 3.11 swirl profile.*

Note that since *OpenFOAM* considers the cylinder as a closed volume from the beginning to the end of the simulation, the pumping losses are not considered.

3.1.3 Glow plug implementation

The glow plug is a heating element. In a simulation it can be modeled by a heat flux coming from a determined area. There are only few references in the literature that model a GP for CFD applications. *Pourfallah et al.* [3] modeled it as a cylinder penetrating through the combustion chamber, see Figure 3.5.

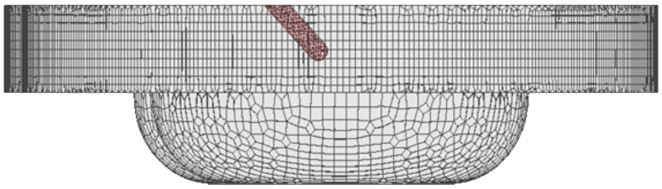

Figure 3.5: *Pourfallah GP model for a CFD simulation. The GP penetrates deeply in the combustion chamber. Adapted from [3]*

Since our model is axisymmetric, the only possible location for the GP is at the very center of the cylinder. Even if on the actual engine it is not perfectly centered (see Figure 2.11).

During the simulation phase, the mounting of the GP on the bench was not known beforehand. Two models of the GP were thus created.

First, a flush mounted GP was modeled (see Figure 3.6). To do so, a patch was created on the cylinder head, using a *set* with *topoSet* which is then converted into a patch with the *createPatch* pre-processing tool.

Then a deep GP was modeled (see Figure 3.6). After several attempts that resulted in a shrinkage of the GP as the piston was going up, a solution to this problem was found. First a patch is created on the cylinder head next to the future GP placement. Then this patch is extruded with *extrudeMesh* in order to create a cavity in the mesh with two new patches. These patches names are very important, the motion solver is looking for the names "*piston*", "*cylinderHead*" and "*liner*" to create the engine mesh between those boundaries. The lower part of the GP has to be called "*cylinderHead*" so that the area on the right of the GP will not be a part of the engineMesh and thus will not shrink with the GP. Finally, since the mesh was extruded, the clearance was adapted in order to keep the same compression ratio for both models.

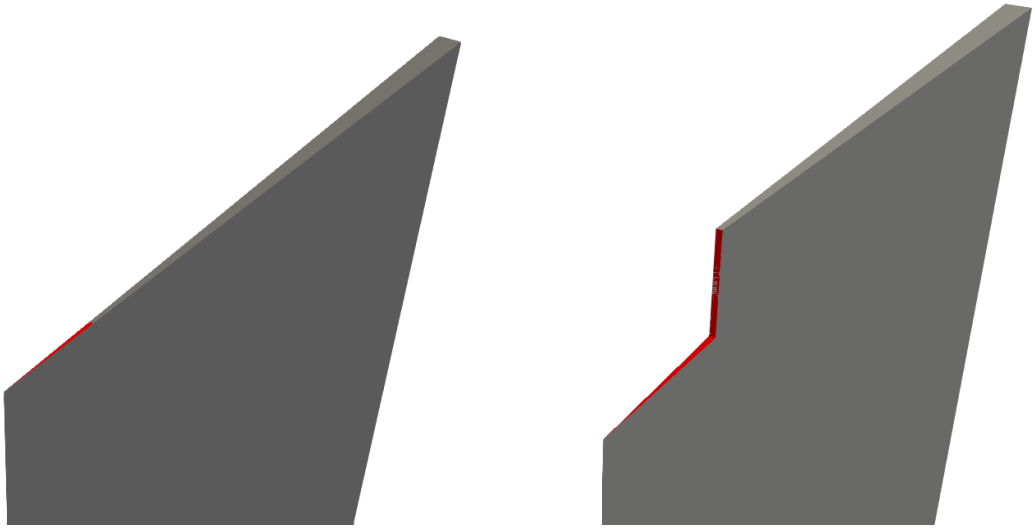

Figure 3.6: *The flush GP patch is located next to the axis. The deep GP increases its contact area with the gases.*

The heat flux was then applied in the T file in the initial time directory. In this file it is possible to specify the temperature as a gradient. According to Fourier's law, the thermal gradient is linked to the heat flux (Equation (3.8)).

$$q = -k\nabla T \tag{3.8}$$

The flux in [W/m^2] is equal to the P_{GP} divided by the contact area between the mixture and the GP. And k is the thermal conductivity [W/m/K] directly obtained from the simulation.

3.2 Validation

The purpose of this validation is to prove that the simulation model is accurate enough to predict the trend of experimental results. First, a study concerning simulation inaccuracies will be presented followed by a comparison between our simulation and experimental results.

3.2.1 Oscillations

In the process of designing an *OpenFOAM* model that reflects the reality, issues in the simulation were found. Oscillations in the pressure and in the function object *Qdot* have been observed. The oscillations in the pressure trace are shown in Figure 3.7. They can be acceptable for maximal pressure or the IMEP computation. However when the pressure derivative is needed, as for the MPRR or the HRR, the derivative is marred with random oscillations.

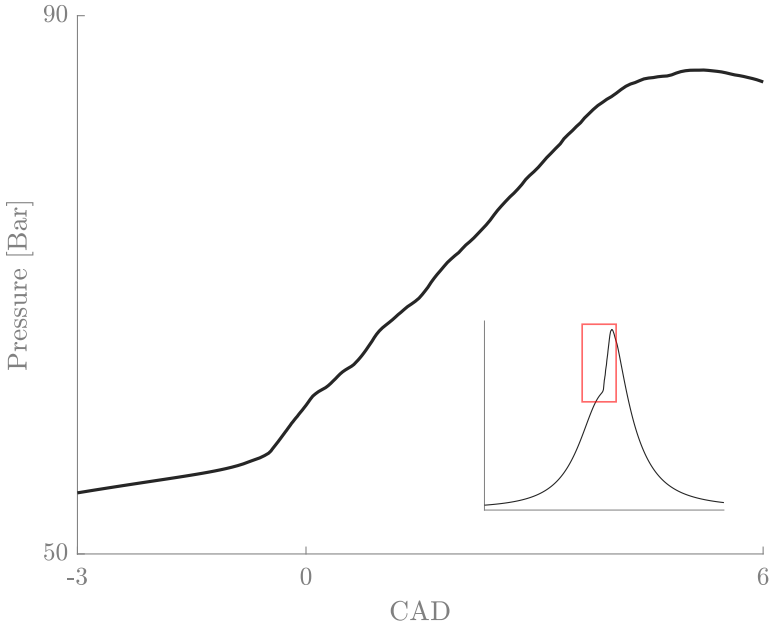

Figure 3.7: *The pressure trace shows erratic oscillations.*

Then waves in the velocity field can be observed in Figure 3.8. A fast gas motion is going back and forth between the *axis* and the *liner*. The magnitude of those velocities can reach up to 50 [m/s]. Since the pressure and the velocity field are linked to each other and that the timing of those oscillations matches the noise apparition, it can be stated that those two events are linked.

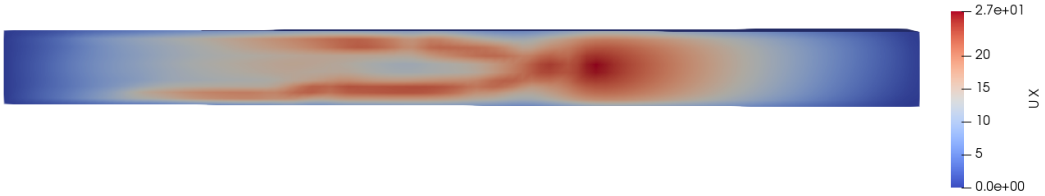

Figure 3.8: *Velocity field in the X direction at -3 CAD. Strong waves can be seen.*

Then those oscillations can also be seen on the HHR retrieved from the function object *Qdot* as it can be seen in Figure 3.9.

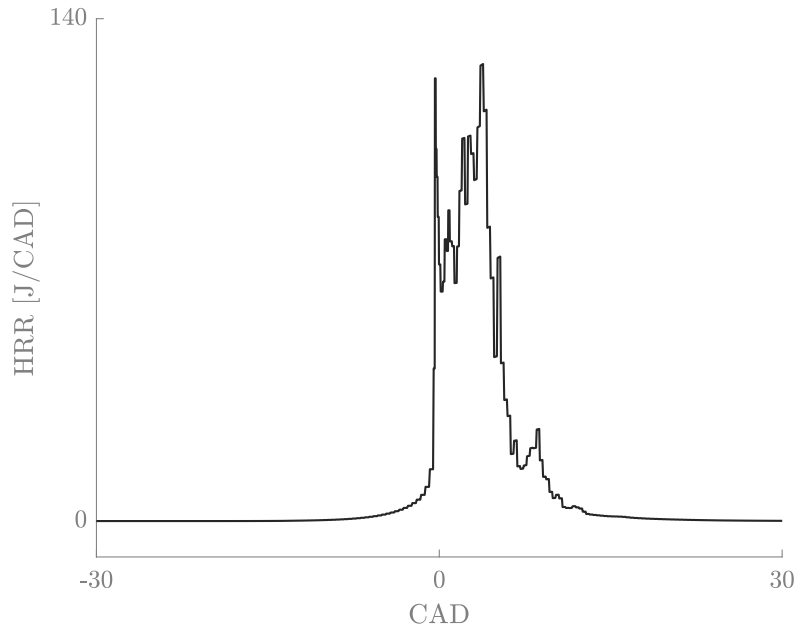

Figure 3.9: *HRR computed with Qdot. The trace shows erratic oscillations around TDC.*

The variation in the *Qdot* comes from variations in the species concentration and in the reaction rate (see Equation (3.2)). It is a difficult issue to tackle since the origin of those fluctuations is unknown. If the assumption is made that the initial fluctuation comes from the pressure. Those pressure fluctuations induce fluctuations in local temperatures, which acts on the reaction rate which then acts on the species concentration and the heat release and then again on the pressure.
However the effect of this noise on the CHR is limited. Even if the species concentration fluctuates, the mass is conserved. The hypothesis is made that if the HRR increases rapidly, a decrease of a similar amount is expected just after. This would result in a correct mean value. Further investigations should be made to confirm that hypothesis.

To find the source of those oscillations, several tests have been done by investigating the effect of some parameters.

Time step

First, in order to see if the fluctuations come from a physical phenomenon or from the simulation itself, a study on the time step was pursued. If by reducing the time step, the fluctuations are similar (similar period), this means that the simulation depicts well a physical phenomenon occurring. If not, the problem comes from the simulation itself.

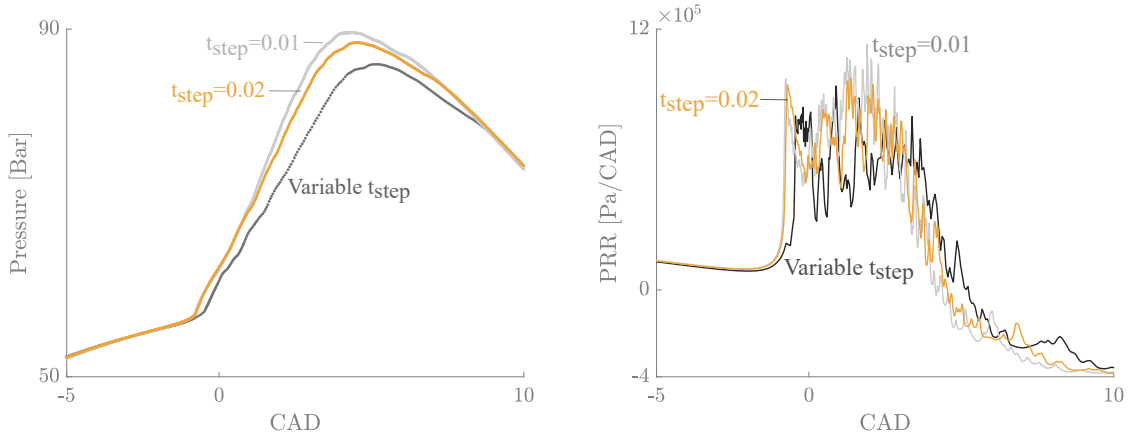

Figure 3.10: *Pressure trace and pressure rise rate for different time steps. A pattern of oscillations for a time step reduction cannot be observed.*

In Figure 3.10, two simulations with a fixed time step are compared with one with a variable one. The fixed time steps are of 0.01 [CAD] for the first one and of 0.02 for the second one. It can be seen that the pressure curves and the fluctuations are different in all three cases. In Figure 3.10, the pressure derivative is shown and confirm the difference between the three cases. This means that the fluctuations are simulation related. In the following analysis, only cases with variable time steps are compared so it will not have an impact on the conclusions. It has been done to save computational time.

Chemistry mechanism

Secondly, since the oscillations are stronger during combustion, it is reasonable to think that they can find their origin in the chemistry mechanism.

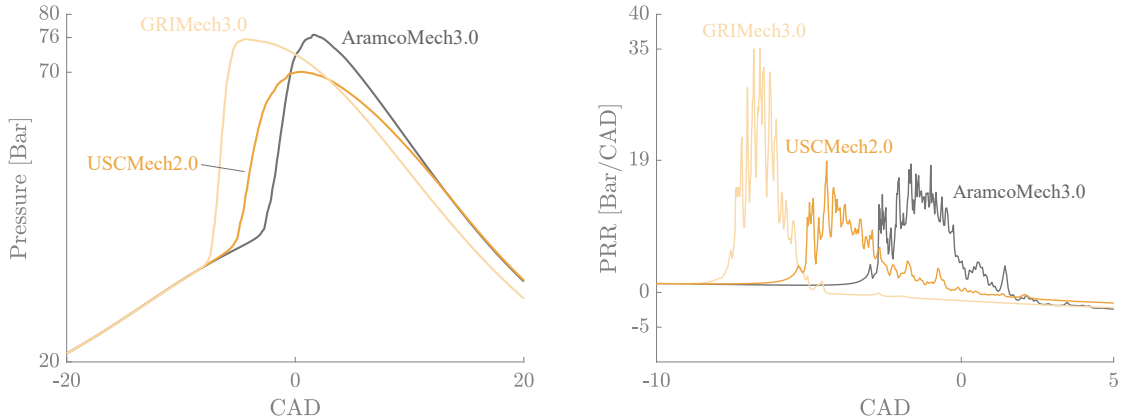

Figure 3.11: *Pressure trace and pressure rise rate for different chemistry mechanisms. They affects greatly the pressure evolution. However the oscillations do not seem to depend on the mechanism.*

Three mechanisms are analyzed : AramcoMech3.0, GRIMech3.0 and USCMech2.0.

Those three mechanisms are suited for HCCI combustion simulation [1]. In Figure 3.11, it can be seen that the mechanism has a significant impact on the pressure trace. To cope for that, tolerances exist in *OpenFOAM* and should be determined but their study is out of the scope of this thesis. The main message of this analysis is that, as seen in Figure 3.11, the fluctuations do not disappear by changing the chemistry mechanism.

Mesh

Thirdly, having a mesh with a high cell aspect ratio could lead to simulation instabilities. The ideal case is to change the mesh in order to have a square cell shape at TDC, where the fields gradients are the largest. However due to the long piston stroke, if at TDC the cells are squared, at BDC they will be very elongated. A remesh during the compression stroke is thus necessary to cope with that. It has been chosen to use from -146 to -50 [CAD] a non-graded mesh. This mesh was constituted of 50 cells between the axis and the liner and 20 cells between the piston and the cylinder head. From -50 to 50 [CAD] a mesh with 100 cells between the axis and the liner and 10 cells between the piston and the cylinder head (see Figure 3.12, bottom). This mesh will be compared with the mesh presented in Section 3.1.2 (see Figure 3.12, top).

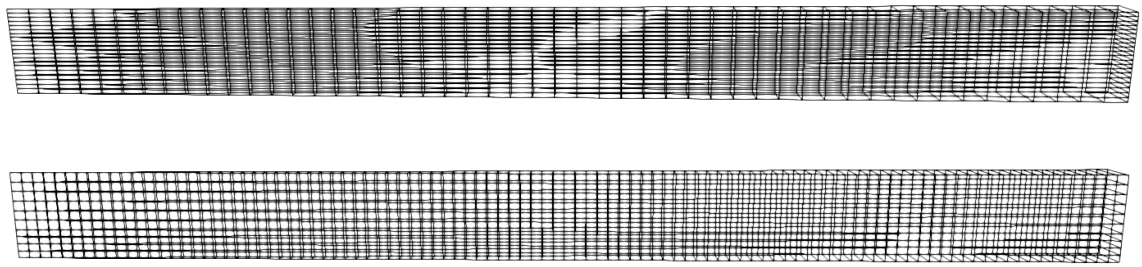

Figure 3.12: *The aspect ratio of the cells at TDC is better for the remesh case (bottom) than for the reference case (top).*

In the Figure 3.13, it can be seen that the pressure traces are very similar. However the oscillations in the PRR are still present in both cases. The poorer aspect ratio at TDC is thus not the reason of the fluctuations.

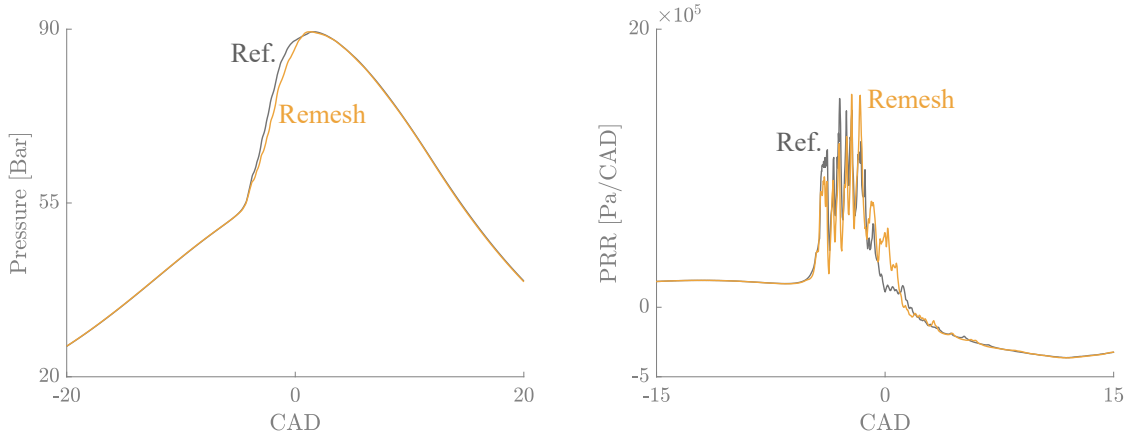

Figure 3.13: *Pressure trace and pressure rise rate with different meshes. The mesh affects slightly the pressure trace but does not remove the oscillations.*

TDAC

Finally, the impact of the Tabulation of Dynamic Adaptive Chemistry on the oscillations has been investigated. TDAC acts between the CFD and the chemistry solver. Since the issue affects the chemistry species as well as the thermodynamic state, the TDAC could be the origin.
In Figure 3.14, it can be seen that the results with and without TDAC are almost identical. Even the oscillations have the same behaviour. This means that the TDAC is not the origin of the oscillations. Note that TDAC reduces considerably the computational time at the cost of negligible result variations.

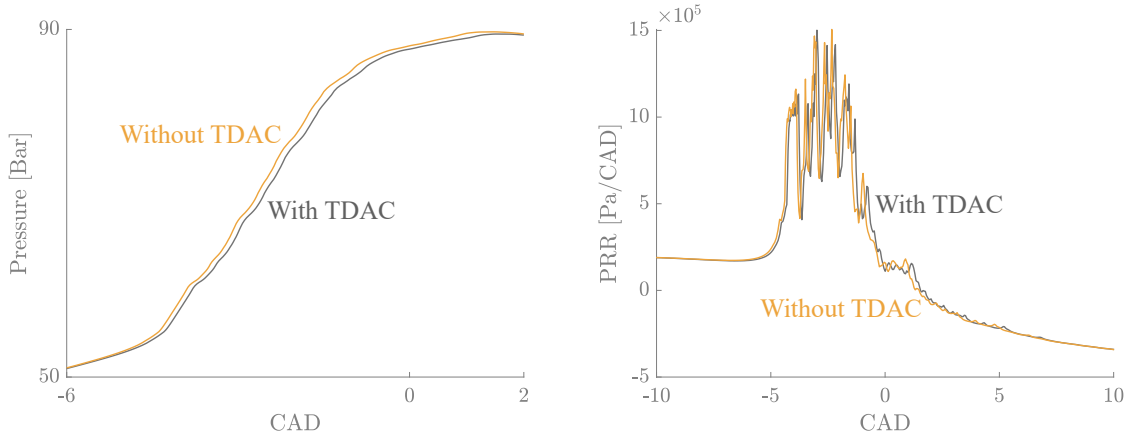

Figure 3.14: *Pressure trace and PRR with and without TDAC. The presence of TDAC does not affect significantly the results or the oscillations.*

3.2.2 Comparison with an experimental case

Ideally, the validation of our simulation should have been done based on experimental results from the UCLouvain HCCI engine. However, due to its recent dismantlement, the engine did not run on methane yet. The latest results using hydrogen are too different to be used in this validation. The choice was therefore made to compare the

simulation with experimental results found in the literature. The experiment with the closest characteristics to the UCLouvain engine is the one performed by *Wang et al.* [20]. Indeed, it is an HCCI engine of similar displacement running on NG. Their engine specifications and parameters are provided in Table 3.1.

Table 3.1: *Wang et al. engine specifications and experimental parameters. [20]*

Engine Specifications		
Engine type	Water-cooled 4 stroke Mono-cylinder	
Geometric compression ratio (τ)	19.5 : 1	
Displacement volume	402	[cm^3]
Cylinder bore (B)	80	[mm]
Piston stroke (S)	80	[mm]
Rotation speed (ω)	800	[rpm]
Parameters		
Intake pressure (p_{in})	1	[bar]
Intake temperature (T_{in})	220	[°C]
Equivalence ratio (ϕ)	0.416	[-]
Fuel	Natural gas	

Although relatively close to our simulation, the experiment of *Wang et al.* differs in several points.

Despite the two fuels being relatively similar, they show different characteristics. The NG has a higher auto-ignition temperature and octane number than methane which makes it more resistant to auto-ignition.
Also, their ratio of specific heats is different which, following an isentropic compression hypothesis, will lead to a lower pressure increase for NG.
Then, regarding the engine characteristics, some parameters are unknown such as the conrod length, the IVC timing, the volumetric efficiency and the swirl.
Finally, the simulation does not take into account all types of losses such as blow-by losses or pumping losses. For the unknown parameters the values provided in the Table 3.2 were chosen.

All those considerations contribute to explain the differences obtained between the simulation and the experiment. The validation performed here is therefore more a comparison to acknowledge the order of magnitude obtained.

Simulations were performed with different chemistry mechanims to see which one fitted the best *Wang et al.* experimental results. Two mechanisms are investigated, AramcoMech3.0 and USC2.0. In Figure 3.15, the pressure traces for the two chemistry mechanisms are compared with the experimental result. It can be seen that AramcoMech3.0 fitted the best the experimental data in terms of combustion duration and phasing. It is the reason why it will be used for all the simulations of this thesis.

Table 3.2: *Hypothesis on Wang et al. experiments*

Conrod length	120.5	[mm]
IVC timing	-146	[CAD]
Volumetric efficiency	1	[-]
Swirl profile	3.11	[-]
Swirl ratio	2.1	[-]

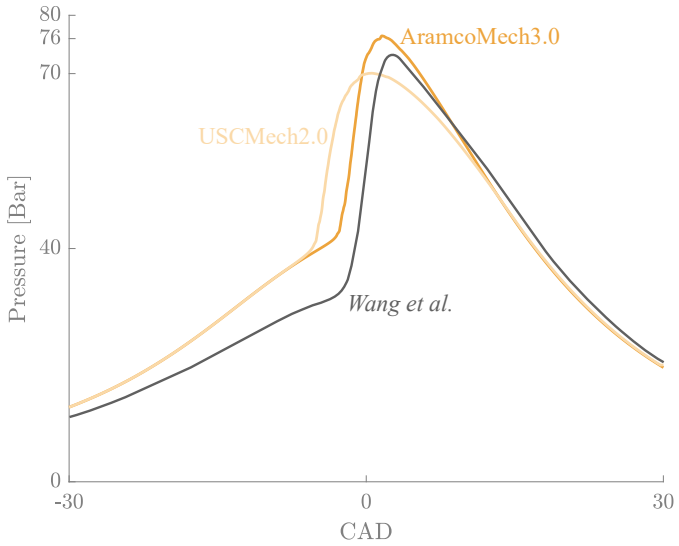

Figure 3.15: *Pressure trace with different chemistry mechanisms compared to experimental results. The AramcoMech mechanism gives a pressure trace which has the closest behavior to the experimental pressure trace.*

The IMEP is then computed from the p-V diagram as explained in Section 1.2.2. An IMEP of 2.61 bars is obtained while *Wang et al.* obtained an IMEP of 2.62 bars. Those values are very close.

As mentioned in Section 1.4.2, the SOC and DOC can be computed from the CHR which is itself computed from the HRR. Their traces are represented respectively in Figures 3.16 and 3.17. The difference between the maximal value of the HRR traces can be justified by the fact that there is no late combustion phase in the simulation unlike the experimental case.

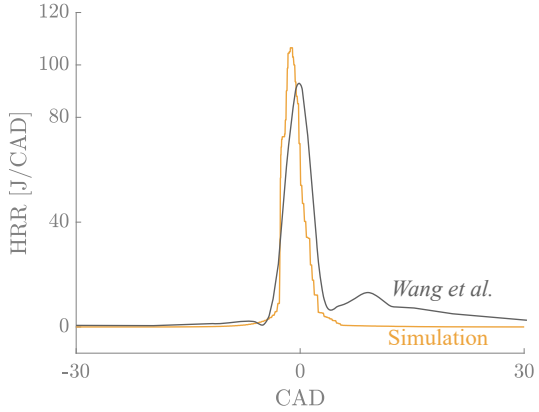

Figure 3.16: *Filtered HRR comparison between the simulation and the experimental results. The HRR simulation results are of the same order as the experimental ones.*

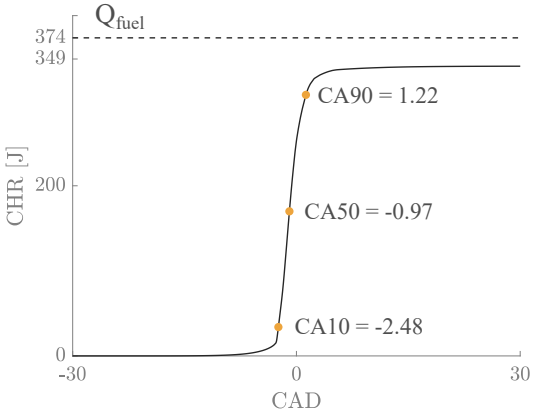

Figure 3.17: *Simulation CHR. sharp increase near TDC can be seen. Q_{fuel} is the total fuel energy contained in the cylinder.*

The comparison of the SOC and DOC is provided in Table 3.3. The difference between the values are small enough to conclude that the simulation SOC and DOC make sense. The combustion efficiency has been computed as explained in Section 4.2.2. A η_{comb} of 93.2 % has been computed from the simulation. *Wang et al.* states a η_{comb} of 94.7 % which is close to the computed value.
By comparing the simulation and experimental results from *Wang et al.*, it can be concluded that the results from the simulation are of the same order than the experimental results.

Table 3.3: *Comparison of SOC and DOC between Wang et al. [20] (experimental) and our validation (simulation).*

	Wang et al.	Simulation
CA10	-2.9	-2.48
CA90	1.12	1.22
DOC	4.02	3.7

Chapter 4

Results

This section presents the main results obtained from this model. First, the simulation losses will be compared with the Hohenberg model. Secondly, the impact of the *Glow Plug* (GP) on the combustion phasing, the IMEP and the thermal stratification will be investigated. Thirdly, being the main goal of this thesis, the increase of the engine performances, its power density, will be covered. Finally, a brief overview of the pollutant emissions produced by the engine will wrap up this analysis.

4.1 Simulation losses

As mentioned in Section 3.1.2, *Qdot* gives the heat released by each reactions, so the wall heat losses are not considered. The pressure curve, on the other hand, takes these losses into account. By subtracting the HRR computed from the pressure and the *Qdot* (Section 1.4.2), it is possible to obtain the losses at the walls over the cycle.
In the framework of an experimental analysis, it is not possible to obtain directly the heat released. To compensate for this, the Hohenberg correlation is used to easily model the losses. Those losses depend on a scaling factor, $\alpha_{scaling}$, as explained in the Section 1.4.3. In the Figure 4.1, the simulation losses and the Hohenberg model are displayed for two temperatures. The coefficient $\alpha_{scaling}$ has been tuned ($\alpha_{scaling}$=375) to fit the simulation losses at 460[K].

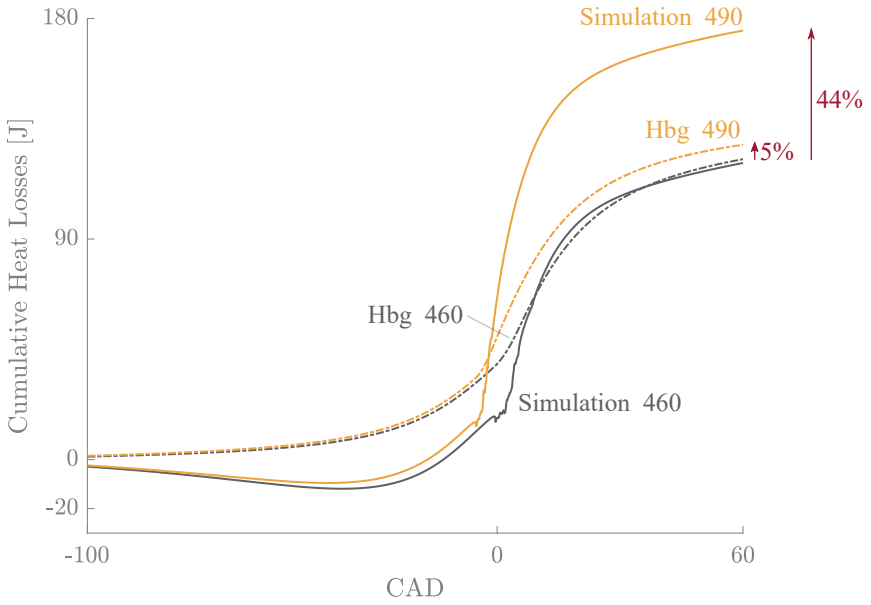

Figure 4.1: *Simulation losses compared with the Hohenberg losses model (Hbg) for a T_{in} of 460[K] and 490 [K]. The simulation losses are very sensitive to an increase of T_{in} compared to the Hohenberg model.*

When the inlet temperature increases, it can be seen that the increase in losses differs between the simulation and the model. Indeed, the increases are significantly different with 5% for the former and 44% for the latter. The share of losses represents 35% of the total heat released when $T_{in} = 460[K]$ both for our simulation and for the Hohenberg model. When $T_{in} = 490[K]$, this value increases to 39% for the Hohenberg losses model and rises to 53% for our simulation.
The amount of the losses and their increase in our simulation are too high compared to the total heat released. It would therefore be preferable to confirm the losses influencing parameters, such as the swirl ratio, via an experimental campaign on the HCCI bench at UCLouvain. In view of this observation, the following results should only be compared with each other. The goal pursued is to analyze the different effects and trends to observe the underlying physical and chemical effects of the GP.

4.2 Glow plug effects

The glow plug is a heating element exactly like a heater that would be placed before the intake manifold to increase the intake temperature. The main differences between a heater and a GP is their location, power and shape. The main question is the following : how is the combustion affected by the type of heat source? This is the reason why an increase in *Glow Plug Power*(P_{GP}) is compared with an increase in T_{in}. In this Section the power of the GP will always be expressed in percentage of the maximal power. The maximal $P_{GP}$was determined in Section 2.2.1 and is equal to 60.9 [W].

4.2.1 Effect on the phasing

To analyze the effect of the GP on the combustion phasing, several simulations were performed. Those simulations start from the same reference case : T_{in}=450 [K], $\phi = 0.38$ and without GP. For one half of the simulations, there is no GP and only the intake temperature is increased. For the other, the intake temperature is kept the same and the P_{GP} is increased.

In the Figure 4.2, for the T_{in} sweep, as T_{in} increase, the combustion starts earlier. For a 6 [K] increase in T_{in}, the CA10 advances of 1.3 [CAD].
For the P_{GP} sweep, the same trend can be seen. Setting the GP at full power has the same effect on SOC as increasing T_{in} of 6 [K]. This effect can be attributed to the fact that the GP is a heating element that will raise the mean in-cylinder temperature. It can be concluded that a GP can control the SOC to some extent.

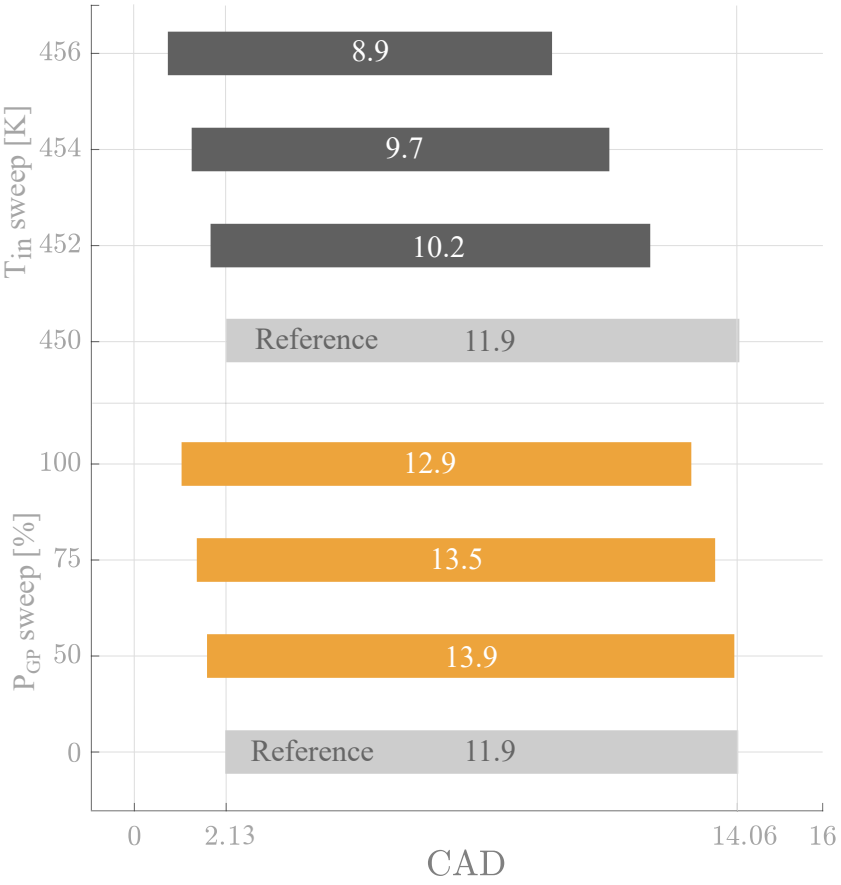

Figure 4.2: *Effect of a T_{in} and a P_{GP} sweep on the SOC and the DOC (CA_{10-90}). Increasing T_{in} and the P_{GP} advance the SOC. The DOC shortens for the T_{in} increase. However for the GP case, it increases and then slightly decreases.*

Then, still in Figure 4.2, as T_{in} increases, the combustion gets shorter of 3.1 [CAD] because the combustion happens closer to TDC. Indeed a CA50 closer to TDC means

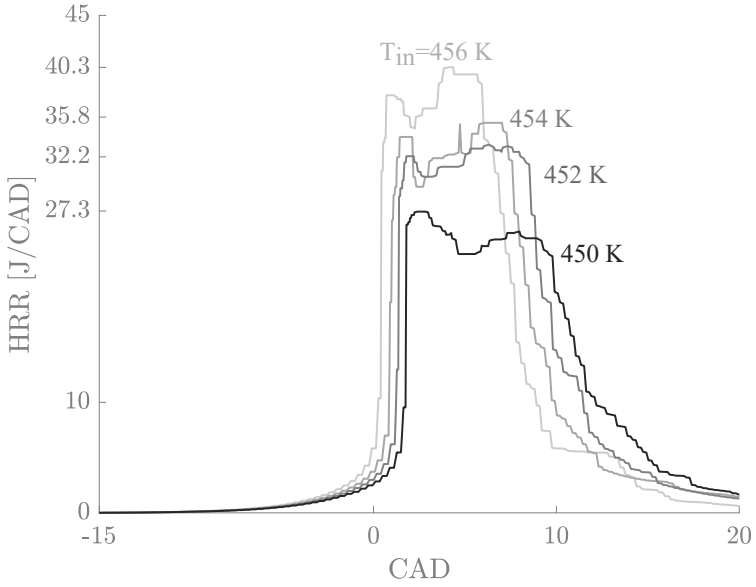

Figure 4.3: *Filtered HRR for a T_{in} sweep. As T_{in} increases, the SOC advances and the DOC decreases.*

that the combustion is occurring in a smaller volume. This leads to higher pressures and a shorter DOC.
For the P_{GP} sweep, the combustion is longer and then gets slightly shorter. This is a first difference that can be noticed between the T_{in} and the P_{GP} sweep. To understand why the DOC is getting longer with the GP, the HRR, from which the Figure 4.2 is obtained, has to be investigated.

In Figure 4.3, the HRR is shown for a T_{in} sweep. It can be seen that as T_{in} increases, the HRR is narrower and move to the left closer to TDC. This trend was already covered previously.
Then in Figure 4.4, the HRR is shown for a P_{GP} sweep. The trend is less obvious than for the T_{in} sweep. As the P_{GP} increases, the combustion start slightly earlier. However from this figure, it cannot be concluded anything on the DOC. It should be noted that the HRR curves have been smoothed using a high order median filter. In this process, the noise has been reduced to facilitate the comparison between the curves.

In order to compare properly the HRR trace between cases and neglect the effect of the phasing with and without GP, they should be compared at the same CA50. In that way, comparing two simulations with the same phasing but with the heat brought with two different ways (with T_{in} or with a GP) could highlight the GP effect. A T_{in} of 452 [K] has to be set to obtain the same phasing as a T_{in} of 450 [K] but with a GP at full power. In Figure 4.5, two cases, with and without GP, that have the same phasing are compared. It can be seen that the increase of HRR is smoother and less abrupt than in the case without GP. Even if this trend is not obvious in the Figure 4.5, it is confirmed by the Figure 4.2.

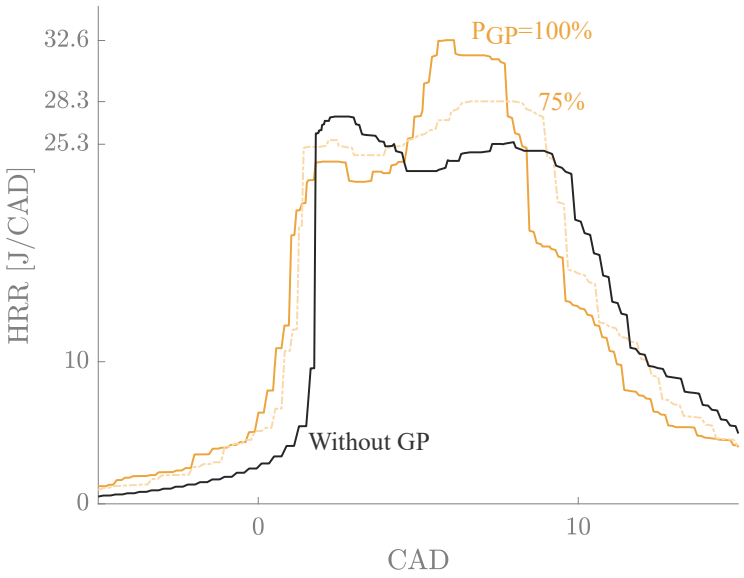

Figure 4.4: *Filtered HRR for a P_{GP} sweep. As the P_{GP} increases the SOC advances.*

It can be assumed that as the P_{GP} increases, the thermal stratification increases which broadens the HRR and thus extends the DOC. This effect is counteracted by the fact that as P_{GP} increases, the SOC advances which reduces the DOC.
At high P_{GP} the second effect is getting larger than the first one. In the end, this results in a higher DOC with the GP which decreases as the P_{GP} increases. The GP effect on thermal stratification will be investigated in Section 4.3.

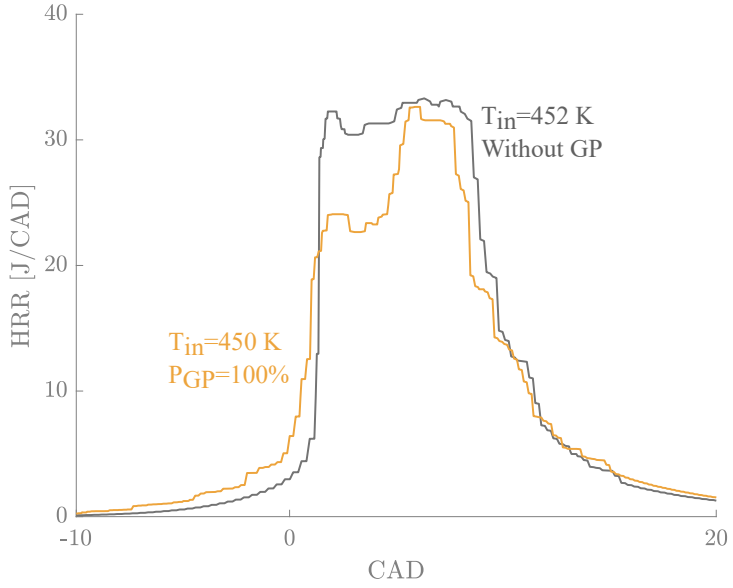

Figure 4.5: *Filtered HRR comparison between a case with and without GP at equivalent CA50. The reason why the DOC is longer with the GP might be due to the thermal stratification.*

4.2.2 Effect on the IMEP

It is well known in the literature that the intake temperature influences greatly the IMEP [20]. The comparison between a T_{in} or a P_{GP} increase can be done for the IMEP. Before studying the effect of the GP on the IMEP two preliminary analyses have to be made.

The first one is the effect of a T_{in} and a P_{GP} sweep on the combustion efficiency. In the Figure 4.6, as T_{in} increases, the combustion efficiency increases as well. At high temperatures the conditions are more suited for a better fuel oxidation. For the P_{GP} sweep, the same trend can be observed. The combustion efficiency is similar between the GP case and its equivalent CA50 case without GP. An increase of 1.6 % in η_{comb} can be observed from the reference case at 450 [K]. The combustion efficiency will be detailed in Section 4.5.

The second analysis is related to the intake charge density. As T_{in} increases, the density of the mixture decreases. Since ϕ is kept constant, the amount of fuel decreases which leads to a FuelMEP reduction as seen in Figure 4.7. The FuelMEP shows a decrease of roughly 0.2 % every Kelvin.
For the GP case, the T_{in} is constant during the P_{GP} sweep. The intake density is not affected during the sweep and thus the FuelMEP is constant. However this should be tested experimentally. The amount of heat transferred from the GP to the mixture during the intake stroke is unknown. It might affect the FuelMEP.

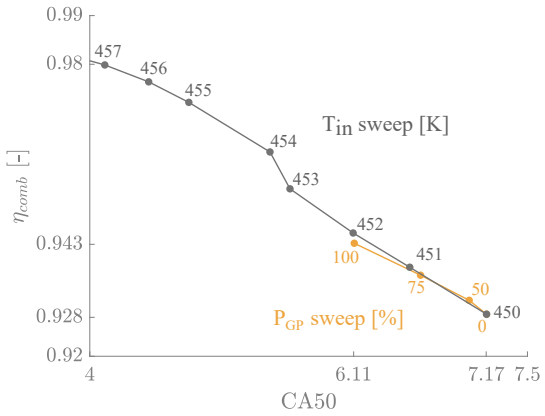

Figure 4.6: *Combustion efficiency for a T_{in} and a P_{GP} sweep. For both cases, the combustion efficiency increases due to better fuel oxidization. Computed from Eq.* (1.5).

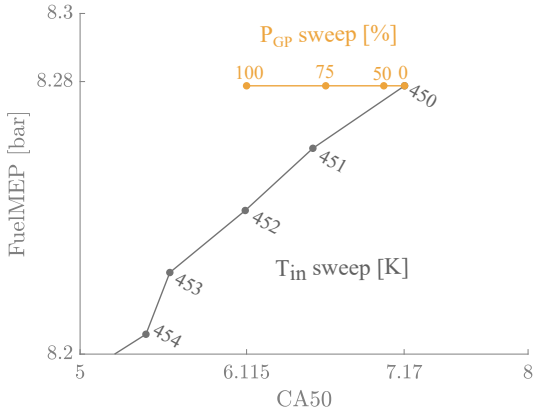

Figure 4.7: *FuelMEP for a T_{in} and a P_{GP} sweep. The FuelMEP decreases with the intake density. Since the density does not decreases with the P_{GP} sweep, the FuelMEP is not affected by the P_{GP} sweep.*

The variation of combustion efficiency and FuelMEP lead to variation in IMEP. For an intake temperature sweep, the IMEP is expected to be optimal for a certain phasing. In the Figure 4.8, the reference case is taken at T_{in}=450 [K].
At low temperatures, the combustion efficiency is low and the combustion happens late which leads to a low IMEP.
At high temperatures, the combustion efficiency increases and the SOC moves closer to TDC. However, the FuelMEP shows a decrease and the losses increase. Overall, this

leads also to a low IMEP.
Between those extrema, there is an IMEP optimum just after TDC. It means that it is more interesting to delay slightly the CA50 to get the best IMEP possible.

The P_{GP} sweep shows a strong increase in IMEP. Increasing the P_{GP} at 100 % will advance the SOC. This leads to a combustion happening closer to TDC. Also, the combustion efficiency is increasing.
However since the GP is in the cylinder, the intake charge density is independent on the P_{GP}. Which means that the FuelMEP is not affected as in the T_{in} sweep case. Furthermore, the GP is located on the axis of the cylinder, the near-wall gases are thus not affected. The wall heat losses are thus unchanged. Those effects lead to an overall increase of the IMEP.

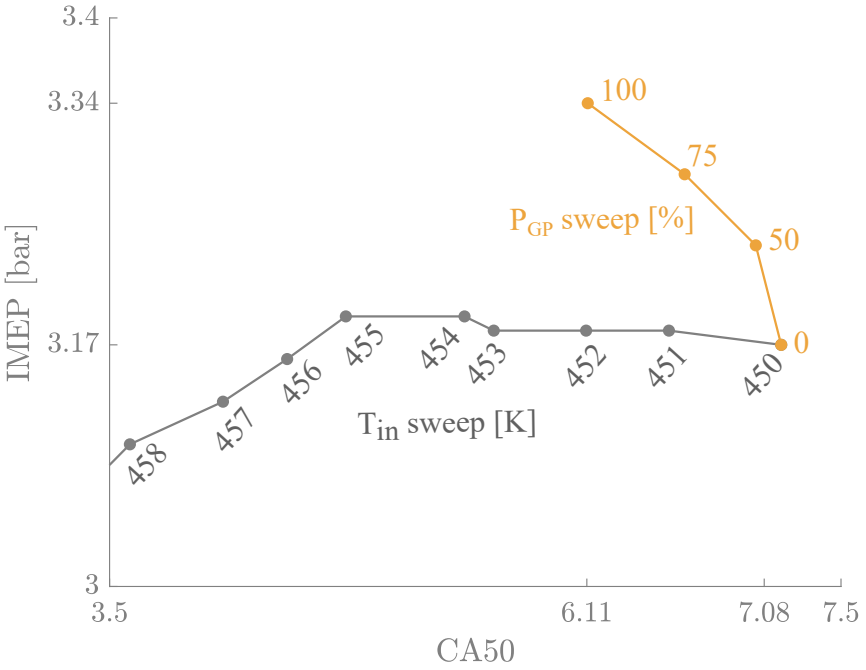

Figure 4.8: *IMEP for a T_{in} and a P_{GP} sweep. For the T_{in} sweep the, the IMEP is maximal slightly before TDC. For the GP case, the IMEP is higher because the GP heat does not affect the near wall gases temperature which limit the parietal losses.*

To summarize, the GP can control the combustion phasing only to certain extent. Indeed at full power the GP moves the CA50 only of 1 [CAD]. Then a GP can increase the IMEP of 5.36 % compared to a case without GP with a similar phasing. The main differences between the case without GP at 452 [K] and the case with GP at 450 [K] are the FuelIMEP and mainly the reduction in wall heat losses. This leads to an η_{ind} with the GP of 40.3 % compared to only 38.6 % without.

4.3 Glow plug thermal stratification

The slower increase in the HRR is the result of thermal stratification. Indeed the hotter areas in the mixture ignite first and the colder areas ignite later. This results in a longer DOC.

A way to confirm that the GP induces stratification is to look at the temperature mass PDF of the unburned gases. It represents the mass that are within a specified temperature range. It is then divided by the entire volume to obtain the units of a density.
In the Figure 4.9, it seems that the GP does not affect the temperature mass PDF. There are two reasons for that. First the GP is fairly small and does not affect the entire in-cylinder mixture. Second, the GP is placed right above the thinnest part of the wedge. The weight of the gases in this area is small compared to the rest of the volume where the mixture is less affected. From the Figure 4.9, it cannot be concluded that there is no thermal stratification. It can only be concluded that the GP does not affect the entire in-cylinder temperature.

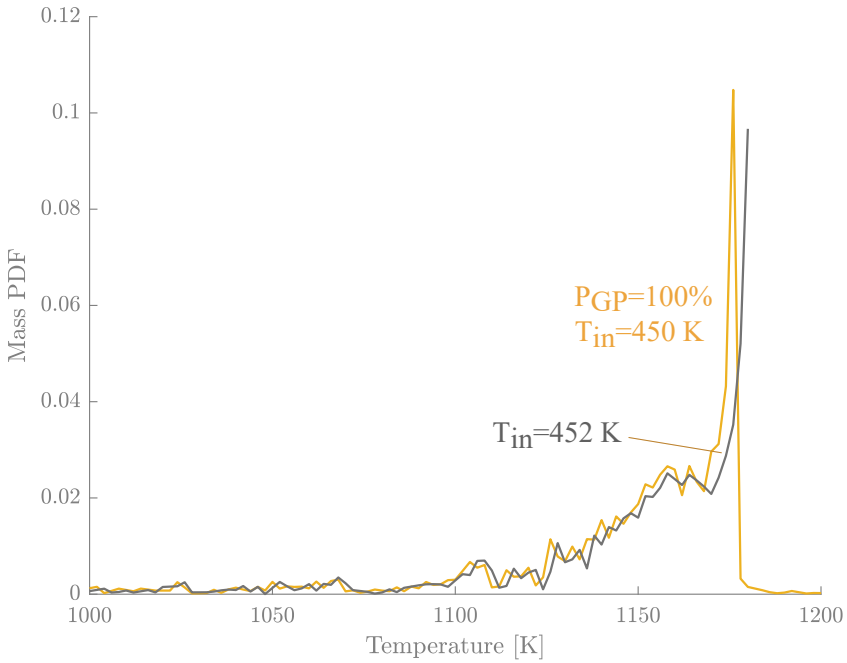

Figure 4.9: *Thermal mass PDF at -10 [CAD]. No significant difference can be observed between the two cases. The GP does not affect the entire in-cylinder mass.*

To understand the effect of the GP, one can use *paraView* to see directly the evolution of the combustion. In the Figure 4.10, several fields are depicted for a case with a GP at full power and a T_{in} of 450 [K].
First, it can be seen that the temperature at -10 [CAD] close to the GP is very high. This temperature is the result of a very local combustion happening around the GP. This local combustion can be seen by a decrease in the methane concentration and an increase in the carbon dioxide concentration near the GP. This local combustion starts

very early, around -50 [CAD]. At -10 [CAD] only 1.12 % of the methane has burned. This early combustion barely affects the CA10. This kind of local combustion around the GP can also be observed in *Pourfallah et al.* [3]. The main combustion happens only at 1 [CAD] where the thermodynamic conditions are prone to auto-ignition not only around the GP but in the entire cylinder.

A hypothesis can thus be made on the effect of the GP on the stratification. In the early stages of the compression, the GP heats up the charge very locally. Since the swirl velocity at the axis of the cylinder is null, the heat is not convected. Then the heat brought by the GP is large enough to allow a local combustion. But since at -10 [CAD] only 1.12 % of the mixture has ignited, the rise of pressure in the cylinder due to this combustion is not sufficient to ignite the entire mixture. Until 1 [CAD] (CA10), where the compression heating is sufficient for the rest of the mixture to be prone to ignition. At that point, since the combustion has already started close to the GP, it will extend very quickly. And unlike a traditional HCCI engine where the fuel molecules break all at once, the combustion is smoother and less spontaneous but still very fast.
The thermal stratification obtained is different from the one obtained by WDI or EGR. In this case it is a more local stratification. Its beneficial effect on the PRR will be studied in the next section.

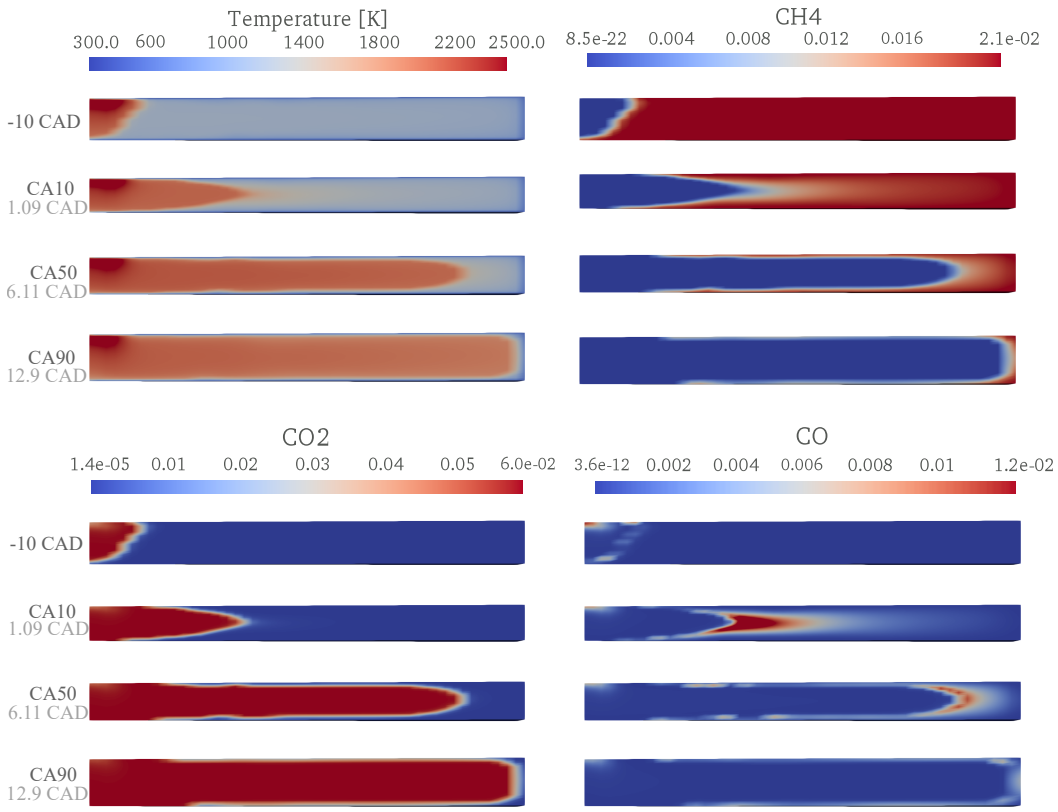

Figure 4.10: *Evolution of the temperature, the CH_4, CO and CO_2 concentration in the cylinder. Before the main combustion, around 1% of the fuel has already burned near the GP.*

4.4 Power density increase

HCCI engines have a low power density. Indeed, the amount of fuel per cycle has to be limited in order to keep an acceptable MPRR and thus a low ringing intensity. Since the GP has the effect of broadening the HRR, it reduces the MPRR. Thus, with the GP, the charge could be richer while still reaching reasonable MPRR.

As the charge equivalence ratio increases, the heat released increases as well. A higher pressure is thus reached which leads to more work produced and thus a higher IMEP. This trend can be observed in the Figure 4.11. Both cases have the same initial CA50. For the reason explained in Section 4.2.2 the GP has always a higher IMEP.

The increase of ϕ leads to a higher MPRR. In the Figure 4.12, the pressure trace of the case without GP suddenly increases when the combustion strikes. This effect is even more pronounced with a greater ϕ. However, in the case with the GP, the pressure curve is not a broken line. The curve is much smoother due to the pre-combustion that has already occurred near the GP. This results in lower MPRR and thus in lower ringing intensity. This smoothing effect increases with the fueling.

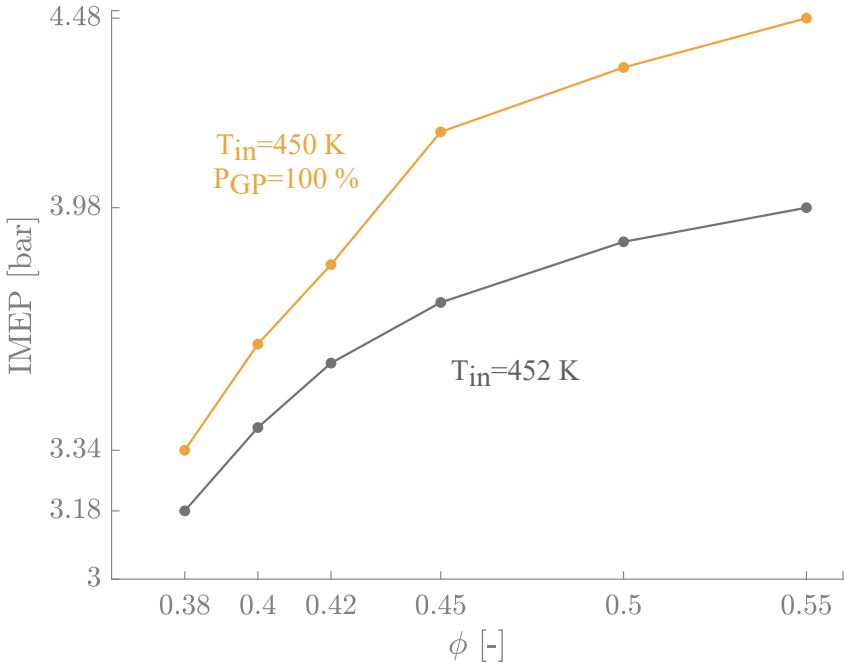

Figure 4.11: *Evolution of the IMEP for a ϕ sweep. An increase of ϕ increases the IMEP which is always higher for the GP case.*

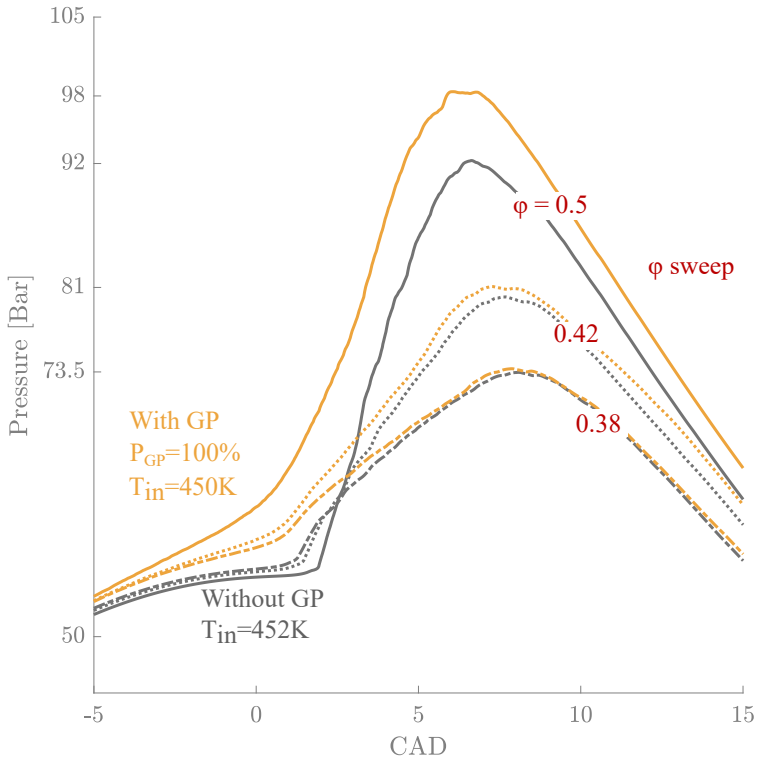

Figure 4.12: *Pressure trace for a ϕ sweep. The GP reduces the MPRR by smoothing the combustion. The smoothing effect of the GP increases with the fueling.*

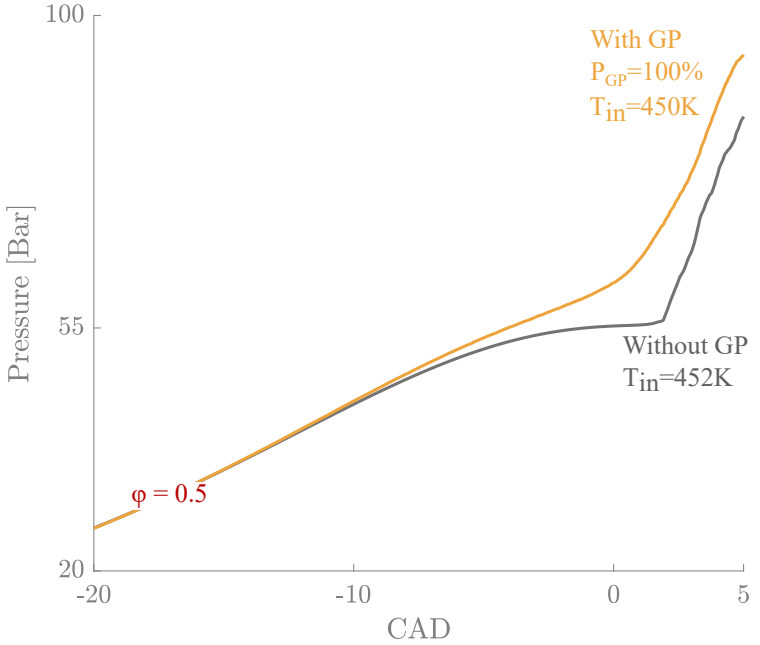

Figure 4.13: *Onset of the combustion on the pressure trace. The smoothing effect of the GP starts very early, around -10 [CAD].*

Looking more closely at the pressure trace, the difference at the onset of combustion becomes more noticeable (Figure 4.13). The early combustion of a fraction of the methane mentioned in the section 4.3 releases a small amount of heat that causes a slight increase in pressure. This earlier increase results in a smoother transition from this pre-combustion to the combustion of the rest of the methane.

In Figure 4.14, two cases are compared. A reference case with a T_{in} of 452 [K] where a ϕ sweep is applied and a case with a GP always set at full power but with a lower T_{in} of 450[K]. The two starting points where, $\phi = 0.38$, have the same CA50. It can be seen that the one with the GP has already a larger IMEP.
In the reference case, the gray line, it can be seen that the RI increases exponentially with the equivalence ratio. The limit of ringing for the UCLouvain experimental bench is set at 5 [MW/m^2] which would allow a maximal ϕ around 0.45.
The GP has the effect of decreasing the RI and increasing the IMEP. It means that higher values of IMEP can be reached while staying under the ringing limit. The amount of fuel cannot be increased significantly, but a maximal increase of 12 % in IMEP can be achieved. This is due to the smoothing of the combustion done by the GP and the fact that the P_{GP} increase does not affect much the parietal losses.

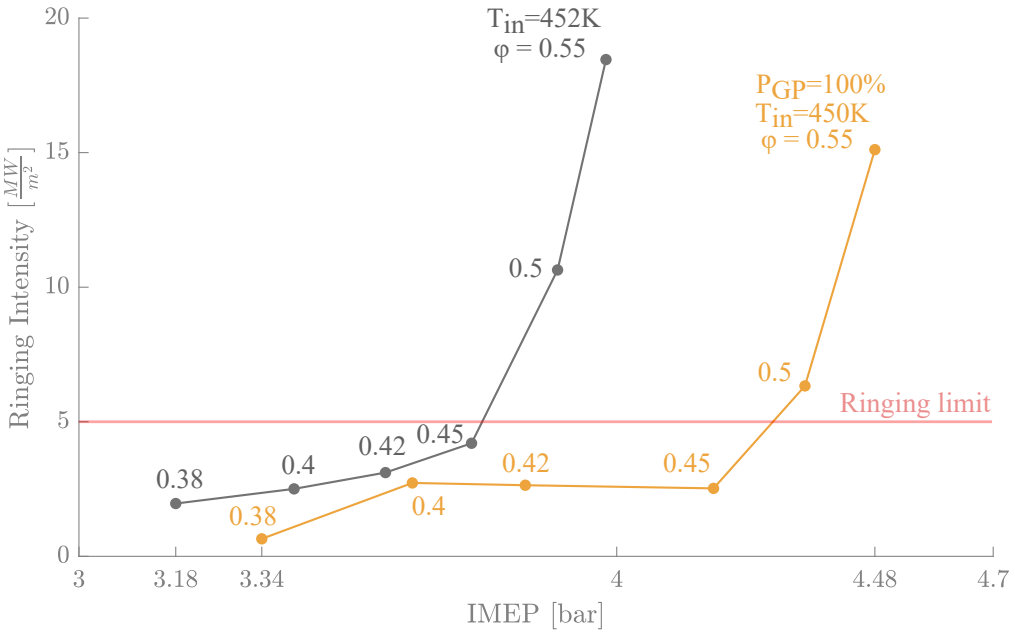

Figure 4.14: *Ringing intensity for a load sweep. The GP can increase the IMEP while staying under the ringing limit. However the fueling cannot be significantly increased.*

4.5 Emissions

As previously mentioned in Section 4.2.2 and especially in Figure 4.6, a T_{in} or a P_{GP} sweep has an impact on the combustion efficiency. The exhaust gas composition is related to the combustion efficiency. If there is a lot of unburned methane at the exhaust, it is directly a loss of fuel that could have been used to achieve more power. Since

carbon monoxide is also a fuel, its presence at the exhaust also reflects a decrease in the overall efficiency. This is the reason why their concentration in the exhaust should be investigated. Unfortunately, a study regarding the NOx was not possible since their mechanism was not embedded in the *OpenFOAM* simulation.

First, it is necessary to define a coefficient that would represent the remaining fraction of unburned methane. It is defined as follows:

$$k_{CH4} = 1 - \frac{x_{CH4,exhaust}}{x_{CH4,initial}} \tag{4.1}$$

If this coefficient is equal to one, it means that there is no more methane in the exhaust gases.
In the Figure 4.15, the same two cases are compared as in the Section 4.2.2 (ϕ=0.38). As T_{in} increases, the fuel is better oxidized. The same trend can be seen for the P_{GP} sweep. The GP brings heat inside the cylinder which reduces the amount of residual methane. It can be concluded that both the T_{in} sweep and the P_{GP} decrease the amount of residual methane.

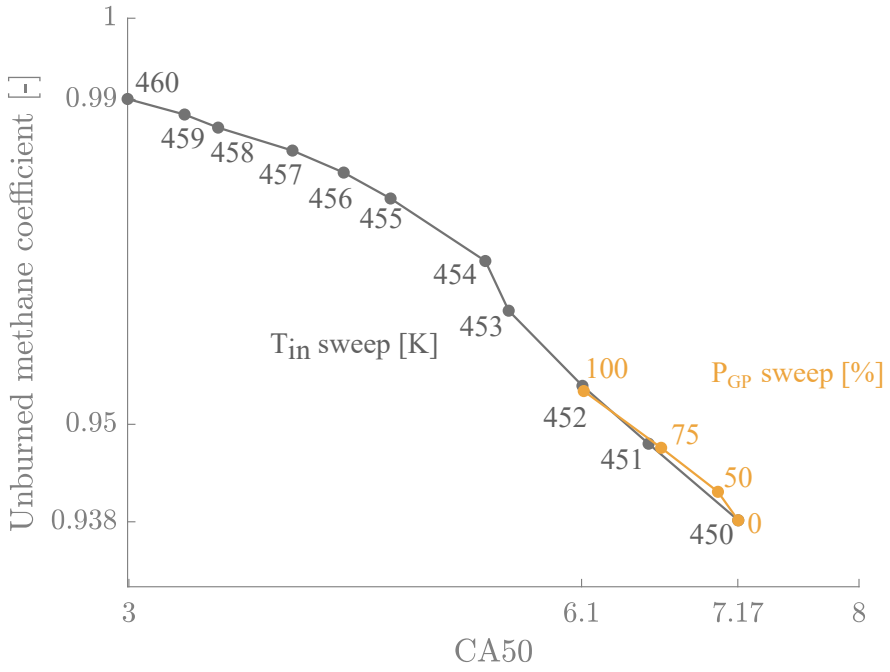

Figure 4.15: *Methane remaining fraction for a T_{in} and a P_{GP} sweep. For both case the fuel oxidation increases.*

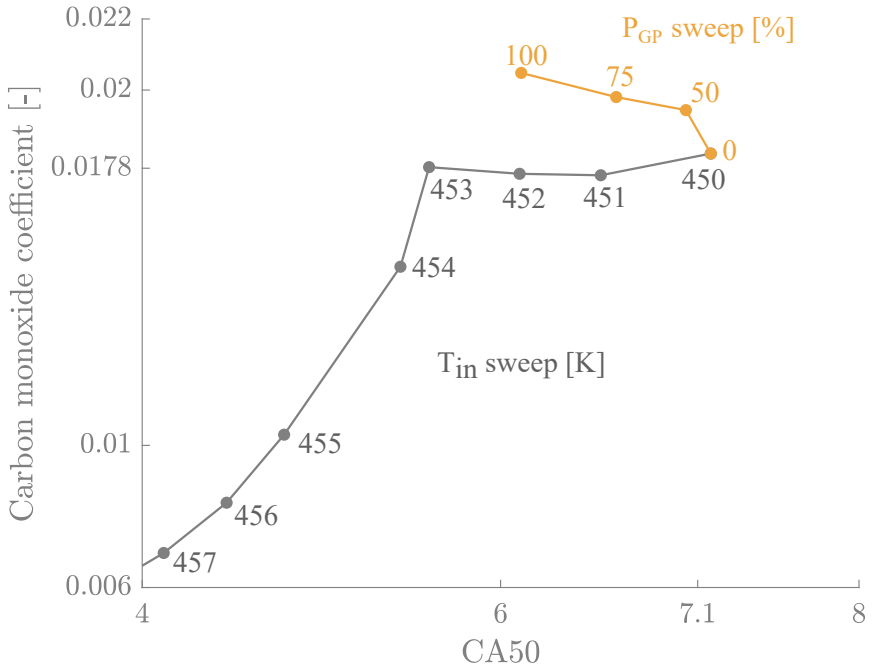

Figure 4.16: *Carbon monoxide coefficient for a T_{in} sweep and a P_{GP} sweep. For the T_{in} sweep, the DOC gets shorter thus the CO increases. For the P_{GP} sweep the opposite effect can be seen.*

To quantify the amount of CO in the exhaust gases, the CO coefficient can be used [44]. It is defined in equation (4.2) and quantifies the completeness of the combustion. If it is equal to zero, the combustion is fully complete. In other words, all the methane has been converted in CO2 instead in CO.

$$k_{CO} = \frac{x_{CO}}{x_{CO} + x_{CO2}} \tag{4.2}$$

In Figure 4.16, it can be observed that the k_{CO} decreases for the T_{in} sweep and increases for the P_{GP} sweep.
As explained in Section 1.2.2, the production of CO is temperature dependent. As the temperature increases, less CO is produced until very high temperatures are reached where the CO production starts to increase again.
For the T_{in} sweep, the DOC becomes shorter. In other words, the same amount of heat is released over a shorter duration which leads to a higher T_{max}. The production of CO and therefore k_{CO} are decreasing with T_{in} [45].
The GP has the effect of increasing the DOC. The T_{max} thus decreases and the production of CO increases. As the P_{GP} increases, the near-GP gases face very high temperatures. This creates a local source of CO. Those two reasons lead to an overall higher CO emission with the GP.

The trend of the combustion efficiency is very similar to the remaining methane concentration. It means that the increase of CO, for the GP case, is marginal compared to the decrease in unburned methane. The mass fraction of CO and methane in the exhaust

gases is similar but the CO LHV is lower. This also explains why the combustion efficiency seems to be led by the unburned methane concentration.

Conclusion

The present work has tried to contribute to the energy transition by proposing an improvement in HCCI engines. By using a glow plug, it is possible to enhance their combustion behavior in order to increase their IMEP and their power density.

In the first chapter, the HCCI engine principle was presented as well as its advantages and drawbacks. The pollutant emissions have also been analyzed in order to highlight the low emissions from the HCCI engine. Particular attention has been paid to thermal stratification, since it is the key principle implemented in this work. Finally, the different theoretical developments have been detailed to allow the reader to understand the origin of the subsequent results.

The second chapter focused on the experimental part of the thesis. Although the results are derived from numerical simulations, they are based on the geometry and parameters of the research bench of the UCLouvain. The intrinsic functioning of the glow plug was explained to understand the consequences of its use. Finally, the safety aspects of the use of a prototype such as the HCCI engine were briefly explained.

The third chapter was composed of two parts. The first one focused on an explanation of the functioning of the numerical simulation and its environment. The second part presented a validation of the simulations which was conducted by comparing experimental and simulation results. Eventhough some differences were noted on the experimental parameters, the obtained results were considered close enough and consistents enough to validate the simulation.

The fourth chapter presented the obtained numerical results. In terms of combustion efficiency, similar results were obtained with and without the glow plug but the effect on phasing resulted in a 5% increase in IMEP. By increasing the load, the rise in IMEP reached 12% while staying under the ringing limit. The effects of thermal stratification were found to be strongly local, but the glow plug was able to generate an early burn of 1% of the methane, making the total combustion smoother. In terms of emissions, an increase in CO production was observed but remains marginal. Regarding parietal losses, the obtained results did not follow the used correlation. Therefore, it would be preferable to carry out an experimental campaign to confirm the values and the trend obtained with temperature variations.

It has been proven in this work that a glow plug can enhance the HCCI combustion.

However the practical implementation of a glow plug reveals new constrains and and nuance the choice of its use. First, in this study, the electrical consumption of the glow plug has been ignored. Considering the chosen glow plug model and without taking the conversion to electrical energy, it would consume around 3 % of the engine power. Knowing that the glow plug increases the power of 12 %, its consumption is not negligible.
Second, the reaction time of the glow plug is slow which limit its use to stationary operations.
Third, glow plugs are not made to be continuously powered. Their life-time will therefore be reduced which will increase the engine maintenance costs.
Finally, besides affecting the mixture temperature, a glow plug will also heat up the cylinder head. The cooling system should then be revised to avoid overheating problems.
Those practical considerations moderate the positive effect of the glow plug on the combustion.

Outlook for future work

The use of a glow plug allows to control the combustion, as demonstrated in this thesis. However, the results were affected with simulation noise. Further investigations should be pursue to determine the origin of those oscillations. The objective would be to have a fully reliable model that could predict experimental outcomes.

Since the results of this work are exclusively numerical, it would be interesting to compare them with experimental results. Indeed, the values obtained for the amount of heat losses seem very high and therefore need to be confirmed by experimental results.

To go further, the influence of the position of the glow plug could be investigated. It can be expected that placing the GP off-center will affect more in-cylinder gases. Indeed, the higher off-center gases velocities due to the swirl profile induces a higher convection effect. Setting the GP deeper will increase the heat exchange area. The quantity of in-cylinder gases affected by the GP will also be increased.

Finally, increasing the swirl could increase the convection of the heat provided by the glow plug. A study combining the glow plug and a swirl flap for swirl ratio tuning might complete this study.

Bibliography

[1] M. Pochet, "Use of electrofuel blends in homogeneous-charge compression-ignition engines," Ph.D. dissertation, UCL-Université Catholique de Louvain, 2020.

[2] F. Contino and H. Jeanmart, "Lmeca2220: Internal combustion engines," 2021.

[3] M. Pourfallah, M. Armin, and A. A. Ranjbar, "A numerical study on the effect of thermal and charge stratification on the hcci natural gas engine," *International Journal of Ambient Energy*, pp. 1–10, 2019.

[4] B. Lawler, J. Lacey, O. Güralp, P. Najt, and Z. Filipi, "Hcci combustion with an actively controlled glow plug: The effects on heat release, thermal stratification, efficiency, and emissions," *Applied energy*, vol. 211, pp. 809–819, 2018.

[5] Office of the European Union, "Going climate-neutral by 2050. a strategic long-term vision for a prosperous, modern, competitive and climate-neutral eu economy," 2019.

[6] Industrie De Nora S.p.A., Energy Storage: De Nora - Electrode and Water Technologies that work! [Online]. Available from: `https://denora.com/products/applications/energy-storage.html`, [Accessed 3rd May 2021].

[7] J. Martin and P. Wauters, *Thermal Power Plants, Energetic and Exergetic approaches*, ser. Cours universitaires. Presses universitaires de Louvain, 2009.

[8] M. Götz, J. Lefebvre, F. Mörs, A. M. Koch, F. Graf, S. Bajohr, R. Reimert, and T. Kolb, "Renewable power-to-gas: A technological and economic review," *Renewable energy*, vol. 85, pp. 1371–1390, 2016.

[9] F. Van de Putte and S. Hosselet, "Use of electrofuels in homogeneous charge compression ignition engines: Numerical study of oxy-combustion potential," 2020, Supervisor : Jeamart, Hervé.

[10] T. Collette and A. Gatin, "Increasing hcci power density through thermal stratification: Impact of water direct injection," 2019, Supervisor : Jeanmart, Hervé.

[11] Combustion Propulsion Lab, Next-generation IC Engine Combustion: Combustion & Propulsion Lab.: UNIST, [Online]. Available from: `https://csyoo.unist.ac.kr/research/hcci-combustion/`, [Accessed 5rd May 2021].

[12] S. Soylu, "Examination of combustion characteristics and phasing strategies of a natural gas hcci engine," *Energy conversion and management*, vol. 46, no. 1, pp. 101–119, 2005.

[13] Sunndar Dannana, What is the Atkinson cycle, [Online]. Available from: `https://extrudesign.com/atkinson-cycle/`, [Accessed 8th June 2021].

[14] A. Peters, H. E. Wichmann, T. Tuch, J. Heinrich, and J. Heyder, "Respiratory effects are associated with the number of ultrafine particles.," *American journal of respiratory and critical care medicine*, vol. 155, no. 4, pp. 1376–1383, 1997.

[15] M. Sjöberg, J. E. Dec, A. Babajimopoulos, and D. Assanis, "Comparing enhanced natural thermal stratification against retarded combustion phasing for smoothing of hcci heat-release rates," *SAE transactions*, pp. 1557–1575, 2004.

[16] M. Vozár, "After ignition, direct water injection (ai-wdi) dew point based closed loop algorithm logic," 2020.

[17] S. Voshtani, M. Reyhanian, M. Ehteram, and V. Hosseini, "Investigating various effects of reformer gas enrichment on a natural gas-fueled hcci combustion engine," *international journal of hydrogen energy*, vol. 39, no. 34, pp. 19 799–19 809, 2014.

[18] A. Y. Nobakht, R. K. Saray, and A. Rahimi, "A parametric study on natural gas fueled hcci combustion engine using a multi-zone combustion model," *Fuel*, vol. 90, no. 4, pp. 1508–1514, 2011.

[19] P. Amneus, D. Nilsson, F. Mauss, M. Christensen, and B. Johansson, "Homogeneous charge compression ignition engine: Experiments and detailed kinetic calculations," in The Fourth Symposium on Diagnostics and Modeling of Combustion in Internal Combustion Engines, Comodia, vol. 98, 1998, pp. 567–572.

[20] Z. Wang, G. Du, Z. Li, X. Wang, and D. Wang, "Study on the combustion characteristics of a high compression ratio hcci engine fueled with natural gas," *Fuel*, vol. 255, p. 115 701, 2019.

[21] B. Lawler, S. Joshi, J. Lacey, O. Guralp, P. Najt, and Z. Filipi, "Understanding the effect of wall conditions and engine geometry on thermal stratification and hcci combustion," in *Internal Combustion Engine Division Fall Technical Conference*, American Society of Mechanical Engineers, vol. 46162, 2014, V001T03A020.

[22] J. E. Dec and M. Sjöberg, "Isolating the effects of fuel chemistry on combustion phasing in an hcci engine and the potential of fuel stratification for ignition control," *SAE transactions*, pp. 239–257, 2004.

[23] A. Gharehghani, "Load limits of an hcci engine fueled with natural gas, ethanol, and methanol," *Fuel*, vol. 239, pp. 1001–1014, 2019.

[24] R. K. Maurya and A. K. Agarwal, "Experimental investigation on the effect of intake air temperature and air–fuel ratio on cycle-to-cycle variations of hcci combustion and performance parameters," *Applied Energy*, vol. 88, no. 4, pp. 1153–1163, 2011.

[25] J. G. Antunes, R. Mikalsen, and A. Roskilly, "An investigation of hydrogen-fuelled hcci engine performance and operation," *International journal of hydrogen energy*, vol. 33, no. 20, pp. 5823–5828, 2008.

[26] C. R. Ferguson and A. T. Kirkpatrick, Internal combustion engines: applied thermosciences. John Wiley & Sons, 2015.

[27] J. Eng, "Characterization of pressure waves in hcci combustion," SAE Technical Paper, Tech. Rep., 2002.

[28] J. E. Dec, W. Hwang, and M. Sjöberg, "An investigation of thermal stratification in hcci engines using chemiluminescence imaging," *SAE Transactions*, pp. 759–776, 2006.

[29] J. E. Dec and W. Hwang, "Characterizing the development of thermal stratification in an hcci engine using planar-imaging thermometry," *SAE International Journal of Engines*, vol. 2, no. 1, pp. 421–438, 2009.

[30] E. Yildar, G. Kuenne, C. He, R. Schiessl, M.-S. Benzinger, M. Neurohr, F. Di Mare, A. Sadiki, and J. Janicka, "Understanding the influences of thermal and mixture inhomogeneities on the auto-ignition process in a controlled auto-ignition

(cai) engine using les," *Oil & Gas Sciences and Technology–Revue d'IFP Energies nouvelles*, vol. 72, no. 6, p. 33, 2017.

[31] S. S. Bhaduri, "Experimental studies on hcci combustion of biomass syngas towards tar tolerant operation," Ph.D. dissertation, UCL-Université Catholique de Louvain, 2015.

[32] H. S. Soyhan, H. Yasar, H. Walmsley, B. Head, G. Kalghatgi, and C. Sorusbay, "Evaluation of heat transfer correlations for hcci engine modeling," *Applied Thermal Engineering*, vol. 29, no. 2-3, pp. 541–549, 2009.

[33] G. Woschni, "A universally applicable equation for the instantaneous heat transfer coefficient in the internal combustion engine," SAE Technical paper, Tech. Rep., 1967.

[34] Thermodynamics and Fluid Mechanics Group and Annand, WJD, "Heat transfer in the cylinders of reciprocating internal combustion engines," *Proceedings of the Institution of Mechanical Engineers*, vol. 177, no. 1, pp. 973–996, 1963.

[35] Hohenberg and Günter, "Advanced approaches for heat transfer calculations," *SAE Transactions*, pp. 2788–2806, 1979.

[36] Bosch Auto Parts Canada, Bougies de préchauffage, [Online]. Available from: `https://www.boschautoparts.ca/fr/auto/diesel-parts/ca-glow-plugs`, [Accessed 10th April 2021].

[37] M. S. Endiz, M. Özcan, M. A. Eri̇şmi̇ş, M. yağci, and H. Günay, "The simulation and production of glow plugs based on thermal modeling.," *Turkish Journal of Electrical Engineering & Computer Sciences*, vol. 23, 2015.

[38] V. J. Abate, "Natural gas ignition delay study under diesel engine conditions in a combustion bomb with glow plug assist," Ph.D. dissertation, 2001.

[39] Bosch, Product information automotive - glow plugs, [Online]. Available from: `https://aa-boschap-uk.resource.bosch.com/media/parts/engine_systems__auto_parts_1/diesel__engine_systems_1/glow_plugs/pia_glow_plugs_en_58333.pdf`, [Accessed 10th April 2021].

[40] Linak, Actionneurs linéaire LA23, [Online]. Available from: `https://www.fr.linak.be/produits/actionneurs-lineaires/la23/\#/description`, [Accessed 13 June 2021].

[41] OpenFOAM, [Online]. Available from: `https://openfoam.org/`, [Accessed 20th May 2021].

[42] F. Contino, Reactions and Kinetics in OpenFOAM 6, slide 10. [Online]. Available: `http://cfd.tips/1803`.

[43] A. De Risi, T. Donateo, and D. Laforgia, "Theoretical investigation on the influence of physical parameters on soot and nox engine emissions," in *Internal Combustion Engine Division Spring Technical Conference*, American Society of Mechanical Engineers, vol. 80111, 2001, pp. 53–64.

[44] M. Papalexandris, *Combustion and Fuels*. Presses universitaires de Louvain, 2020.

[45] Z. Chun-hua, P. Jiang-Ru, T. Juan-Juan, and L. Jing, "Effects of intake temperature and excessive air coefficient on combustion characteristics and emissions of hcci combustion," *Procedia Environmental Sciences*, vol. 11, pp. 1119–1127, 2011.

Appendix A

A.1 P&ID

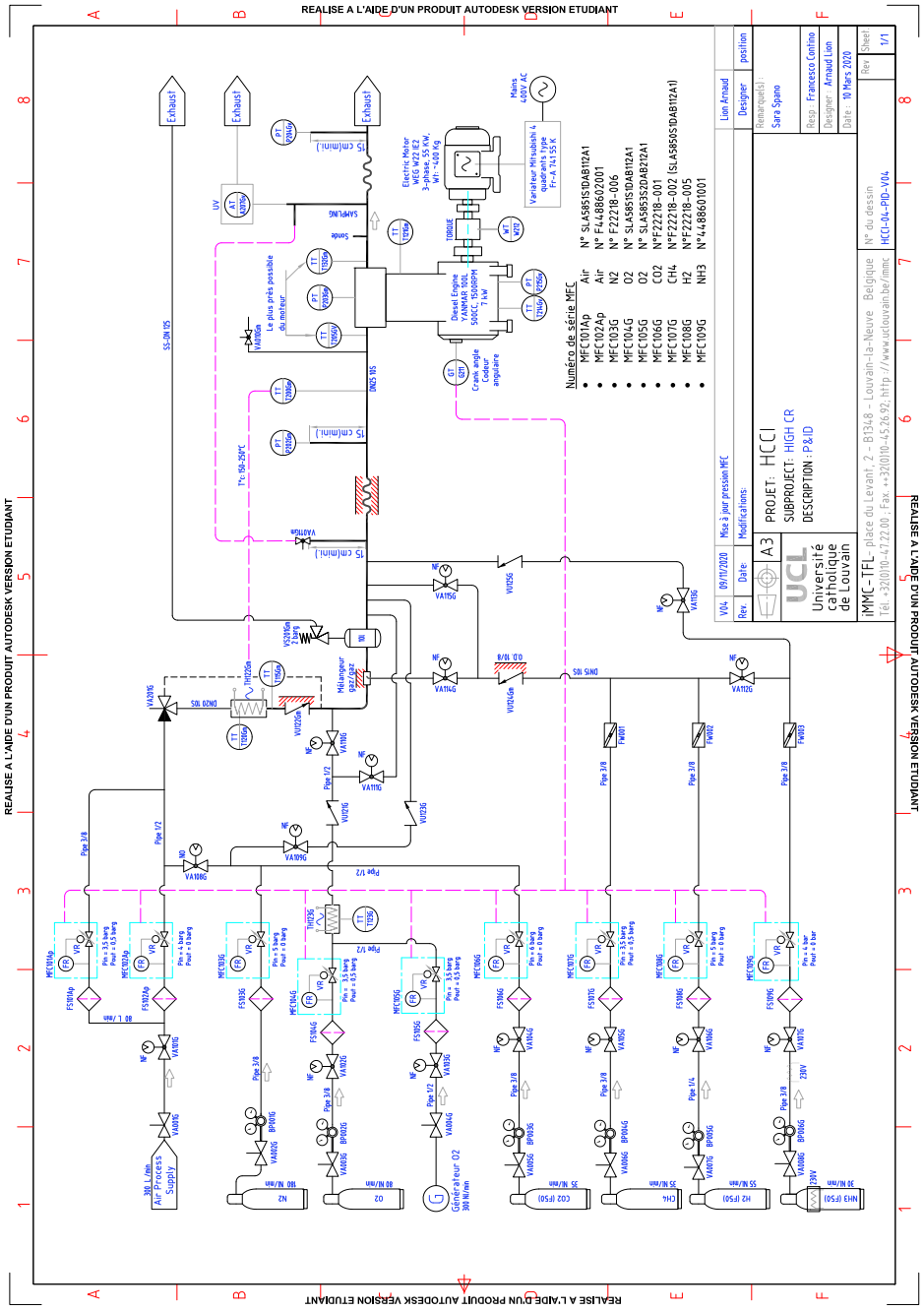

A.2 Plan de zonage

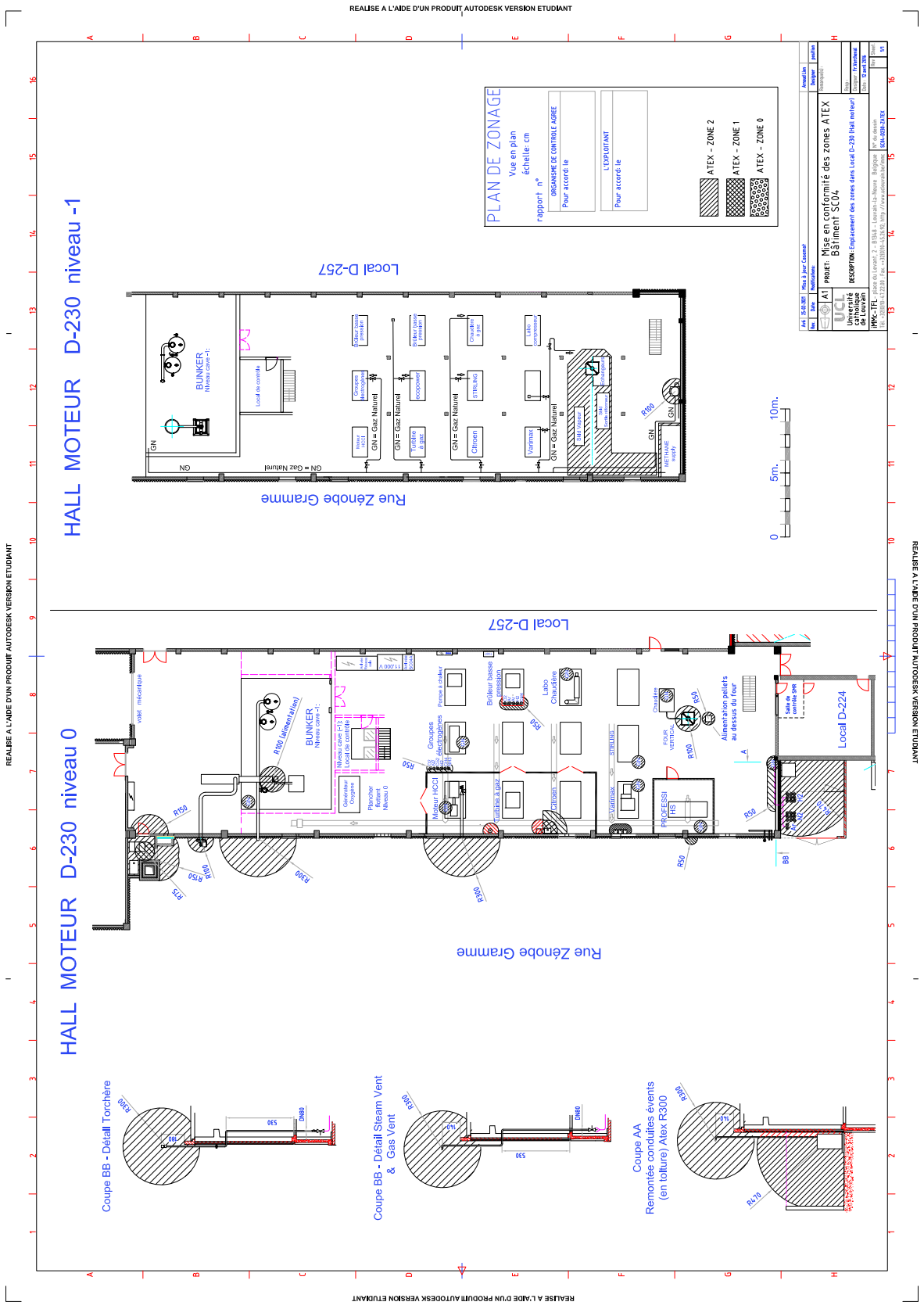

UNIVERSITÉ CATHOLIQUE DE LOUVAIN
École polytechnique de Louvain
Rue Archimède, 1 bte L6.11.01, 1348 Louvain-la-Neuve, Belgique | **www.uclouvain.be/epl**